University of Nevada, Reno

Relationship of base-metal skarn mineralization to Carlin-type gold mineralization at the Archimedes gold deposit, Eureka, Nevada

A thesis submitted in partial fulfillment of the requirements
for the degree of Master of Science in Geology

by
Matthew H. Hastings

Dr. Tommy B. Thompson/Thesis Advisor

December 2008

THE GRADUATE SCHOOL

We recommend that the thesis
prepared under our supervision by

MATTHEW H. HASTINGS

entitled

Relationship of base-metal skarn mineralization to Carlin-type gold mineralization at the Archimedes gold deposit, Eureka, Nevada

be accepted in partial fulfillment of the
requirements for the degree of

MASTER OF SCIENCE
IN GEOLOGY

Tommy B. Thompson, Ph.D., Advisor

John L. Muntean, Ph.D., Committee Member

Victor R. Vasquez, Ph.D., Graduate School Representative

Marsha H. Read, Ph. D., Associate Dean, Graduate School

December, 2008

Abstract

The Ruby Hill Mine is comprised of three distinctly different gold orebodies occurring near the town of Eureka, Nevada. The deposits are hosted in the Ordovician carbonates immediately adjacent to the Graveyard Flats intrusion, a Cretaceous andesite porphyry. To the west, the Bullwhacker Sill outcrops and plunges gently too the east, presumably to merge with the Graveyard Flats at depth. However, the initial discovery of gold mineralization at Ruby Hill Mine was made over 1000 feet above this skarn and approximately a mile to the west. The two orebodies that make up Archimedes (East and West) appear to be predominantly Carlin-type in their occurrence. The West Archimedes deposit is a sub-horizontal cigar-shaped orebody consisting of oxidized jasperoid and decalcified limestone. Oxidized gold mineralization is principally found in siliceous to variably decalcified breccias associated with intersections of structures such as the East Archimedes fault and the Blanchard-Molly fault system (Dilles et al., 1996). The auriferous jasperoid of West Archimedes is continuous with that that forms the wider orebody to the east. Unlike West Archimedes, the deepest portion of East Archimedes is also host to significant base-metal mineralization with local high-grade sulfide-rich gold. It is here that observations were first made relating to the close proximity of disseminated gold mineralization and base-metal skarn (Dilles, 1996). Gold mineralization also exists approximately 1700-2100 ft below the West Archimedes pit as arsenic sulfide and barite-rich hydrothermal breccias. This orebody is known as Ruby Deeps and is interpreted as being contemporaneous with the Archimedes orebodies. It is thought to be the result of the trapping of ore fluids against the hanging wall of the Bullwhacker Sill.

Based on several different lines of evidence drawn from the study of the different orebodies, the results suggest that the mineralization at Archimedes is related to a much later Carlin-type event rather that simply being the latest parts of the magmatic-hydrothermal system responsible for the base-metal skarn. Detailed petrographic studies and analysis using scanning electron microscope techniques provide the most compelling evidence. Arsenian pyrite replaces andradite garnets in high-grade intervals in deep East Archimedes and barite is commonly found as a late hydrothermal product. Well-preserved replacement textures and unique paragenetic relationships offer excellent examples of overprinting by the later Carlin-type event. Additionally, the fact that faults that cut the Cretaceous Bullwhacker sill at depth are hosts to Carlin-type gold mineralization in the Archimedes orebody is a compelling line of evidence for post-intrusion structures serving as mineralizing fluid conduits. Apatite fission track analysis appears to be supportive of this conclusion, exhibiting potentially two different populations of fission tracks with cooling periods ranging from about 100 Ma-70 Ma as well as 35 Ma-9 Ma. These ages are consistent with typical Carlin-type ages as well as the intrusion of the Graveyard Flats. $\delta^{18}O$ and $\delta^{13}C$ ratios were calculated from carbonates found both in veinlets around mineralized structures as well as wall rock alteration. $\delta^{18}O$ values show strong depletions in the deeper parts of East Archimedes as well as along fault zones within the West Archimedes pit. The data obtained from petrographic studies supported by the AFTA data appear to conclusively suggest a dual event model for the genesis of the unique Archimedes deposit, with each period of mineralization potentially separated by as much as 80 million years.

Acknowledgements

This thesis would not have been possible without funding from the Ralph J. Roberts Center for Research in Economic Geology (CREG) at the University of Nevada, Reno. An enormous debt of gratitude is owed to Ralph Roberts and the many others who have helped establish this world-class program for higher education specifically related to the science of ore deposit geology. Specific thanks are due to Shelley Harvey, the woman who simultaneously does many things at once to keep CREG moving forward and the students moving period.

Thanks are also due to Dr. Tommy B. Thompson, my advisor, who educated me in almost everything I know about ore deposits as well as many other geology-related subjects. Without his input and constructive criticism, this thesis would not be possible. I also would like to thank Dr. John L. Muntean, for serving on my committee and sharing his time, comments, and ideas that contributed significantly to improve the final product. Thanks also go out to Dr. Victor Vasquez, who also served on my committee and offered a unique perspective and intuitive comments that helped improve both my ability to explain my work and most importantly to communicate the most important parts of this study to people who had never seen nor worked at Archimedes.

A huge amount of gratitude is owed to Barrick Gold Company, most notably for donating generously to CREG every year and for continuing to support students through their interest in CREG projects. I would like to thank personnel at Barrick's Ruby Hill Mine for putting up with me rifling through their core, using their office space, and "wandering aimlessly" around their open pit. Their dedication to their jobs, the mine, and most of all safety was an excellent first example for me of how a world-class miner and its employees should function. Specifically, I deeply appreciate the time and patience given by Kevin Russell. He is truly the end-of-the-line authority on Archimedes and his guidance was instrumental in focusing the development of this thesis. Also, I would like to thank James Berry for his help in providing expertise in pit-mapping and, more importantly, a fresh and inquisitive mind that forced me to know what I was talking about to defend against his thoughtful and candid questions. Also deserving thanks are Barrick Exploration geologists Karl Marlowe, Dave Arbonies, and Paul Dobak. These gentlemen were more than generous when it came to logistics and sharing of data and the amount of work that was able to be done because of them smoothing the way ahead cannot be measured.

I would like to thank my friends and coworkers in CREG for their assistance, criticism (both constructive and destructive), and levity. Notably, Wes Sherlock gave much of his time to provide assistance with mineral identification via the SEM as well as reflected light microscopy. Rick Trotman is a good friend who is not afraid to challenge me at every turn and force me to explain my reasoning for things before accepting them to be true. Keith Campbell and Robert Wood are some of the most knowledgeable geologists I've ever met and their patience and willingness to answer my many questions was hugely beneficial.

Finally, I would like to thank my beautiful wife Theresa, for her understanding, compassion, and motivation. She supported me while in school and forced me to take breaks when I needed to and go back to work when I had to. I would never have been able to finish this thesis without her standing beside me and pushing me forward.

Table of Contents

List of Tables

List of Figures

Introduction

The Archimedes system is located approximately one mile west of the town of Eureka, in east-central Nevada (see Figure 1). Archimedes is an interpreted Carlin-type system comprised of three orebodies: West Archimedes, East Archimedes, and Ruby Deeps. It is currently operated by Barrick Gold Co., and retains the name Ruby Hill Mine. Unlike the lead-zinc-silver/gold mineralization mined from Ruby Hill in the late 1800's and early 1900's, the economic gold mineralization at Archimedes is conspicuously devoid of lead or zinc. The Ruby Hill Mine is an oxide operation, involving the crushing and cyanide heap-leaching of the ore. The system was originally separated into two different orebodies (East and West Archimedes) to ease tensions with locals concerning water rights. West Archimedes was mined first, as it was above the water table. As the price of gold rose, East Archimedes became more economically viable and is currently producing. West Archimedes can best be described as an oxidized carbonate-hosted, structurally and lithologically controlled gold deposit. The result is a 780 meter-long cigar shaped orebody plunging approximately S60E at -10^{o}. East Archimedes is the second part of the system, and appears to be a more steeply dipping root to the West Archimedes orebody. East Archimedes is a partially oxidized, steeply plunging, auriferous breccia body.

Perhaps the most interesting thing about this otherwise obviously Carlin-type system (as well as the subject of this project) is the proximity of East Archimedes to the Graveyard Flats andesite porphyry and associated base-metal skarn mineralization. The schematic cross section in Figure 2 defines the inferred relationships of the gold orebodies to intrusive rocks as well as a base metal skarn. The Ruby Deeps orebody is

hosted in the Cambrian Windfall Formation at depths in excess of 1700-2000 ft from the original surface. This orebody occurs in the footwall of a shallowly dipping andesite porphyry sill. This sill is interpreted to have originated as an offshoot of the Graveyard Flats intrusive that was likely emplaced along a preexisting thrust fault. Ruby Deeps is both mineralogically and morphologically different from the Archimedes system, and is characterized by barite/arsenic sulfide hydrothermal breccias with disseminated auriferous arsenian pyrite. The purpose of this project is to explain and differentiate between different types of gold mineralization seen within the Archimedes and Ruby Deeps deposits. The controversy that has arisen from the proximity of these different orebodies and the base-metal skarn at depth has been drawn from the similarities of distal carbonate-replacement deposits and Carlin-type systems. The purpose of the research presented in this study is to evaluate and observe the relationship between the skarn mineralization at depth and the Archimedes and Ruby Deeps orebodies. Conclusions drawn from this research will hopefully shed

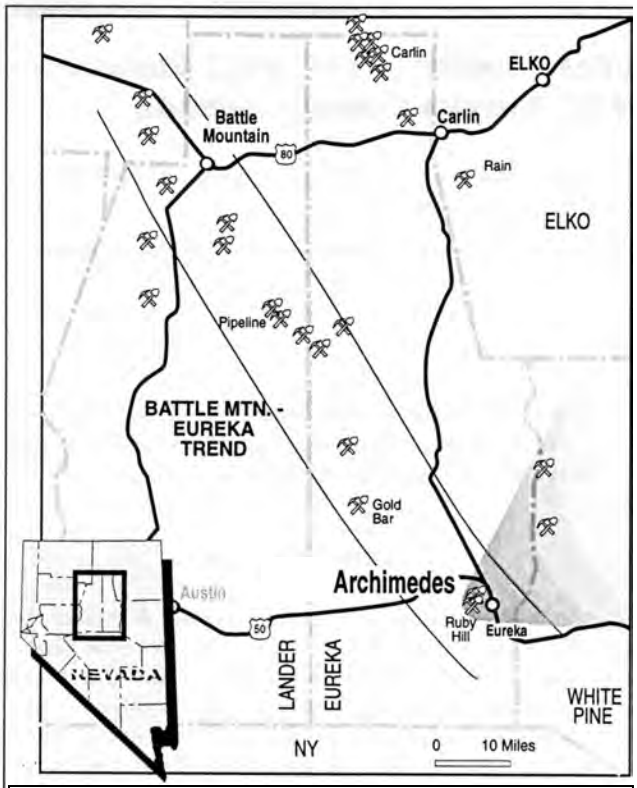

Figure 1. – Location map for Archimedes showing proximity to prolific Battle Mountain-Eureka trend of ore deposits

some light on the complex relationships between these systems and help develop a model for their genesis.

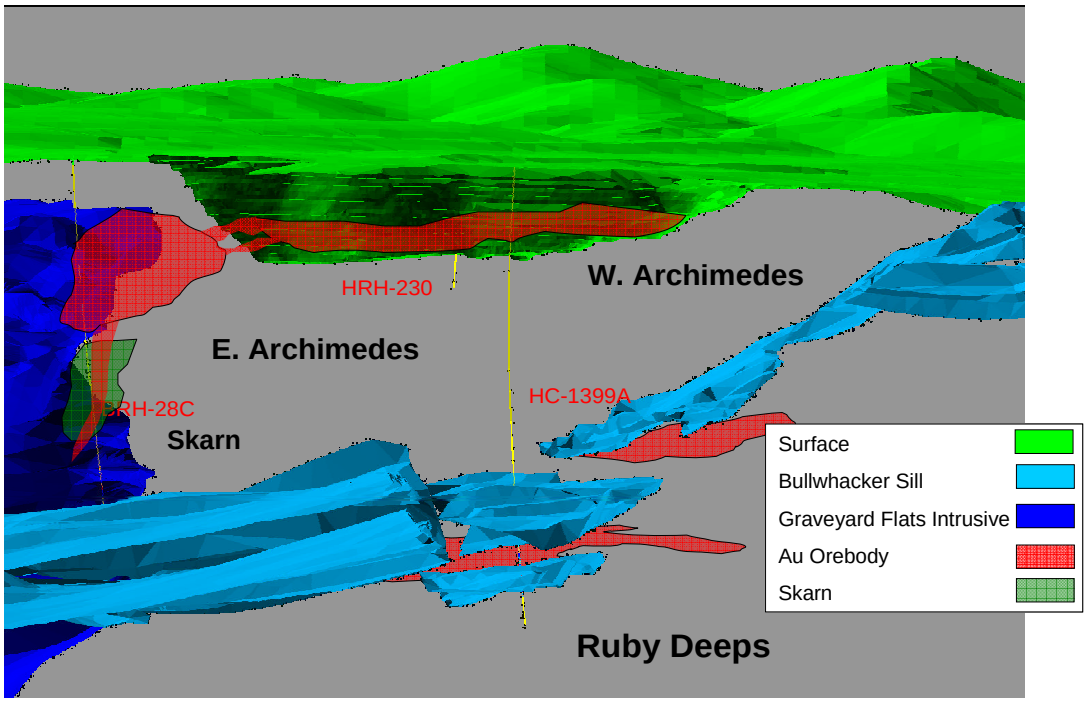

Figure 2. – Schematic 3D cross-section showing the spatial relationships of the different orebodies to the surface as well as intrusive rocks defined by drilling.

Methods

Initially, the surface geology of the area around Archimedes in the northern part of the Eureka District was mapped. Mapping was primarily focused on nearby igneous rocks and alteration associated with them, with the express purpose of relating volcanic events to mineralization. Mapping of these units was done at 1”-1000’ scale. For the most part, the work done in previous reports was very accurate and more detailed than that which could be accomplished in the time available. Therefore, much of the regional

district geology is synthesized from the maps of these previous workers with minor additions or corrections by the author. This regional geology with simplified structure is presented in Figure 9. Accessible exposures in the East Archimedes pit was mapped in January of 2007 at the scale of 1”-200’. In lieu of exposure, over 5000 feet of core was logged and much more was sampled and examined in detail to describe stratigraphy and mineralization at depth. Many drillholes were examined using existing logs to expedite the process of looking for specific styles of alteration or mineralization. The three holes that were logged in detail are HRH-230, BRH-28C, and HC-1399. These holes are representative of the West Archimedes orebody, the East Archimedes orebody, and the Ruby Deeps mineralization, respectively. Over 200 samples were taken, both in rotary chips and diamond-drill core in order to evaluate alteration and mineralization styles using standard and polished thin sections.

Also, a group of samples were taken for stable isotope analysis. Ninety isotope samples were taken and successfully analyzed for carbon and oxygen isotopes from within the mineralized area as well as from unaltered samples from fresh limestone outcrops to the south to act as baseline values. Separates were drilled using high-speed Dremel rotary tools. Carbonates were sampled from veinlets and wall-rocks in the mineralized zones as well as whole rock samples from unaltered carbonates. Fifteen samples of sulfides and sulfates were analyzed for isotopes of sulfur. Minerals were separated from massive replacement zones and veinlets in the unoxidized portions of the orebodies. The purpose of this investigation was to demonstrate any isotopic exchange taking place during mineralization. Sulfur isotopes were also analyzed for geothermometry potential in the sulfide minerals at depth. The objective was to estimate

temperature of formation based on the fractionation of sulfur isotopes in sulfide/sulfate minerals in equilibrium. While a minimum temperature of formation could also be derived from fluid inclusion data, early examination of doubly-polished plates from mineralized zones was discouraging. Samples were taken from silicified zones as well as the massive barite horizons. Any observed fluid inclusions present are in barite and appear to be predominantly secondary. This precludes that any reliable fluid inclusion data would likely be extremely difficult to obtain and likely innaccurate.

In order to better identify paragenesis and mineralogy, over 75 thin and polished sections were analyzed using both an Olympus binocular petrographic microscope and JEOL 840A Scanning Electron Microscope (SEM). Over thirty hours were spent analyzing sections from representative mineralized zones on the electron microscope, obtaining Electron Dispersive Spectra (EDS) and backscatter images of paragenetic relationships of the ore minerals. In addition to paragenesis, the EDS is capable of giving quantitative elemental analysis to determine, for example, relative amount of arsenic within pyrites. Finally, six samples on a transect from East to West were collected from the Bullwhacker Sill and Graveyard Flats intrusive for apatite fission-track dating. Irradiation and fission-track counts were performed by Geotrack International in Sydney, Australia. Geotrack also used their proprietary modeling methods to develop thermal histories and possible explanations for the heating and cooling periods that they describe. A full report from this investigation can be found as Appendix D.

Eureka District History

A brief history of the Eureka mining district is included herein, mostly taken from historical accounts in papers by Curtis (1884), Hague (1892), Roberts et al. (1967), and Nolan (1962),. Today's Ruby Hill Mine lies just west of the town of Eureka, Eureka County, in the northernmost part of the Eureka mining district. The name "Eureka" originates from early mining prospects discovered in the summer of 1864. These prospects are located in New York Canyon on the eastern side of Prospect Mountain, and were originally exploited as the Eureka Mine. The name Eureka also stuck to the town that had sprung up around the workings, and was later assigned to the county. When the Ruby Hill mineralization was discovered in 1867, the focus of mining efforts was shifted to the Ruby Hill area and away from the original Eureka Mine. Two major companies sprouted from Ruby Hill and would make the Eureka district a leading producer of lead, silver, and gold; Eureka Consolidated and the Richmond Mining Co. (Hague, 1892). While the relationship between these two companies could be described as tense at best, they managed to bring new mining and smelting techniques to the area and make it possible for other smaller mines to operate. The bulk of the district's lead production came in the interval from 1870 to 1890, when the Richmond and Eureka Consolidated smelters were in operation. The rich Ruby Hill base-metal deposit was capable of feeding both smelters, with relatively large amounts of gold and silver as by-products. The Eureka Consolidated smelter was located in the northern part of the district, with the

Richmond to the south. The sizeable slag piles from these smelters are still recognizable features of the landscape today.

Figure 3. – Water door installed in the FAD workings by Eureka Corp. in 1941

The extremely rich Ruby Hill ores were, for the most part, exhausted in 1890, although minor production continued from lower grade ores until 1939. The smelters shut down in 1891 in response to the lack of high-grade ore. In 1941, the FAD shaft was sunk by Eureka Consolidated to exploit the new ore horizons in the hanging wall of the Ruby Hill fault. However, upon reaching a depth of 2,500 ft., a higher crosscut on the 2250 level met with a 16,000 gpm water flow within the Martin fault (Figure 3). This took place in 1948, and essentially was the death knell for the Eureka Corporation at Ruby Hill. As of 1959, an economical solution to the flooding could not be found, and the company did not renew the FAD leases. According to Nolan (1962), the early production numbers from the Ruby Hill area are approximately 51.3 t Au, 1,200 t Ag, and 283,575 t Pb from about 1.8 Mt of ore. Most of the Zn was not recovered. During the bonanza years, ores averaged an estimated 0.75 opt Au, 40 opt Ag, and 45% Pb (Curtis, 1884). In 1878, the town's population peaked at 9000, with over fifty mines producing over 700 tons of ore per day for the smelters. In 1892, Hague describes the 88 mile-long Eureka and Palisade railways, which served to connect the

Eureka Consolidated and Richmond smelters with the Central Pacific railroad. This itself shows the importance of Ruby Hill on a large scale. The amount of lead generated by Ruby Hill was sufficient to affect the world market during the most robust years of mining.

In 1960, the lease on the FAD shaft property was picked up by a conglomerate of Newmont Mining Corporation, Cyprus Mining Corporation, and Hecla Mining Company. The FAD shaft was dewatered in 1964 and a crosscut was extended into mineralization (Roberts et al., 1967). Hecla calculated a resource of 2.8 Mt, grading 0.16 opt Au, and 5.7 opt Ag, with 3.7% Pb and 8.3% Zn. However, grades were not particularly amenable for an underground operation, and metallurgical tests were also somewhat discouraging. Thus, the shaft was allowed to flood again and the consortium began to break up. Newmont took their leave in 1976, with Hecla following in 1979. Cyprus remained in the district and explored for a near surface, bulk-mineable gold deposit for two years. Exploration was disappointingly unsuccessful and in 1982 the lease on the property was allowed to revert to Sharon Steel Co., the successor to the Ruby Hill Mining Company. The area was for the most part dormant until 1990, when Homestake began negotiating for the lease on the Ruby Hill property.

Stimulated by the lack of exploration in the past eight years, as well as the magnitude of the district's historical production, Homestake aggressively pursued the lease to the Ruby Hill property. Field work was not begun until 1992, when the negotiations concluded with Sharon Steel (Dilles et al., 1995). Shortly thereafter, a twelve-hole drilling campaign returned several disappointing results, with the exception of hole HRH-138. This particular hole had a somewhat encouraging interval on Mineral

Point that returned approximately 30 ft of 0.046 opt Au from about 30-60 feet below the surface. The next campaign focused on developing any sort of geochemical indicators for finding a larger orebody beneath the pediment. Hole HRH-150 was drilled about 470 ft. east of HRH-138 and returned about 90 ft. of 0.228 opt Au. The disseminated Au mineralization was hosted in silicified, decalcified limestone with anomalous As and Hg values. Moreover, it was completely oxidized, making it amenable to a heap-leaching operation. Further drilling in this area defined a small, fault-bounded orebody, and made it possible to develop a geochemical vector for exploration to the southeast. The next drilling program began in July of 1993, resulting in the discovery of the main portion of the West Archimedes orebody. By August of that same year, drillhole HRH-237 had intercepted 390 ft of 0.106 opt Au in the southeast corner of the pattern. This was essentially the discovery hole for the East Archimedes orebody. In 1997, Homestake announced its plans to develop the West Archimedes orebody, with active drilling to explore the potential of the East Archimedes orebody. Over the next four years, over 700,000 oz Au was mined from West Archimedes prior to its shutdown in 2001. However, just one year later, Barrick Gold Co. would acquire Homestake, and begin plans for reopening the Ruby Hill Mine to pursue the East Archimedes mineralization. Currently, stripping is almost completed and the first ore is being exposed in the new pit.

Tectonic History

The Eureka district is located in the most southeastern end of the Battle Mountain-Eureka trend as defined by the concentrations of gold deposits along the lineament from the area of Battle Mountain extending to Eureka. To understand the area's geology, it is important to address its history. The town of Eureka is interpreted to lie on western edge of the rifted North American craton (Speed & Sleep, 1982). The ancient ensialic margin of the North American continental plate is expressed as what is known as the Sr 0.706 line (Tosdal et al., 2000). This line represents a significant isotopic shift from primary continental crust to a different composition in the accreted rocks (See Figure 4). Additionally, Eureka lies on or very near the eastern edge of the Roberts Mountains Allochthon (RMA). The lower plate rocks beneath the RMA are host to many of the richest and most important gold discoveries within Nevada. The allocthon was thrust onto continental crust due to a series of subduction-related collisions taking place around 370 Ma (Oldow, 1984). A series of island arcs approaching from the west developed several different orogenic events, the most prominent of which are the Antler and Sonoma orogenys. The Late Devonian to Early Mississippian collision of the Antler arc plowed continental shelf sediments up onto the craton, resulting in the emplacement of the RMA (Miller et al., 1992). The Late Permian to Early Triassic Sonoma orogeny resulted in the thrusting of the Golconda allocthon onto the continental crust and over the RMA (Burchfiel et al., 1992).

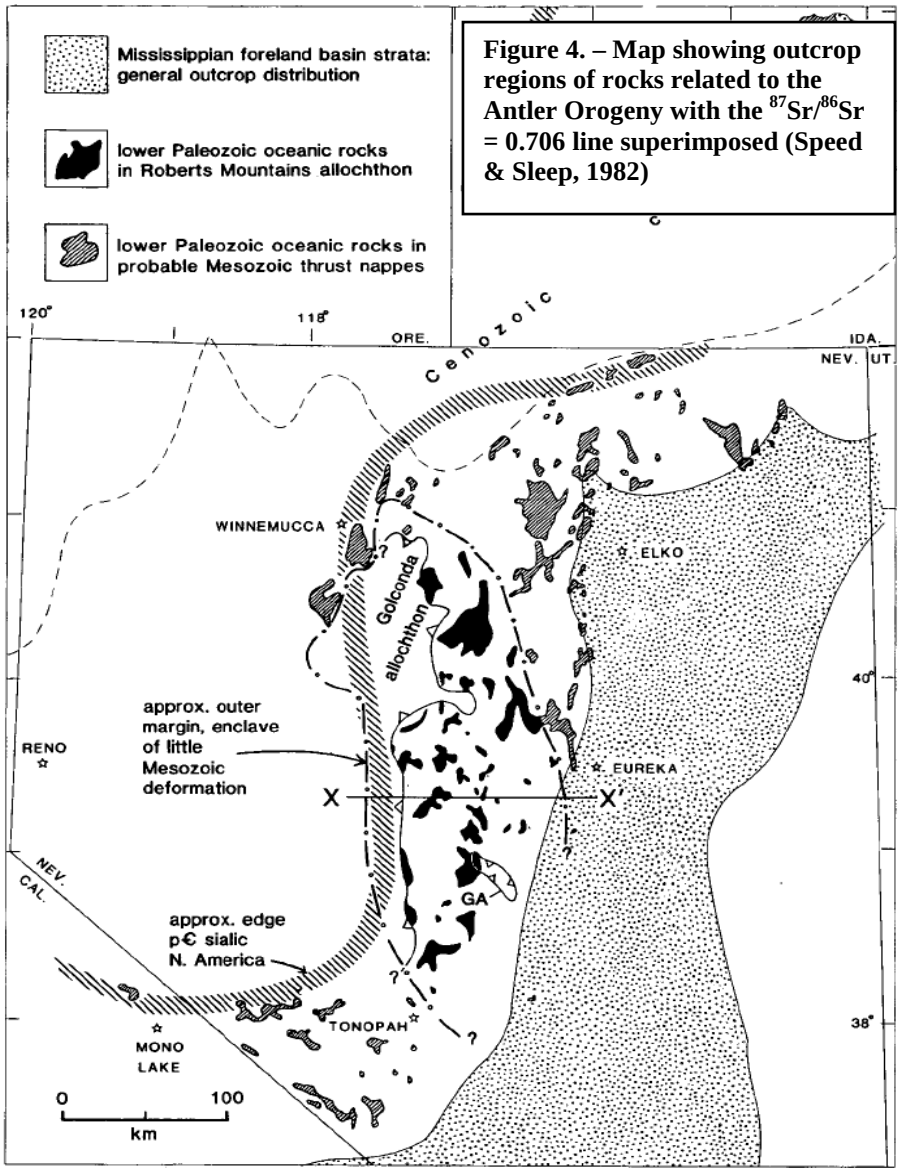

Figure 4. – Map showing outcrop regions of rocks related to the Antler Orogeny with the $^{87}Sr/^{86}Sr$ = 0.706 line superimposed (Speed & Sleep, 1982)

A series of complicated tectonic regimes dominate from the Early Triassic to the Cretaceous. Most of the changes that take place in this time period are related to changing subduction parameters and oblique plate convergence. Many more arcs are accreted in this time and built onto the North American craton, but the most important event during this time was the Nevadan Orogeny. The steepening angle of the subducting plate from

the Middle to Late Triassic caused widespread volcanism and uplift close to the western edge of the craton. This mountain building episode is the source of what is now called the Sierra Nevada (Burchfiel et al., 1992). Also occurring in this time is rifting and extensional tectonics related, again, to the transpressional and oblique plate movement. Some of these aspects continue well into the Cretaceous, but the plates somewhat change alignment. In the early Cretaceous, the Pacific and North American plates collided head on. The establishment of an active continental margin to the west resulted in compressional deformation (folding and faulting), crustal thickening, and widespread magmatism that continued through early Cenozoic time (Grauch et al., 2003).

In Eureka this is best represented by the abundance of 100-110 Ma intrusions (such as the Ruby Hill stock and Graveyard Flats intrusion) and later 80 Ma two-mica granites. Early Tertiary tectonism was characterized by a changing subduction angle to the west and resultant southward migration of volcanic provinces. This also included localized intensely extensional regimes (Seedorff, 1991). From the Middle to Late Tertiary, regional uplift and widespred development of tilted blocks and subsequent valleys resulted in the features we now call the Basin and Range (Christiansen & Yeats, 1992). This time was also characterized by the development of the Northern Nevada Rift. The Northern Nevada Rift (NNR) is approximately 500 km long and extends from southern Nevada to the Oregon-Nevada border (Zoback et al., 1994). Represented by a series of north-northwest trending basaltic and rhyolitic dikes and flows, the NNR was first described as an aeromagnetic anomaly. It is believed that the NNR probably stemmed from a situation similar to the Columbia River Flood Basalts in Oregon. Its development was supported by the extensional tectonic regime that dominated during the

development of the Great Basin. The dike swarms of the NNR are roughly equivalent in age, orientation, and composition to the feeder dikes responsible for over 95% of the 15.5-16.5 Ma Columbia River Flood Basalts (Zoback et al., 1994). The breaching point for the NNR is believed to be the McDermitt Caldera at the northernmost end of the rift. Although not well exposed across the whole of Nevada, the NNR as identified by aeromagnetic data has an orientation perpendicular to the least principal stress direction during the time of emplacement in the Miocene. In other words, the NNR records back-arc extensional tectonics and regional heating in northern Nevada as recently as 15 Ma (Zoback et al., 1994). In the history of northern Nevada, this is perhaps the latest of the widespread heating events, although certain parts of Nevada are hydrothermally heated today.

Stratigraphy

A complete stratigraphic section exists in the Eureka district (Figure 5). The stratigraphy has been well studied, and the following description is only a brief synopsis of detailed work done by Hague (1892), Nolan et al. (1956), Nolan (1962), Dilles et al. (1996), as well as the author's own field and lab observations. The oldest unit exposed in the area of interest is the Cambrian Prospect Mtn. Quartzite, which is at least 1700 ft thick, and the base is not exposed in this area. The Prospect Mtn. Quartzite typically has a slightly higher clay content and larger grain size than the nearby Ordovician Eureka Quartzite (Nolan et al., 1962). The Pioche Shale lies stratigraphically above the Prospect Mtn. Quartzite, and is comprised of approximately 400-500 ft of khaki-colored

micaceous shale with sandy limestone. It varies widely in thickness, likely due to structural deformation (Nolan et al., 1956).

Above the Pioche shale is the Cambrian Eldorado Dolomite. This 2500 ft thick massive dolomite is host to the high-grade carbonate replacement deposits mined at the original Ruby Hill. It is generally bluish-gray in color and is coarsely crystalline. It locally contains darker blue/black dolomite that is much finer grained. Overlying the Eldorado is the 300 ft-thick Cambrian Geddes Limestone, a well bedded dark blue/black carbonaceous limestone with thin dark, shaly bedding. The 650 ft thick Cambrian Secret Canyon Shale overlies the Geddes, and is comprised of two members: the Clark Springs and Lower Shale. The Clarks Spring Mbr. is a thin-bedded silty fine grained limestone with reddish argillaceous partings (Nolan, 1968). The Lower Shale member is mostly composed of grey/green argillaceous shale. The Cambrian Hamburg Dolomite is a 1000 ft thick dark grey massively bedded limestone with banded and mottled dolomite horizons. The Dunderburg Shale, which overlies the Hamburg, is a brownish shale with zones of thin nodular limestone interbedding.

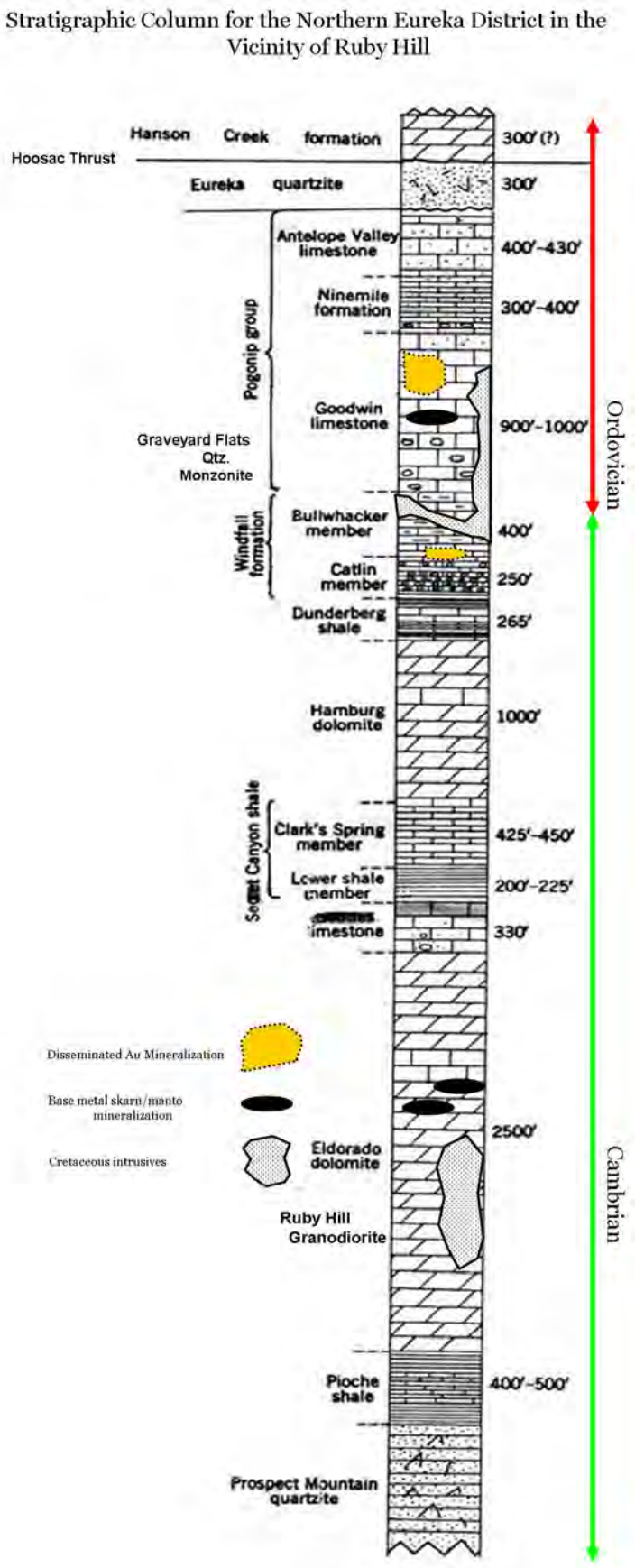

Figure 5. – Stratigraphic column modified from Nolan, (1962). Shows known mineralized stratigraphy as well as intrusive relationships.

The units that host the mineralization in the vicinity of Archimedes are the Cambrian Windfall Formation and the Ordovician Pogonip Group. A generalized map of these units within and in the vicinity of the Archimedes open pit is shown in Plate 1. The Windfall Fm. is comprised of the Bullwhacker Mbr., a yellow/tan platy limestone with shaly/sandy partings with thin buff-colored interbeds (Nolan, 1968). The overlying Catlin Mbr. is a massive limestone with local thinly bedded sandy/silty limestone and abundant chert. Sparse interbedding was observed in both units and is typically < 3 in. thick. Laminations appear to be the most common bedforms in the carbonates. Chert content is variable, but it is more prevalent in the lower-most part of the Catlin. Under the microscope, the unit appears to be comprised of primarily very fine/fine grained sandy limestone (Figure 6A). Chert/quartz grains are abundant, and typically are found near laminations as rounded grains as well as micro-lag in bedding (Figure 6D). Laminations are typically silty, and show an abundance of opaques that appear to be either pyrite or hematite pseudomorphs after pyrite. Other samples from stratigraphic units above and below the Windfall have locally preserved pyrite. Fossil hash is abundant, consisting of brachiopods, gastropods, and local burrowing casts (Figure 6C). The most common texture is fine-grained limestone, with sparse relatively large (>1mm) coarsely-crystalline intraclasts (Figure 6B).

The Ordovician Pogonip Group is comprised of five units (Dilles et al., 1996). The Ordovician Goodwin Limestone was separated into three separate units after closer examination during mining enabled geologists to better differentiate them within the pit. The Pogonip also includes the Antelope Valley Limestone and the Ninemile Formation. The lowermost unit is the 350 ft-thick Lower Goodwin Limestone (Og1). The Og1 is

described as a fine to medium-grained, massively-bedded sandy limestone. A key diagnostic feature of the Og1 is the sparse black/gray

chert nodules that occur ubiquitously throughout (Figure 7A). The chert in the Og1

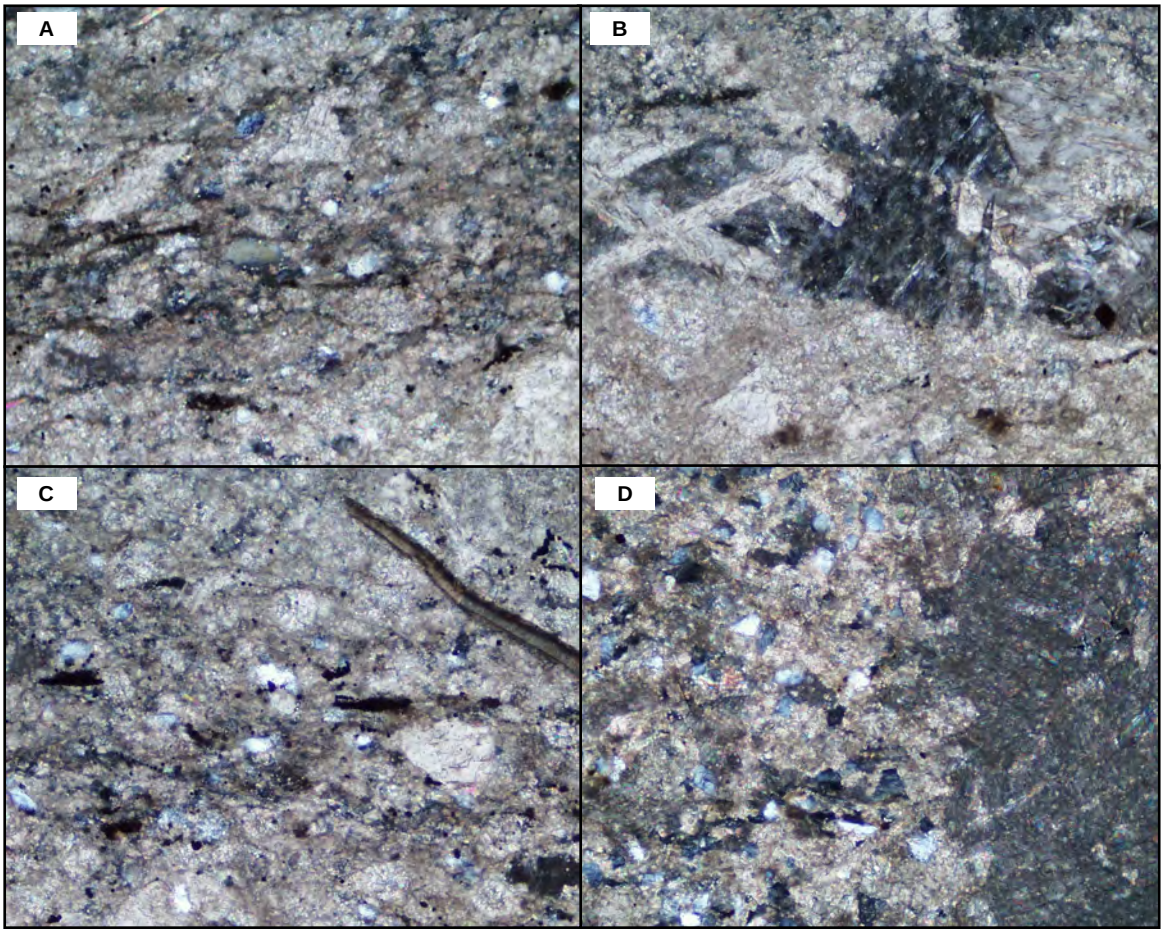

Figure 6. – Photomicrographs of the Windfall formation. A. - Silty lamination with quartz grains 20X, XP; B. - Sparry intraclast in micrite mud 10X, XP; C. - Brach fossil with smaller un-identified fossil hash 10X, XP; D, - Cherty horizons in laminations in the Catlin Mbr. 10X, XP. FOV = (100x) 0.85 mm, (200x) 0.43 mm, (400x) 0.21mm

occurs locally as bedded nodules but more commonly as fragments within the more sanded portions of the limestone. Locally, interbedding looks almost hummocky, but is generally very faint and discontinuous. Indeed, it is very difficult to distinguish these features in the field where exposure is limited. Bedding is generally thicker than 2 ft, but is also relatively faint in outcrop. The lowermost part of the unit is much more shaly,

with relatively abundant fossiliferous lenses. Unlike the other units, the mud content of the Og1 appears to be very low, although this could be a local feature (Figure 7B). The Og1 in the pit area is also characterized by coarse, abundant calcite veins. Sparse (>0.3mm) quartz grains are relatively angular and have a more cryptocrystalline texture. These probably represent the chert fragments. The uppermost part of the Og1 is strongly burrowed and is slightly coarser grained. Much of the gold mineralization of East Archimedes is hosted in Og1 or lower rocks. The upper contact of this unit is typically fairly gradational, but is generally denoted by an increase in silty laminations.

Overlying the Og1 is the lower-laminated member of the Goodwin Limestone (Ogll). It is described as a thinly interbedded fine/medium-grained silty limestone (Dilles et al., 1996). Bedding is generally less than 1”-4” thick and is variably sanded. Laminations are the dominant bedforms, with little apparent burrowing or fossil hash (Figure 7C). Chert content is rather low, but locally occurs as semi-continuous lenses and nodules. Stylolites are also common in this unit. In thin section, the Ogll appears to be a fine-grained silty micrite with fairly abundant (15%) quartz grains (less than 0.01 mm). Quartz grains are well-rounded and for the most part supported by carbonate mud. Silty layers typically contain higher percentages of quartz fragments as well as some euhedral pyrite/hem with organic insoluble material (Figure 7C, 7H). Intraclasts of sparry calcite are common, and could represent diagenetic recrystalization. This unit is known to be a minor ore host, although high grade intervals within this unit along the intersection of the Blanchard and 426 faults are now being examined as possible targets. In the pit, the Ogll displays variable alteration, but is typically more susceptible to argillization due to its higher silt content (Figure 7D).

The uppermost unit within the Goodwin is the Upper Goodwin Limestone (Og2). The most favorable host to the Archimedes mineralization, this unit is approximately 500 ft-thick and is identified by a noted increase in chert and presence of easily identifiable bedding. It is classified as a medium to thickly bedded fine-grained limestone. It is commonly interbedded, varying between wackestone and packstone beds of 1”-8” thickness. Coarser-grained bedding is obvious, especially in the upper part of the unit. Some bioturbation is present, as burrows in excess of ½” width, roughly sub-parallel to bedding are present. Local chert content can be as high as 20%, ranging in color from light gray to black, and occurring as stringers, boudins, and individual nodules. The unit is fine to medium-grained although bedding can include rather coarse horizons that are locally sanded (Figure 7E). It is likely that the increased permeability from sanding and high chert percentages make this unit favorable for the Archimedes mineralization. Generally sparry calcite with sparse quartz grains ranging in size from .1mm to .5 mm is common (Figure 7G). In fossiliferous horizons there appears to be mostly trace fossils with rare brachiopod allochems. Intraclasts of more micritic limestone are abundant, commonly taking an oblong spheroid shape. Veins of calcite are common and could be a product of diagenesis or late hydrothermal activity (Figure 7F). Notably, the Upper Goodwin is rife with stylolites, many of which contain what is probably diagenetic pyrite.

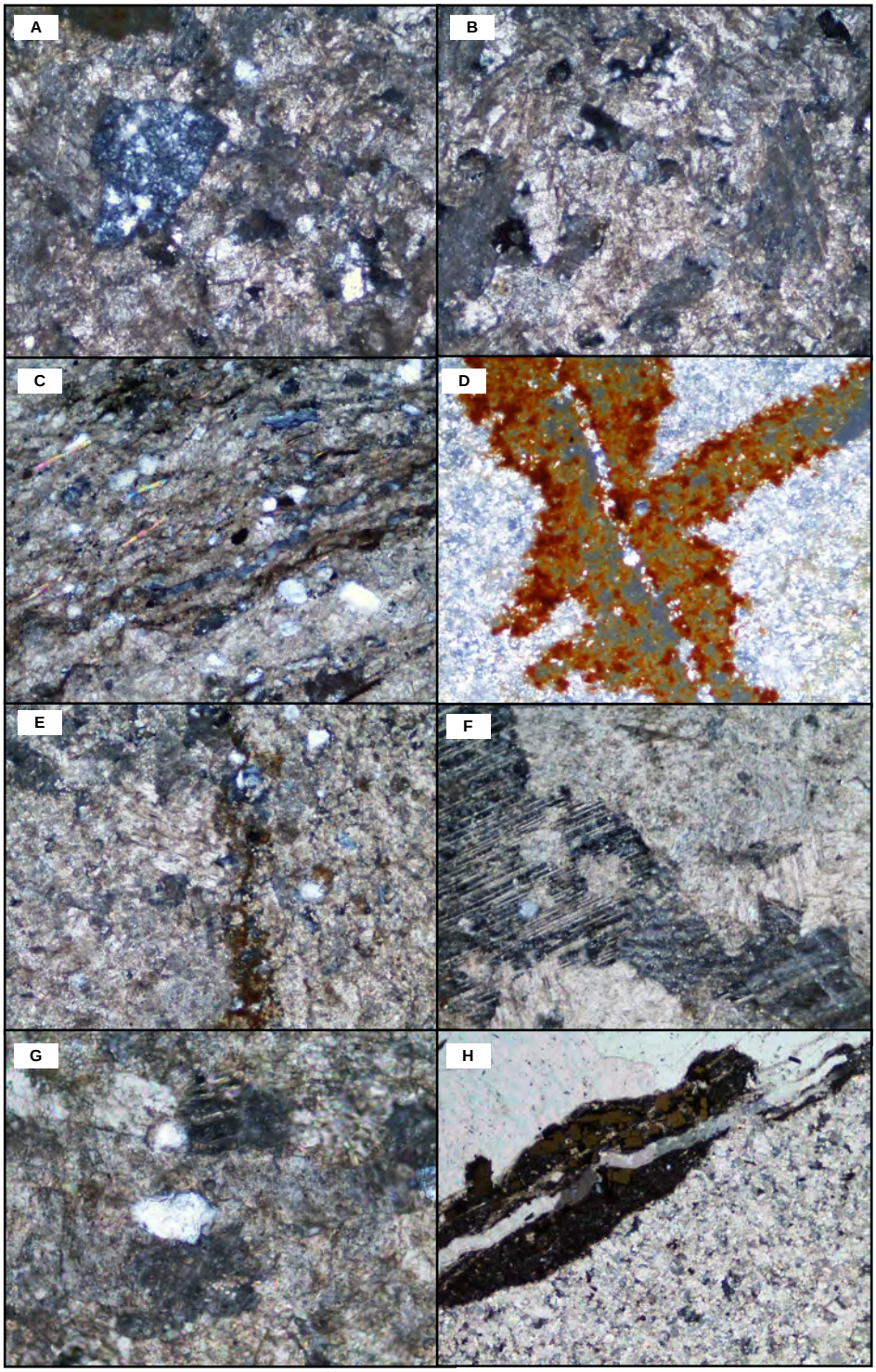

Figure 7. – Photomicrographs showing key differences within the Goodwin Limestone. Lower Goodwin (Og1) A. - Chert frag in sparry cc, 10X, XP; B. - Massive sparry cc with opaques, 10X, XP; Lower Laminated Goodwin (Ogll) C. - Silty laminations with quartz grains and cherty layering 20X, XP; D. - Clay + FeOx alteration in the pit along qtz-calcite veinlets, 20X, XP; Upper Goodwin (Og2) E. - Stylolite with sparry cc (L) and micritic cemented ed mud (R) 10X, XP; F. - Sparry cc w qtz grains 10X, XP; G. - Qtz grains in sparry cc 20X, XP; H. - Stylolite showing different carbonate textures on either sides with pyrite and oganic material along the dissolution horiizon, 10X, XP FOV = (100x) 0.85 mm, (200x) 0.43 mm, (400x) 0.21mm

Fine-grained cubic pyrite and abundant organic material are observed in the stylolites, illustrating the possibility of dissolution and re-deposition (Figure 7H). These relatively insoluble products are deposited after dissolution of carbonates and concentrated over time (Fletcher and Pollard, 1981). Upon making these observations it is believed that these stylolites provided nucleation sites that contribute to the favorability of the Og2 as an ore host.

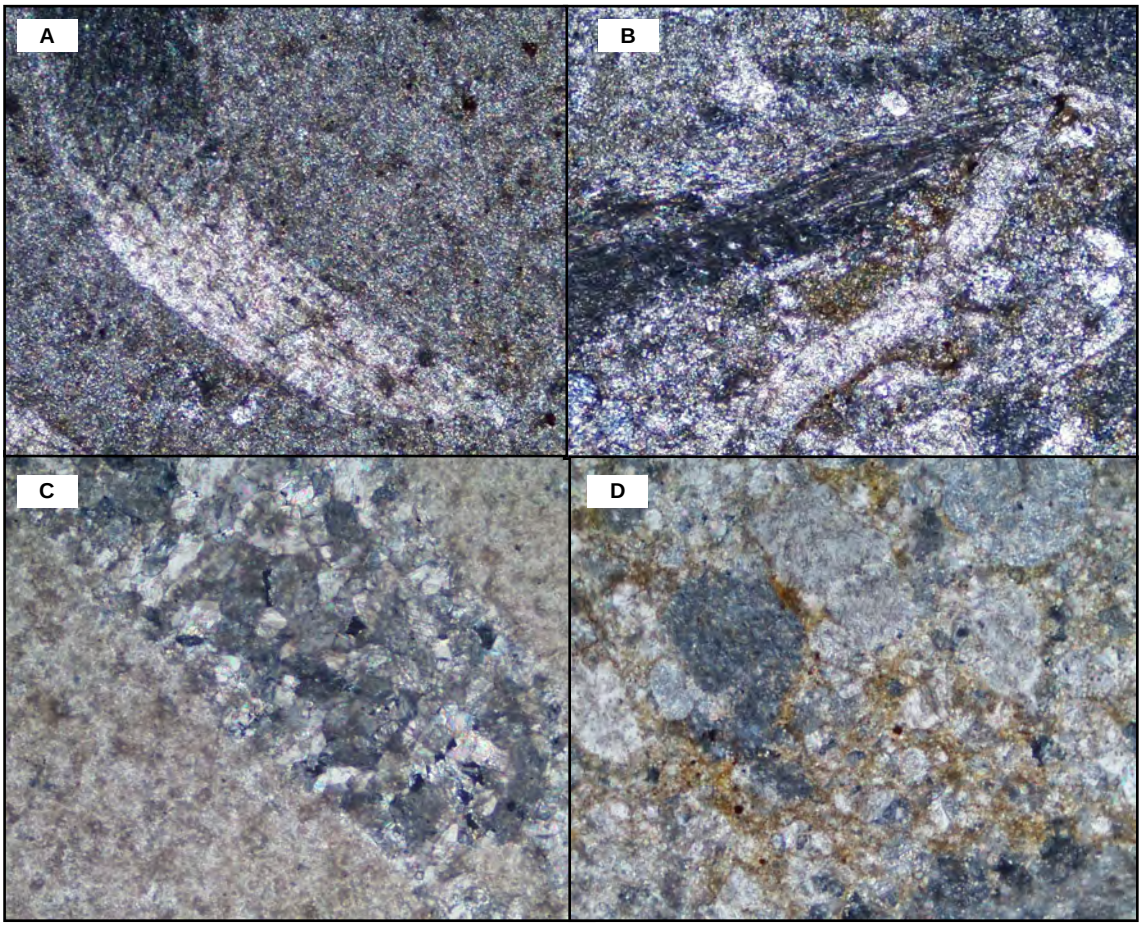

Figure 8. – Photomicrographs of the Ninemile formation. A. - Pelecypod fossil in On, 10X, XP ; B. - Brachiopod fossil hash in On, 10X, XP; C. - Sparry replacement of fossilized material 10X, XP; D. - Primary sedimentary slump breccia 10X, XP FOV = (100x) 0.85 mm, (200x) 0.43 mm, (400x) 0.21mm

Above the Goodwin Limestone is the Ninemile Formation (On). The Ninemile is an olive drab very fine grained mudstone that is typically thinly bedded. Although

predominantly fine-grained carbonate, it also contains very fine-grained silty limestone. It is fossiliferous locally with 10-50% mud matrix (Figure 8A). More fossiliferous zones tend to be more coarse-grained. Locally, sparry calcite is dominant due to replacement of fossiliferous material by coarser calcite (Figure 8C). Local interbedding of coarse fossil hash (up to 30%) is common in this unit (Figure 8B). which prompted Dilles et al. (1996) to break it up into two members. Today, it is considered a single unit, as the bioclastic horizons have been observed to occur throughout the thickness of the unit. The Ninemile is also host to several different types of slump features that are easily visible in both hand sample and thin section (Figure 8D). While these slump breccias are common, they tend to be fairly localized and allow the Ninemile to retain its more massive texture overall. The permeability contrast between this unit and the Og2 has been proposed as a reason for the gold mineralization within the Og2 (Dilles et al., 1996). Finally, the Antelope Valley Limestone (Oav) overlies the Ninemile, and is approximately 450-600 ft-thick. The Oav is generally fine-grained with local coarse-grained lenses and thin bedding. This unit can be denoted by the abundant chert near its base, with sparse fossil hash dispersed throughout the unit.

Igneous Rocks

The igneous rocks within the Northern Eureka District likely hold some key as to the age of mineralization at Archimedes. The fact that contemporaneous magmatism is a characteristic of skarns and not necessarily Carlin-type deposits is enough cause for a closer look at the igneous rocks in the district. Their distribution is displayed in the

regional geologic map in Figure 9. To achieve a better understanding of these rocks as well as the processes responsible for their emplacement, samples were taken for detailed petrographic analysis as well as whole rock geochemistry. Whole-rock geochemical data is available in Appendix A. It would appear that there are at least two discreet periods of magmatism within the Northern Eureka district. The oldest of these is the pulse of Cretaceous magmatism represented by a number of porphyritic intrusions. This period coincides with the Sevier Orogeny, and likely is related to the intense period of magmatism that affected the western U.S. as periods of rapid subduction occurred to the west. The second period of magmatism apparently took place during the Late Eocene/Early Oligocene based on radiometric dates from extrusive rocks. These rocks range in composition from rhyolites to basalts, and crop out at Target Hill as well as Richmond Mtn.

The oldest intrusive units in the northern part of the district are the Cretaceous Graveyard Flats porphyry and Ruby Hill Stock. The Graveyard Flats intrusion was discovered beneath alluvium while drilling near East Archimedes in 1993 (Dilles et al., 1996). Its extent is not known, but appears to be much larger than other intrusions such as the Ruby Hill Stock found in the district. The Graveyard Flats intrusion has been identified as an andesite porphyry, with quartz and plagioclase phenocrysts in an aphanitic matrix (Langlois, 1971). The primary composition of the rock likely was comprised of around 15% quartz, 25% feldspar, as much as 10% biotite and hornblendes set in a fine-grained groundmass. The original mineralogy of the intrusion is strongly masked by the extensive argillic alteration in the area of the pit as well as in drill core. Most of the prior work focused primarily on the Bullwhacker Sill, now believed to be the

western-most expression of the Graveyard Flats intrusive (See Plate 2). The sill is variably altered, but exhibits propylitic, argillic, and weak sericitic alteration in and around the Bullwhacker and T.L. mine dumps (Langlois, 1971). Much of Langlois' investigations were performed on samples from mine dumps, with the most argillized samples coming from drill holes. The observations in Langlois' study are consistent with the author's investigations of the Graveyard Flats intrusion. The Graveyard Flats intrusion is extensively argillized in almost all samples, with quartz, sericite, kaolinite, chlorite, pyrite, calcite and minor epidote as common alteration products. Locally, sericite/kaolinite replaces plagioclase phenocrysts completely and retains the original lath-like shape (Figure 12B). Also present are minor quantities of apatite and rutile. Sodium cobaltinitrite staining of billets of the Graveyard Flats reveals that over 80% of the rock is comprised of clays, with little to no visible K-feldspar alteration (Figure 12B & 12C). This has also been confirmed through petrographic examination. Textural differences within the intrusive suggest the possibility of multiple phases of intrusion (Dilles et al., 1996). Pendant-shaped propylitized zones within the larger intrusion appear to be texturally similar, yet have different alteration styles and different geochemistry (Figure 10). Alteration contacts are abrupt and distinct. It is possible that the pendant-shaped propylitic zones are remnants of the original propylitic alteration from the initial intrusive phase, and that the pervasive argillic alteration was a later effect of the Carlin-type hydrothermal system. Although speculative, this conclusion is supported by the lack of dramatic textural changes that would be observed in an intrusive contact.

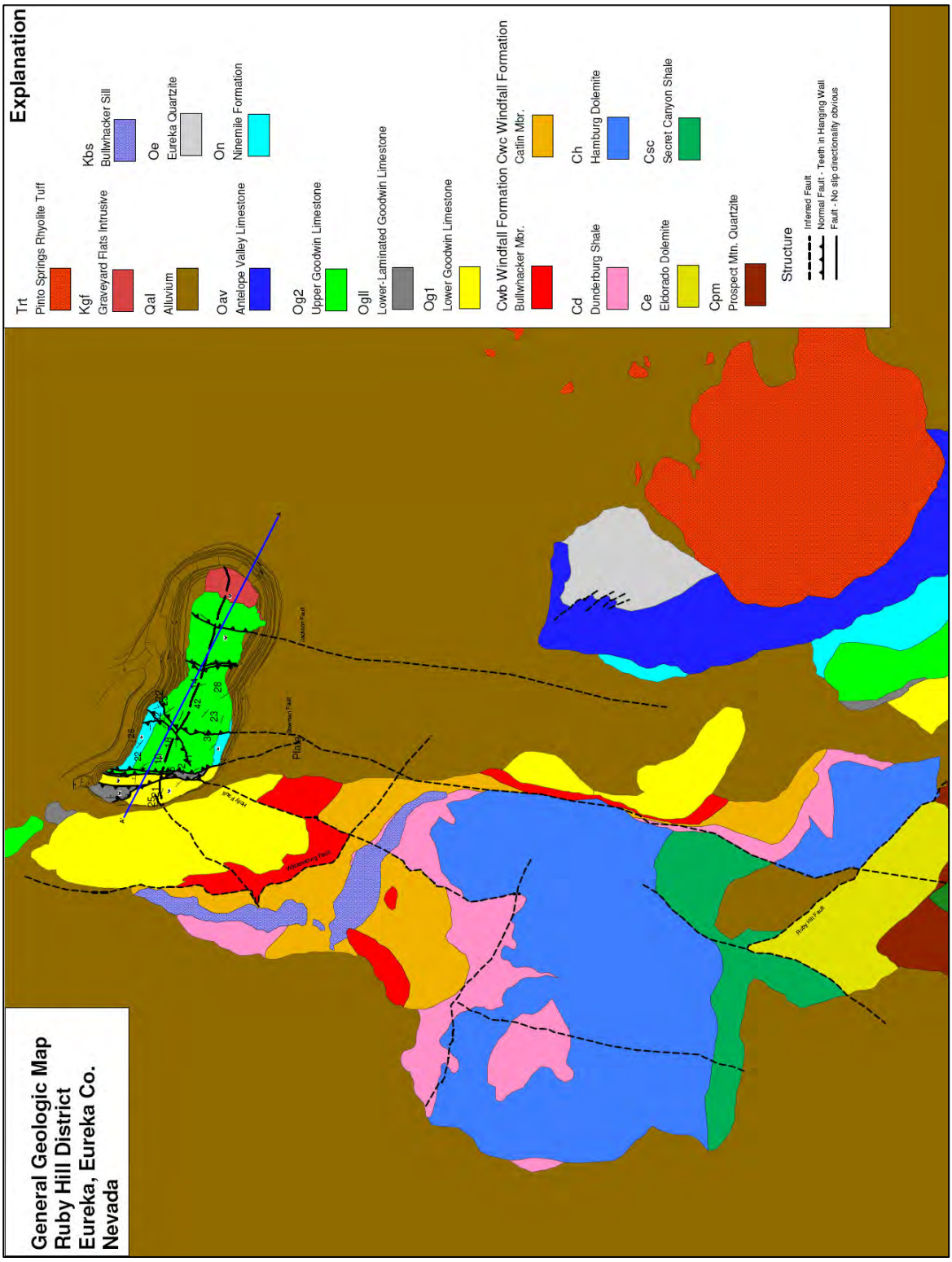

Figure 9. – Generalized geologic map of the northern Eureka District showing lithologic units, age dates of intrusive rocks, and pit geology for the Archimedes deposit. Mapping by Nolan, 1964; Russell & Chadwick, 2002; and the author, 2007..

Figure 10. - Sulfidic Graveyard Flats andesite porphyry shown with moderate propylitic alteration. Zones of this unoxidized material are dispersed throughout the predominantly oxidized intrusive. Coarse pyrite is common in these zones as well as chlorite ± calcite.

Differences between the mineralogy and geochemistry of these samples can potentially be explained by the intense alteration of the Graveyard Flats intrusive. Extensive argillic alteration of this rock has completely eliminated the Mg/Fe-rich phases such as pyroxene, biotite, and amphibole. In rare cases, the preservation of Mg/Fe minerals is only in the presence of iron-oxide minerals that retain the characteristic cleavage planes of the primary phenocrysts such as horblende (Figure 12F). The removal

of these elements, subsequent increase in Al due to volume loss, and the addition of Si are what shift the Graveyard Flats intrusive to the more Si-rich compositions (Figure 11). Dating of the Graveyard Flats intrusion has yielded a K/Ar date on sericite of about 110 ± 5 Ma, with the assumption being that alteration is only slightly younger than intrusion,

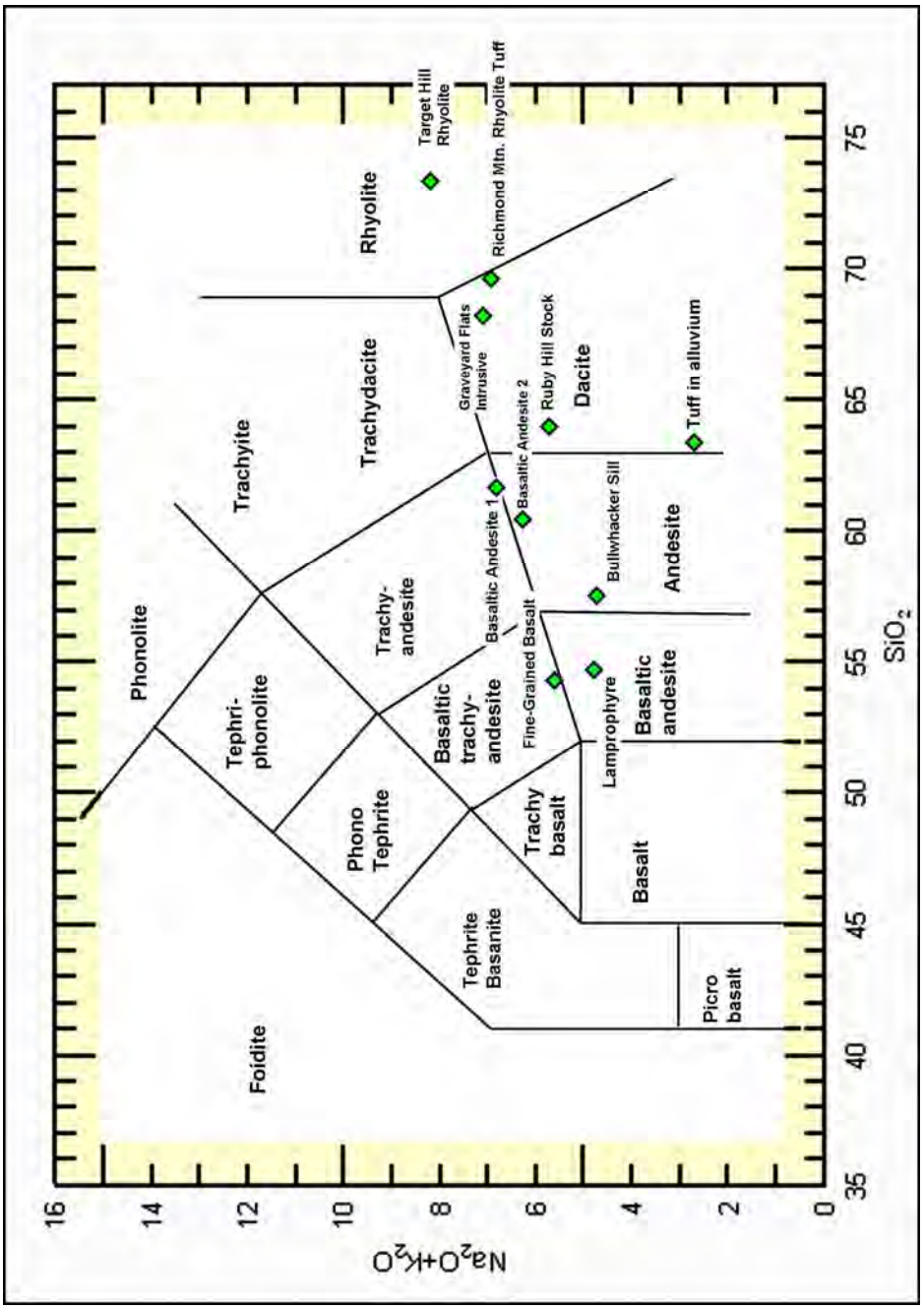

Figure 11. – Total alkali/silica diagram showing relative compositions of the igneous rocks of the Eureka District. Shifts in the compositions of these rocks from what is described in literature and this paper are probably due to hydrothermal alteration and the chemical gains/losses that accompany those processes.

and is not necessarily associated with gold mineralization (Margolis, 1996).

The aforementioned Bullwhacker Sill is described as an andesite porphyry with abundant quartz phenocrysts that is typically emplaced between the Windfall Fm. and Dunderburg Shale, probably along a pre-existing thrust fault (Langlois, 1971). Early descriptions of the Bullwhacker Sill referred to it as a quartz porphyry, primarily due to the absence of obvious mafic phenocrysts and local destruction of feldspars (Nolan, 1962). Primary igneous textures in the sill are difficult to observe in altered samples, but can be demonstrated to have likely been similar to those of the Graveyard Flats quartz monzonite. In less altered samples, remnant biotite and hornblende fragments are common and obvious. Alteration in the sill is dominantly argillic, with local silicification. Phenocrysts in the sill have been completely replaced by kaolinite ± sericite ± calcite. Locally kaolinite replaces adularia in the deepest and eastern parts of the sill. Kaolinite appears to be later than sericite in some of the samples that were analyzed. Quartz phenocrysts remain, but are overgrown by hydrothermal, growth-zoned, chalcedonic silica locally. Illite and sericite are also common within the most argillized portions of the sill and can constitute as much as 10% of the rock. Quartz phenocrysts as well as altered plagioclase phenocrysts are present in similar abundances and are much better preserved within the sill to the west. Sericite in the Bullwhacker Sill has been dated at 91.8±2.4 Ma, but it is possible that the sill was altered much later than that (Langlois, 1971). However, it is worth noting that the samples taken by Langlois were from surface samples that did not show the argillization that is characteristic of mineralized zones in and around the Ruby Deeps orebody.

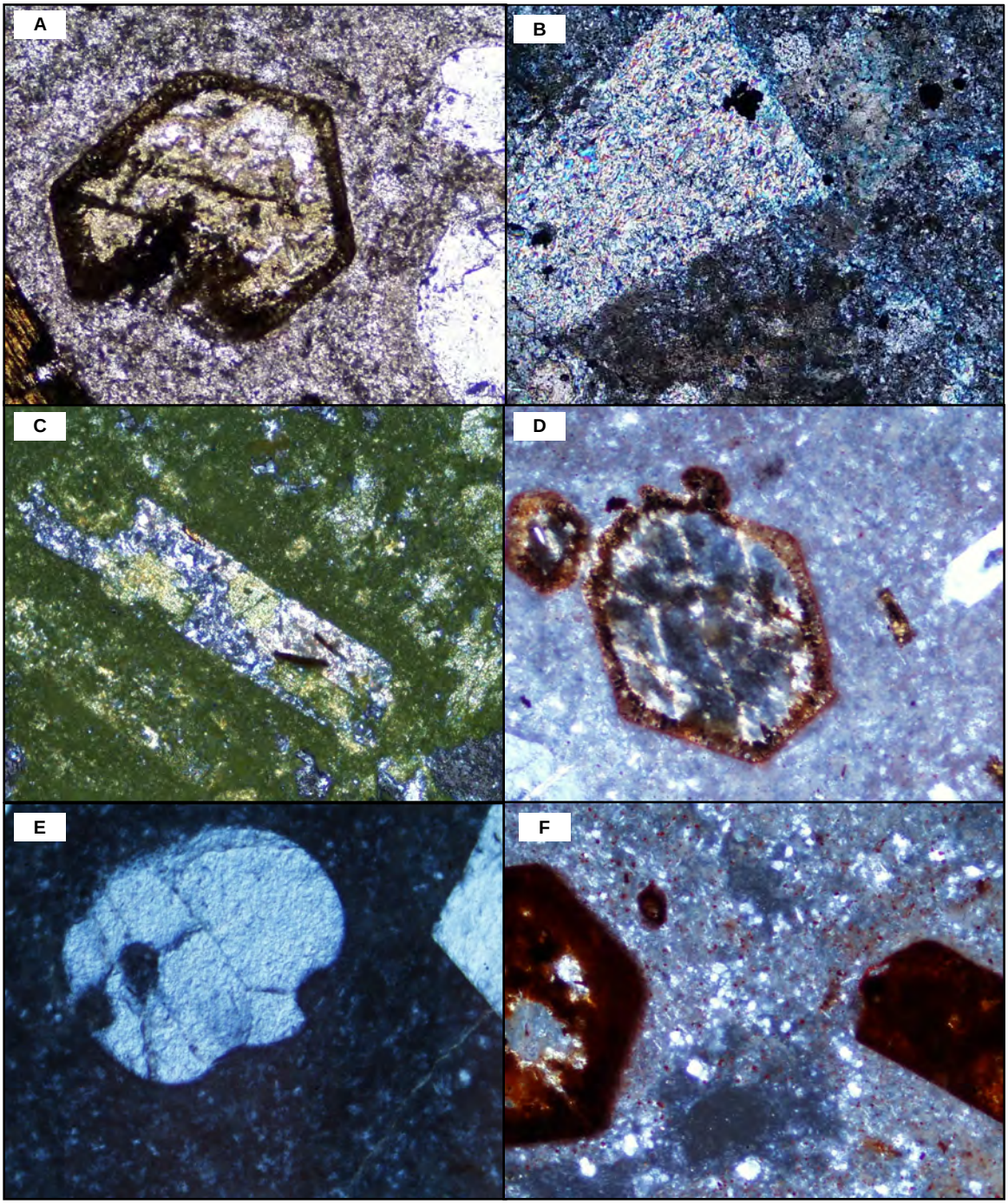

Figure 12. – Photomicrographs of the Graveyard Flats Intrusive. A. – Altered amphibole pheno in fine matrix with hornblende and qtz phenos in the lower left and right, respectively, 10X PP; B. – Argillized intrusive showing complete sericitization of feldspar phenocryst. Dark spots in this sample are pyrite with arsenian rims , 10X XP; C. – Argillized sample with complete replacement of feldspar lath by clay minerals, 20X XP; D. – Chloritized amphibole pheno, 10X XP; E. – Partially resorbed qtz phenocryst, 10x XP; F. - Iron-oxide stained amphibole and hornblende phenocrysts, probably after chloritization, 10X XP. FOV = (100x) 0.85 mm, (200x) 0.43 mm, (400x) 0.21mm

The Ruby Hill or “Mineral Hill” stock is a granodiorite that is exposed on Ruby Hill in two areas (Langlois, 1971). It is believed to be responsible for the carbonate replacement mineralization that defined the Ruby Hill Pb-Zn-Au ores (Nolan, 1962; Vikre, 1998). Compositionally different from the Graveyard Flats, the Ruby Hill Stock contains relatively fresh hornblende, sericitized plagioclase, and coarse biotite locally altered to chlorite (Dilles et al., 1996). Vikre dated the Ruby Hill Stock at approximately 106 Ma using $^{40}Ar/^{39}Ar$ on igneous biotites (1998). However, K/Ar dating of sericite yields an age of 95 ± 2.4 Ma, indicating that alteration took place soon after crystallization (Langlois, 1971). If alteration took place immediately after the intrusion of the Ruby Hill and Graveyard Flats intrusives, any sort of retrograde alteration associated with the Pb-Zn-Au mineralization would have to be Cretaceous in age. This issue is the source of much of the controversy regarding the mineralization at Archimedes.

The Target Hill Rhyolite Dome is a prominent feature in the landscape, and is an excellent example of the classic volcanic dome complex. It is a rhyolite, with quartz and sanidine phenocrysts commonly in an aphanitic groundmass (Dilles et al., 1996). It is presumed to be part of the Pinto Peak Rhyolite and is generally included as a sequence of flows, domes, and breccias (Blake et al., 1975). The dome has undergone little, if any, alteration, although the surrounding carbonates exhibit some decalcification, recrystallization, and silicification in the form of mottled purple/brown jasperiods. Flow banding is common. A glassy vitrophyre is exposed to the north and south of the hill, indicating the basal chill zone of the dome, although in some cases it appears to occur within the dome itself. A U-Pb date on the Target Hill rhyolite yields an age of roughly 38 ± 5 Ma (Blake et al., 1975). K/Ar dates of the Pinto Springs tuff and Richmond Mtn.

volcanics of the northern Eureka district clusters around 35 Ma (Blake et al., 1975). It is also noted that compositionally and texturally, the Target Hill Rhyolite Dome is very similar to the rhyolite tuffs that crop out in and around the Eureka Township and on the western side of Richmond Mountain. This tuff represents the northernmost expression of the Pinto Basin Tuff member of the Pinto Peak Rhyolite.

The Richmond Mountain volcanic rocks are a suite of extrusive rocks comprised of basaltic andesite with minor olivine. These rocks are predominantly flows, but also seem to occur as intrusive dikes to the north (Nolan, 1962). Texturally, they are coarse-grained porphyritic with well developed quartz-eyes as well as more aphanitic dikes with abundant pyroxenes and minor olivine (Hague, 1892). Olivine remnants were seen in thin sections only sparsely this study. Whole-rock geochemical analysis of these more mafic andesites plot in the basaltic andesite field on a total alkali-silica diagram (Figure 11). The Richmond Mtn. andesites have been dated at 34.3 ± 0.7 Ma by K/Ar methods, and represent the more mafic assemblage of bimodal volcanism taking place in the northern Eureka district at this time (Blake et al., 1975).

An andesitic crystal-lithic tuff exposed in the highwall of the E. Archimedes expansion was sampled in core initially and then in the pit at a later time when exposure was sufficient. This tuff occurs unconformably overlies the Graveyard Flats intrusion and is locally found interbedded within the alluvium. The tuff appears to have been reworked where found in the alluvium and contains abundant rounded lithic fragments and is poorly welded. It appears to be slightly more welded where it overlies the intrusion and contains phenocrysts of quartz, plagioclase, sanidine, and local biotite. Biotites are fresh whereas phenocrysts of plagioclase have locally been altered to kaolinite. This is likely a

weathering feature. This tuff was used as a control for the apatite fission track data that was performed. It is assumed that these tuffs have not experienced hydrothermal alteration and as such the apatites should essentially reflect an original thermal history starting with cooling from eruption. The composition and textures in this tuff are very similar to those found in the tuffs to the south exposed in and around the Rustler pit. These tuffs have been called the extrusive phases of rhyodacitic dikes and are described to be variably weathered and not geochemically anomalous (Wilson, 1986). The dikes themselves are locally argillically altered with destruction of biotite and conversion of plagioclase to sericite/kaolinite. Within the Rustler pit, the dikes are altered with variable intensity and are dominantly fresh. Local iron-oxide stained zones in the rhyodacites are attributed to weathering of biotites and hornblendes (Wilson, 1986). The rhyodacites have been dated at approximately 36 Ma (McKee et al., 1971). The dates obtained from apatite fission track dating concur roughly with this date and provide evidence that these tuffs at Archimedes could be correlative with those from the Windfall-Rustler areas.

Due to the extensive alteration of a number of the whole-rock samples, rare earth element (REE) profiles for each sample are used to differentiate between phases of magmatism due to their relative immobility (Scambelluri et al., 2001). Chondrite normalized REE plots are available in Figure 13 (Nakamura, 1974). While most of

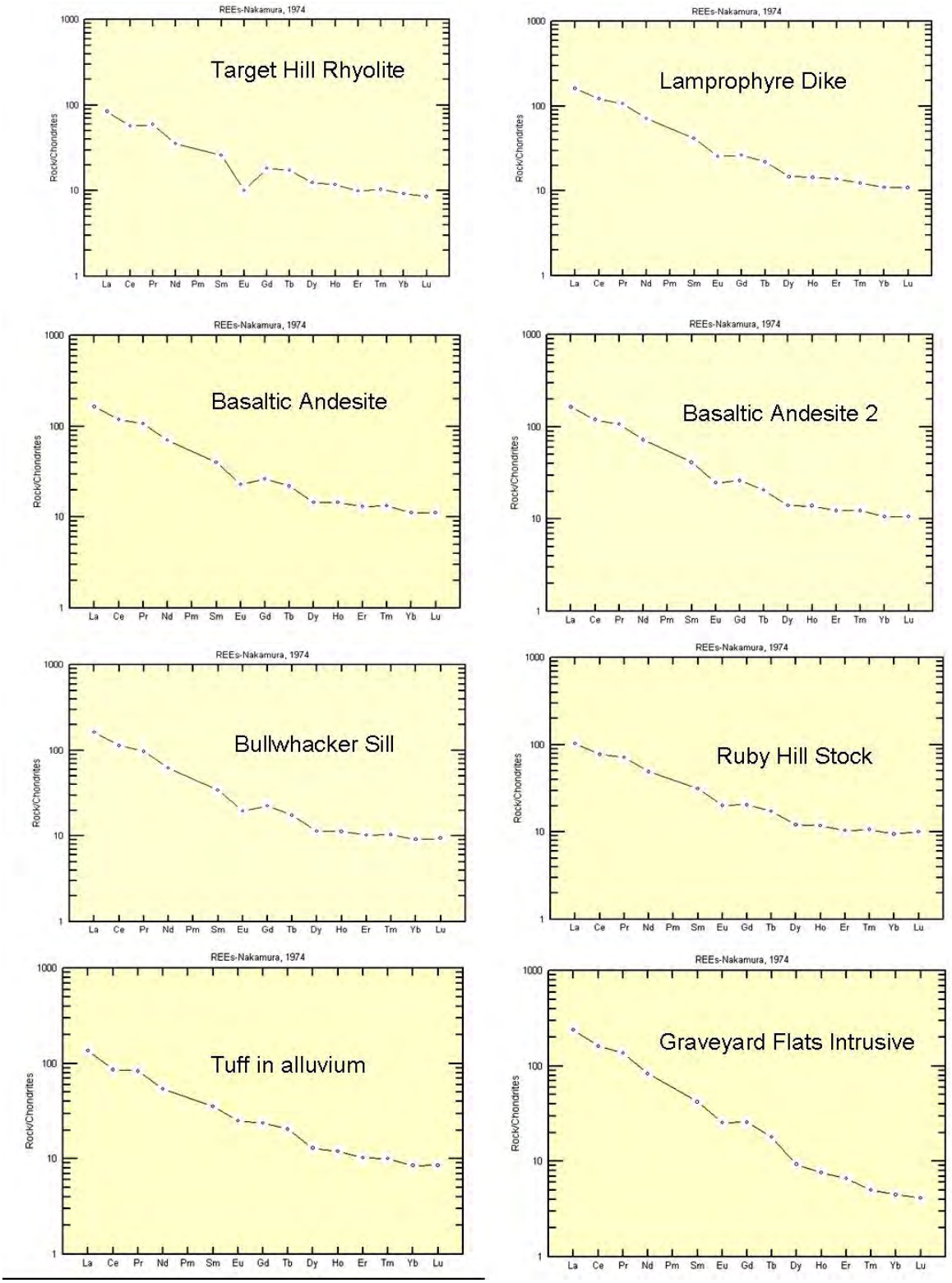

Figure 13. – Chondrite-normalized plots of REE compositions for igneous rocks of the Eureka district.

the samples appear to have relatively similar REE patterns, there are some notable differences. The Target Hill rhyolites as well as the rhyolite tuffs show a common Eu depletion that is significantly more pronounced than other rocks in the district. The negative Eu anomaly is generally related to the crystallization of plagioclase feldspar and is typical for more evolved magmas (Weill & Drake, 1973). Petrography supports this conclusion and identifies much higher plagioclase content in the rhyolites relative to other rocks in the district. As seen in Figure 11, the rhyolite tuff that crops out around the town of Eureka is of a slightly different major-element composition than that of the Target Hill Rhyolite, whereas REE plots show an almost identical composition (Figure 13).

The Graveyard Flats andesite porphyry also shows a depletion in the heavy REEs relative to the Bullwhacker Sill. While this would seem to negate the hypothesis that these rocks are genetically contemporaneous, there is perhaps a different explanation. The sample of Graveyard Flats that was analyzed for whole-rock geochemistry came from the developing East Archimedes pit in a zone that was returning poor cyanide leach assays relative to the fire assays. As the pit developed, it became apparent that there were different alteration styles present within the intrusive itself. While the bulk of the Graveyard Flats appears to be argillically altered with very little sulfide content, there are isolated pods of propylitized rock with abundant sulfide present. It has been noted that the Graveyard Flats andesite porphyry was likely a multiple-stage intrusion, and the author hypothesizes that these pendant-shaped propylitic zones are perhaps a later stage of the Graveyard Flats intrusion. Thus, the Graveyard Flats sample taken from this

sulfide-rich zone in the pit was likely from one of these pendants, and might record the geochemical signature of a later pulse of geochemically distinct magmatism.

Structure

The Archimedes gold deposit was formed in the structurally complex Eureka District, at the toe of the Roberts Mountains Allocthon. Much of the structural complexity in the northern Eureka District is derived from the deformational events described earlier in the geologic history section. A detailed geologic map of the pit area can be found in Plate 1. A district-scale simplified geologic map is in Figure 9. The district wide deformation is mainly due to pre-Cretaceous events that folded, overturned, and displaced the Cambrian section along a series of thrust faults (Nolan, 1962). In the pit area, bedding dips moderately to steeply to the NE, as much as 60^{o} locally. Moving further north and east, bedding flattens out to between 10 and 20 degrees NE. The hinge axis of this fold likely runs to the E and plunges in that direction. To the south, the Cambrian section is exposed on Prospect Mountain and is much more complex. Bedding is locally

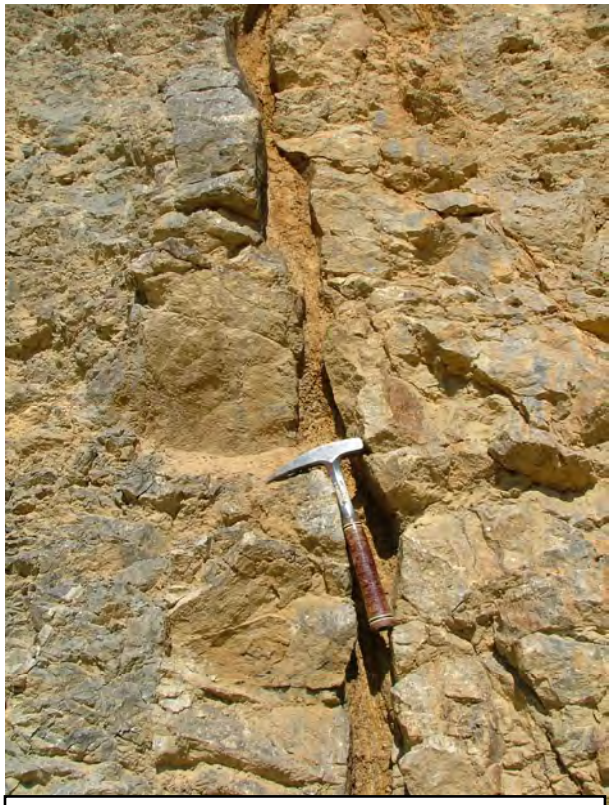

Figure 14. – 426 fault in SW wall of West Archimedes pit. Blue-green recrystallized carbonate suggests this structure was a fluid-flow path.

overturned and sectioned by a number of thrust faults that are likely all part of the larger Hoosac thrust fault. The Hoosac thrust displaces Paleozoic rocks which are believe to have been folded just prior to the Cretaceous (Nolan, 1972). The hanging wall of the Hoosac thrust contains Archimedes as well as most of the other known ore deposits in the district. Based on the fact that this mineralization is channeled along Hoosac-related thrust faults and the age of intrusives are well known, the thrusts in the area likely occurred prior to their emplacement. This hanging wall is in turn sectioned by multiple thrusting events such as the Dugout, Diamond Tunnel, and Champion thrust faults (Vikre, 1998).

The Cretaceous volcanism responsible for the Graveyard Flats intrusive and Ruby Hill stock further deformed the Paleozoic rocks, with later Basin-and-Range normal faulting breaking the district into an alternating series of horsts and grabens (Vikre, 1998). This type of faulting is best represented by the Bowman fault and its splays to the north. The Holly and 150 faults are high angle normal faults dipping to the east, and have excellent exposure in the western part of the pit. This fault system in particular becomes very important when looking at cross-cutting relationships regarding ore-deposition and age of faulting. Notably, the 150 fault has been demonstrated by drilling to offset the Bullwhacker Sill down to the east as much as 150 meters (Barrick Gold Corp., Unpublished Drill Data). Also, the 150-Holly system is host to decalcified/locally jasperoidal ore-grade rock concentrated in and around the structures. This key relationship will be revisited in later discussion. To the east, there are more normal faults that play a significant role in the development of Archimedes. The 194 and 426 faults appear to be relatively low angle normal faults, but dip in opposite directions, east and

west respectively. The 426 is well expressed in the southwest wall of the Archimedes pit (Figure 14). The Armpit fault is a splay of the 194 fault and is best expressed in the northeastern wall of the pit (Figure 15). At depth, there is evidence that the 194 is older than the 426 and is displaced down to the east of the 426.

The detailed cross section A-A' (Plate 2) has been drawn on a NW trending strike line that roughly follows the plane of the Blanchard fault. It displays the down-dropped block that hosts Archimedes, as well as the Bullwhacker Sill at depth. The section was generated from surface observations within the pit as well as drillhole information to assist with interpretation at depth. Literally hundreds of holes were used in 3D modeling software to step through sections and assist with geologic interpretation. Due to the lack of closely spaced holes at depth, some contacts have been inferred. Within the area of the Archimedes system, the host rocks of the Pogonip group strike roughly northwest and dip to the northeast between 15^{o} and 35^{o} Gold-bearing fluid pathways have been both channeled and displaced by faulting in the area, indicating both pre- and post-mineral

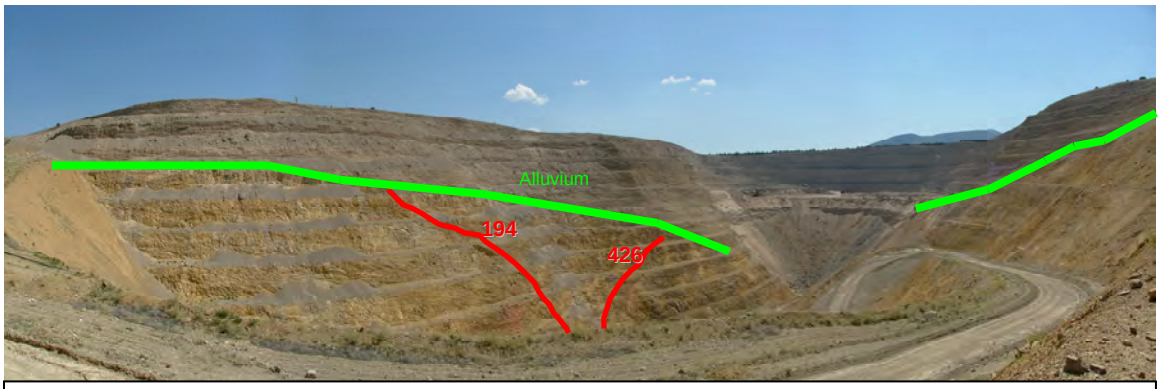

Figure 15. - View of the developing East Archimedes pit from the 6220 bench of the West Archimedes pit. Structure has been superimposed.

deformation (Russell, 1996). The West Archimedes deposit lies in a downthrown block of the Pogonip section, between the north-trending high-angle Holly fault system and the East Archimedes fault (Plate 2).

The oldest structures in the area are thought to be the high-angle N-NE trending faults that are best expressed at the district scale by the Jackson and Bowman faults (Nolan, 1962). These structures run roughly N-NE and exhibit significant displacement both vertically as well as laterally. Although little information exists regarding slip-indicators on the Bowman, detailed pit-mapping shows it to have a significant right-lateral component of movement, with displacement of some units over a kilometer to the south (Russel & Chadwick, 2002). The primary fault associated with gold mineralization is the Blanchard fault. The Blanchard is a W-NW trending, steeply north-dipping normal fault. It exhibits down-to-the-north offsets with as much as 300 ft of post-mineral offset. The surface traces of some of these faults are difficult to delineate, even with excellent the exposure found in the Archimedes pit. Mineralization in East Archimedes was likely also related to the intersections of these fault systems, and retains a wider profile (Dilles et al., 1996). Other high-angle normal faults to the east appear to have localized and concentrated later ore-fluids that were probably responsible for the Archimedes system. Examples of this can be seen in West Archimedes, where the orebody widens and branches out along the more N-NE trending high angle faults intersecting with the Blanchard (Russell, 1996). As the East Archimedes pit develops, the nature of the faults to the east will become more apparent, but are currently not well understood. Assisting in the interpretation of the complex structure is the fact that the Bullwhacker Sill is offset by most of the faults in the pit. The sill is a unit that can be confidently identified in logging, and thus can be trusted more than the erratically logged contacts in the carbonate rocks. Deep drilling that intersects the sill has been very helpful in identifying faults at depth even before they are exposed at the current level in the pit (Plate 2).

One of the earliest identified faults in the Archimedes system was the 271 fault, now referred to as the East Archimedes fault. The East Archimedes fault is a high angle, east-dipping fault that intersects the Blanchard fault in the pit. The intersection of these two mineralized faults is believed to have been one reason for the location and shape of the East Archimedes orebody (Dilles et al., 1996). The inferred trace of the East Archimedes fault can be seen in the long section (Plate 2). The Graveyard Flats fault is another high-angle down-to-the-east N-NE trending fault within the pit. This structure appears to have down-dropped the East Archimedes orebody, and exhibits over 200 ft of offset. This fault is later than others, and appears to cut mineralization. West Archimedes has probably experienced a significant amount of erosion, as the top of the system is no longer present. Mineralized clasts are found in the overlying alluvium, indicating that erosion did take place after mineralization. This also prevents any idea as to the original shape or extent of the Archimedes system. Faults in the Archimedes pit are not known to be associated with elevated base-metal values or calc-silicate alteration, indicating that they were not sources for high-temperature fluids during skarning.

Another fault that likely played a role in the development of the Archimedes system is the Jackson fault. It is the easternmost in a series of high-displacement, high-angle, normal faults that define the mineralized Paleozoic section in the Eureka District. Total displacement on this fault is estimated to be as much as 5,000 ft, and the fault is believed to be pre-mineral. This is despite the theory that most of the relatively large normal faults are related to Tertiary basin-and-range tectonics (Vikre, 1998). Although not well understood, it is believed that the Graveyard Flats intrusion likely came up along

a pre-existing weakness in the crust, the surface expression of which might be the Jackson fault.

Mineralization and Alteration

At the heart of the controversy surrounding the mineralization at Archimedes lies the fact that there are several distinct styles of mineralization and alteration within the deposit. Detailed petrographic analysis as well as SEM work has been instrumental in defining paragenetic relationships of sulfides and alteration overprinting. The distribution of the three mineralized zones discussed in this study is generally described in Figure 16. The important observation is that the gold deposits in the Archimedes system are present as three morphologically distinct types that include: oxidized jasperoid-hosted gold mineralization, base-metal skarn-hosted gold mineralization, and sulfide-rich reduced Carlin-type mineralization. It is important to remember that most of what is known about deep East Archimedes is from a very few drill holes. As a result, this gives us little evidence for lateral changes or zonations in alteration at depth, important in classification for both Carlin-type and Au-skarn deposits. Hence, the division of the types of mineralization is based on observation of three isolated assemblages that are very different from each other, yet might encompass a wide range of textures and mineralogy.

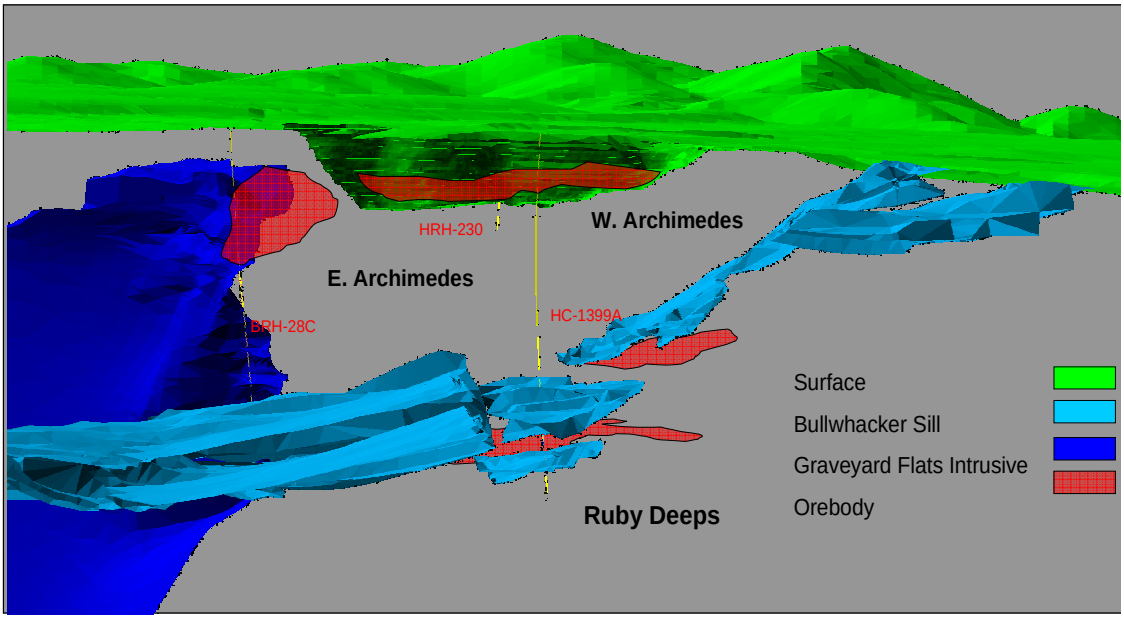

Figure 16. – Schematic 3D cross section of the Archimedes area showing the relationships of the intrusive rocks to the morphologically distinct Au-mineralized zones in the vicinity of the pit. Looking southwest.

Jasperoid-hosted Gold Mineralization

First is the oxidized Carlin-type disseminated gold, referred to as Type A by Margolis (1997). This style of gold mineralization occurs as both jasperoid and variably decalcified breccias in the higher levels of the system (Figure 17). The West Archimedes orebody was roughly cigar-shaped with bulges along fault intersections, indicating that these structures were instrumental in focusing the mineralizing fluids. The entirety of the West Archimedes orebody was hosted in the decalcified and silicified Goodwin Limestone, specifically the upper Og2 sub-unit. Gold is found to be strongly proportional to degree of silicification. East Archimedes is more lobate in two dimensions, and extends to greater depths than did West Archimedes. Additionally, a large percentage of the East Archimedes orebody is found in this type of mineralization. Local pod-like

bodies at depth in this zone are less oxidized, and contain auriferous arsenian pyrite and marcasite (Figure 18E). Gold generally occurs as sub-micron sized grains on the margins of oxidized pyrite as well as fractures within the jasperoid. Grains as large as 1.5 µm in diameter have been seen in the West Archimedes jasperoid (Dilles et al. 1996). Visible

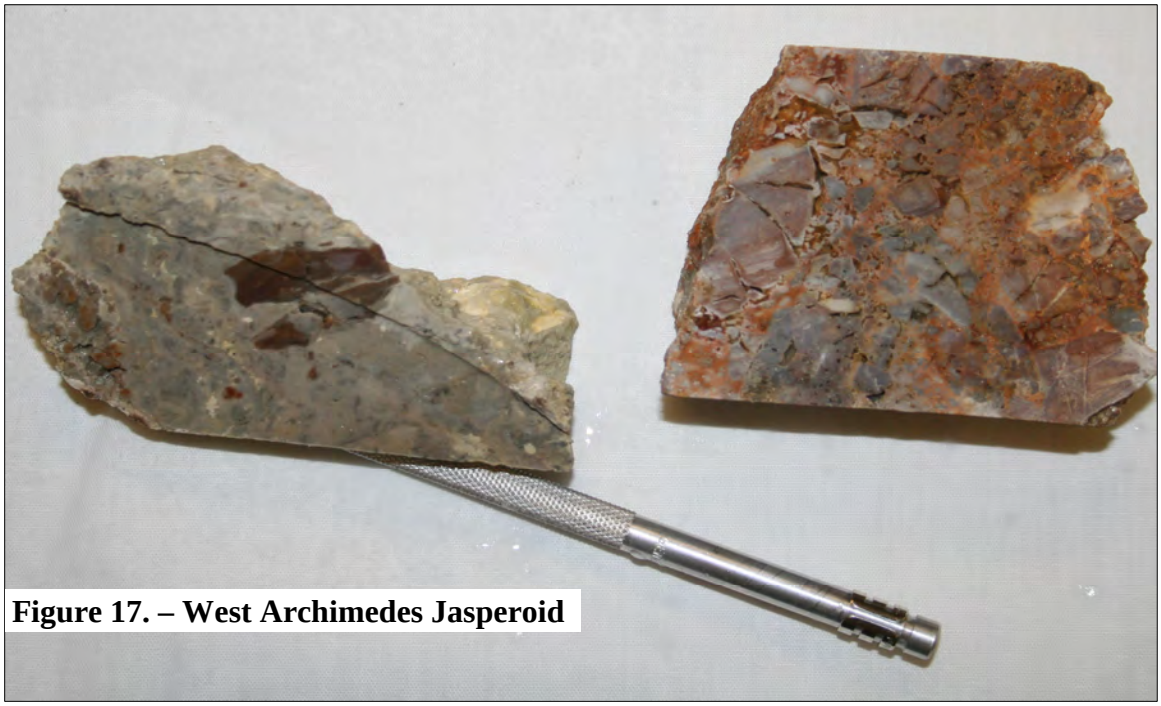

Figure 17. – West Archimedes Jasperoid

gold in East Archimedes has not been detected.

Silicification is present as jasperoid, with replacement style quartz occurring, making up 10-95% volume of the rock, as fine-grained anhedral intergrown grains. Alteration in this zone is restricted to brownish/white jasperoid breccias with a rind of decalcified, argillaceous limestone (Margolis, 1997). Silicification is restricted primarily to the core of the orebodies, but locally extends along high-angle faults. Locally, quartz can also be seen to develop as chalcedonic overgrowths on replaced limestone fragments as well as coarse comb quartz in vugs. The vuggy texture of the jasperoids likely is due to early decarbonatization in the ore zones. In the East Archimedes jasperoid, Fe-sulfates

are common (dominantly jarosite), typically as pseudomorphs after pyrite (Figure 19). Remnant arsenopyrite inclusions are found in many of these sulfates, and locally coalesce on the outer margins of the sulfates. Breccias are extensively oxidized to depths in excess of 1000 ft. Clasts of lower strata can be found locally within the jasperoid and the base-metal sulfide and calc-silicate skarn (Margolis, 1997). Cinnabar is widespread in the jasperoid, occurring in small concentrations and grains up to 10 µm in diameter. Unusual copper minerals are common in the jasperoids, usually in the form of native copper along with varying abundances of tin and cobalt. These minerals appear yellowish in polished section, and were originally mistaken for native gold. SEM analysis proved them to be native metals with little, if any, other elements (Figure 20). Barite is fairly common in the moderately silicified zones, and is commonly associated with the highest grade intervals. Iron oxides are generally limonitic with abundant hematite pseudomorphs after pyrite (Figures 18A, 18B, & 18C). In many cases, the limestones have been decalcified to the point of pronounced volume loss. Locally, this volume loss has resulted in compaction and sanding due to accumulation of sedimentary quartz as carbonate was removed (Figure 7C).

The intensely silicified orebodies in Archimedes are surrounded by an argillic “carapace” of friable variably decalcified limestone (Plate 3). These more argillaceous zones are comprised of a mix of silica, kaolinite, illite, iron-oxides, and calcite (Dilles et al., 1996). Lower-grade ore is associated with this decalcified rind, a

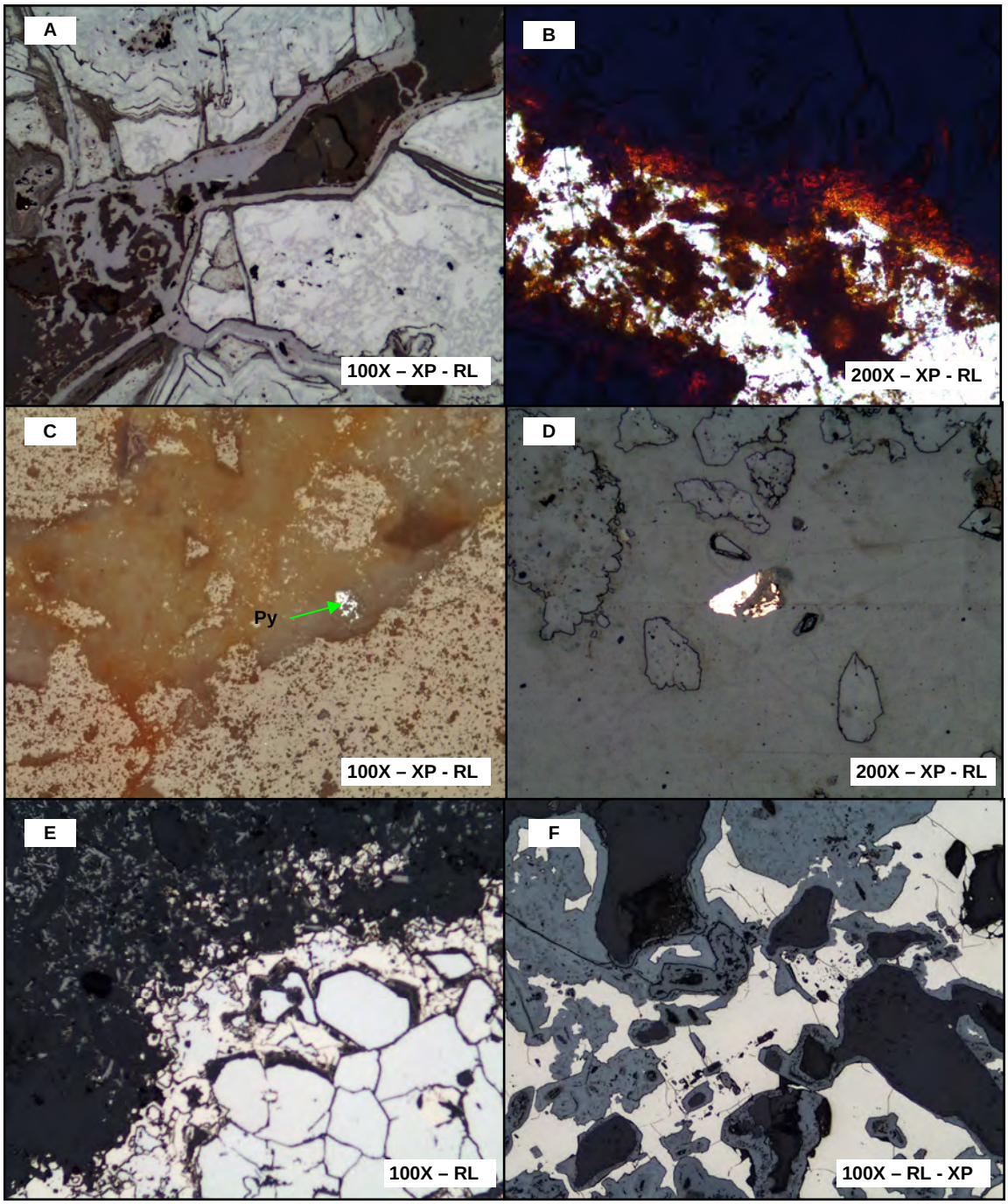

Figure 18. – Photomicrographs from the oxidized East Archimedes zone; A. – hematite after pyrite showing zonation of oxidation; B. – Hematite/jarosite staining in jasperoids; C. – Jasperoid breccia with abundant hematite and local remnant sulfide; D. – Unusual copper – cobalt – tin mineral in jasperoid breccia; E. – At the base of the oxidized zone, arsenian marcasite/pyrite on well preserved arsenopyrite; F. – Hematite after pyrite in partially oxidized ore zone. FOV = (100x) 0.85 mm, (200x) 0.43 mm, (400x) 0.21mm

typical feature in most, if not all, Carlin-type systems. In the area of the pit, friable decalcified rock is moderately to intensely limonitic with locally fresh limestone horizons. These relict limestone “eyelets” are preserved along bedding (Dilles et al., 1996). Late calcite/siderite veinlets and vein breccias in structural zones are common. Dark-brown carbonate-cemented crackle breccias have been observed even in weakly decalcified rock and are comprised of coarsely crystalline calcite and siderite. They appear to have a diagenetic origin due to cross-cutting relationships with jasperoid and chalcedonic quartz veinlets. Local quartz veinlets occur as fracture fill and as chalcedonic druse on fractures both in the jasperoid as well as the decalcified areas. Argillic zones below the main orebodies are barren and occur mainly in the Og2 up to 260ft from the main orebodies (Dilles et al., 1996). Argillization is most pervasive and intense in units with higher percentages of shaly or silty partings such as the Ogll. There are intensely argillized zones within the pit that are dominantly kaolinite-illite assemblages with minor hematite-jarosite staining (Plate 3). These present an almost-total replacement of the original host-rock by clays and occur locally in the Ogll as well as the lowermost Ninemile.

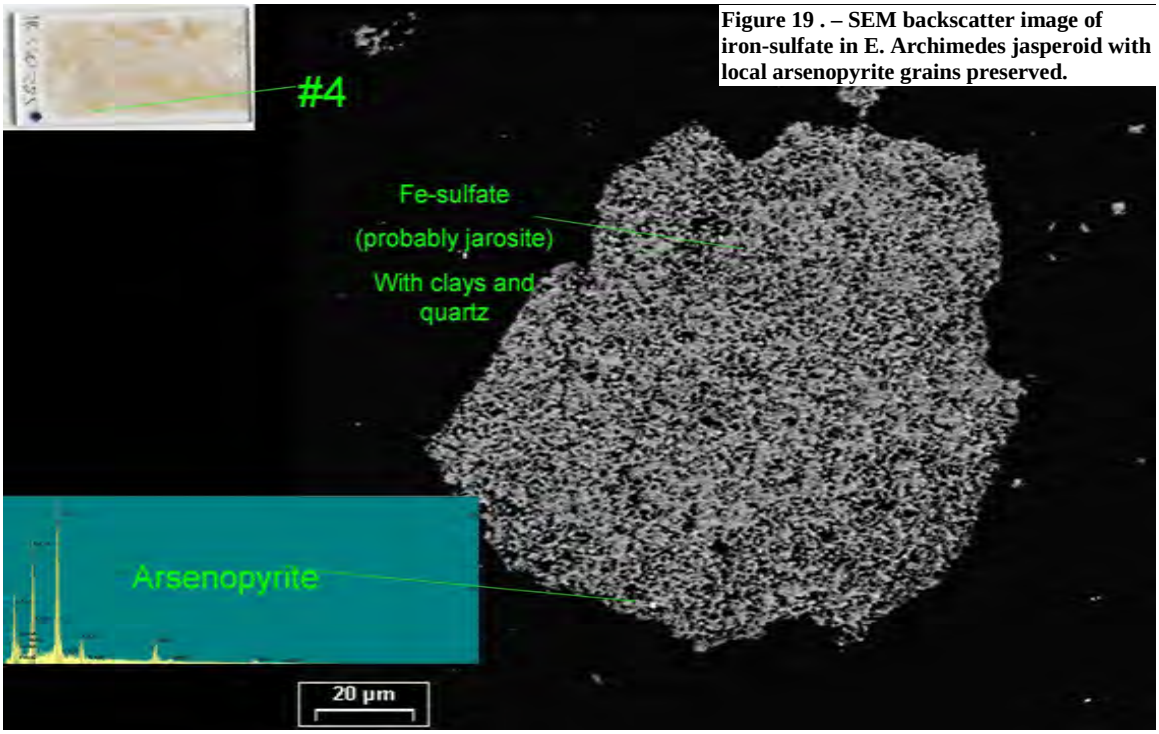

Figure 19 . – SEM backscatter image of iron-sulfate in E. Archimedes jasperoid with local arsenopyrite grains preserved.

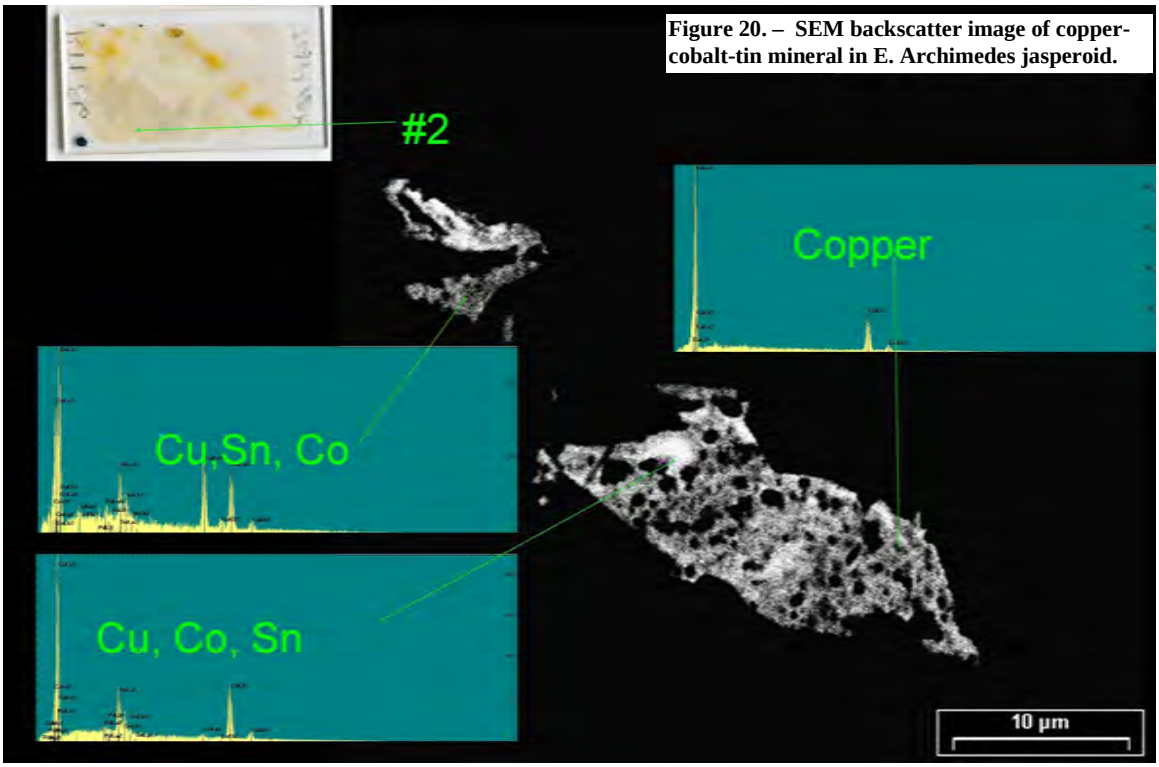

Figure 20. – SEM backscatter image of copper-cobalt-tin mineral in E. Archimedes jasperoid.

Base-Metal Skarn

The second type of mineralization is the skarn-hosted, base metal sulfide-rich horizons (Figure 21). The top sample in Figure 21 is from core in the skarn zone of deep East Archimedes. The pale-green massive garnet occurs in the Cambrian Windfall Fm. beneath the western lip of the intrusive (Plate 2). It can be considered a calcic skarn due

Figure 21. - East Archimedes Skarn

to the weak/trace presence of pyroxene or other Mg-rich minerals in the assemblages. Although base-metal sulfide mineralization persists into the lower Goodwin, the prograde skarn appears to have been concentrated in or around carbonate units that have the most exposure to heat and fluids from the intrusive. This refers to the lips and protrusions of the Graveyard Flats at depth and the fact that the most intense garnet skarn is developed there. The prograde skarn alteration assemblage is comprised of grandite garnet (Ad39-

99) ± wollastonite ±minor scapolite ± minor pyroxene. Grandite is by far the most abundant calc-silicate mineral in the alteration assemblage. The garnets are typically weakly birefringent, 0.5-2mm, relatively euhedral, and show oscillatory zoning (Figures 22A & 22B) (Margolis, 1998). Garnets locally have jagged pyrite cores, indicating that they preferentially grew on pre-existing pyrite grains in the carbonate host rocks. Quartz fragments are also commonly found in the cores of garnet grains. Wollastonite is a common alteration product in the more distal parts of the calc-silicate alteration, but is locally replaced by carbonate. Euhedral prismatic apatite occurs within wollastonite/carbonate as well as garnets. No pyroxene-dominant zone has been identified in this or any other study. Samples from the prograde are typically quartz-poor but locally retrograde-altered samples have cryptocrystalline quartz developed as a late fracture-fill. Margolis mentions that quartz is more common in zones with sphalerite and galena, which was found to be consistent after petrographic work on the prograde skarn. However, there were no skarn samples analyzed in which sphalerite and galena were absent. Massive garnet skarn has lower concentrations of sphalerite and galena but has a wide range of the other types of sulfides present. These will be discussed later as they are generally found to be paragenetically later than the garnets and probably are contemporaneous with the retrograde skarn. This is consistent with other base-metal skarns where sulfides generally occur during the later waning phases of metasomatism where temperatures are low (Kim, 2007). In thin section, weak overprinting is common and may reflect either retrograde skarn alteration, distal Carlin-type alteration, or some combination of the two.

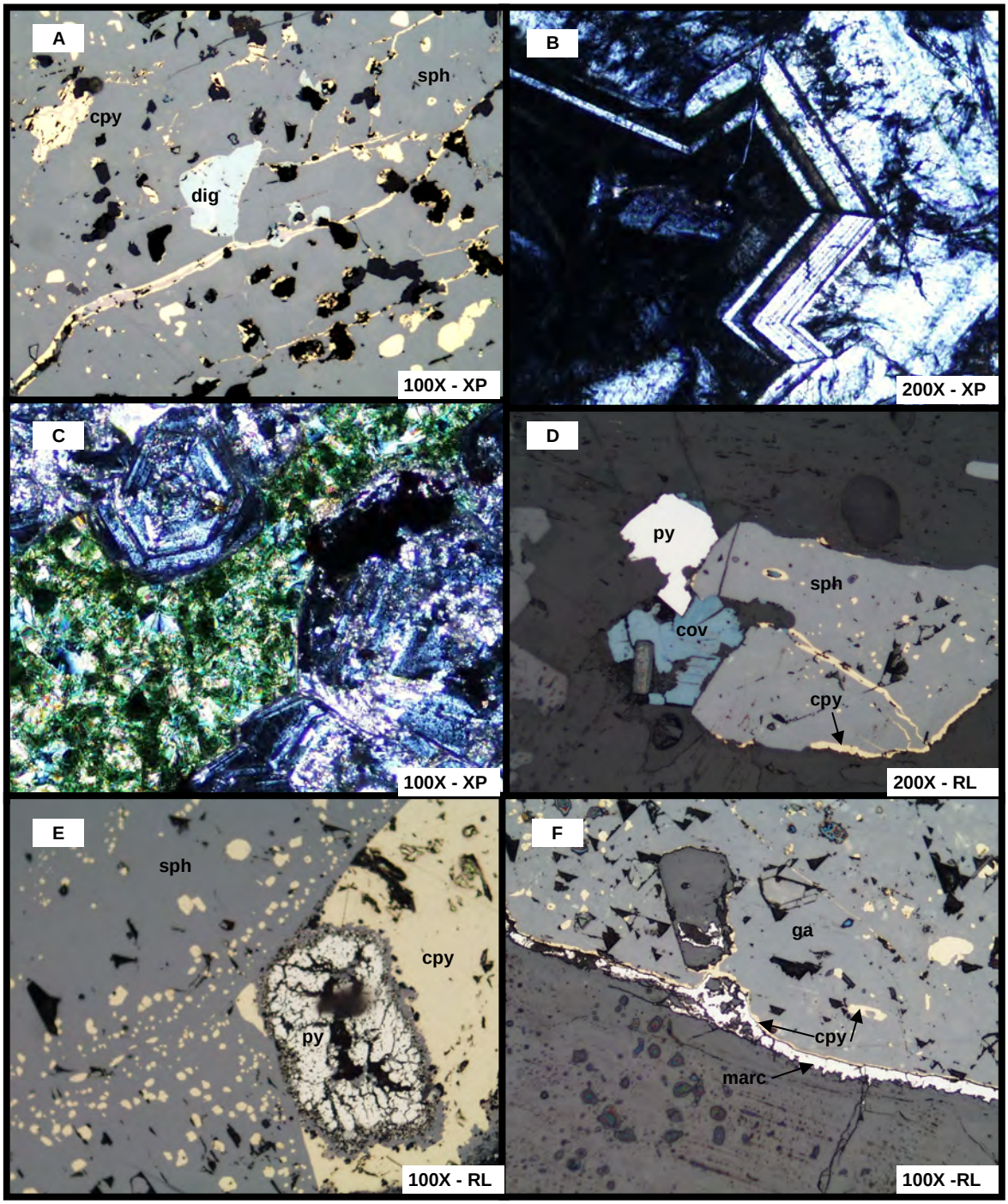

Figure 22. – Photomicrographs from the preserved skarn zone in the Archimedes system; A. – Early digenite enclosed by sphalerite with chalcopyrite "disease"; B. – Banding in andradite garnets caused by varying compositions within the garnets; C. – Stilpnomelane interstitial to andraditic garnets; D. – Covellite with pyrite, sphalerite and chalcopyrite; E. – "Shattered" pyrite grain overgrown by sphalerite and subsequently by chalcopyrite; F. – Sphalerite with chalcopyrite "disease" with rim of marcasite (non-arsenian). FOV = (100x) 0.85 mm, (200x) 0.43 mm, (400x) 0.21mm

Retrograde alteration in the calc-silicate zone is commonly reflected by a chlorite ± calcite ± adularia ± pyrite ± stilpnomelane assemblage. Stilpnomelane is well-developed within the massive garnet skarn, likely as a product of retrograde alteration of the garnets (Figure 22C). In the more obviously retrograde zones, sulfides are more prevalent. These include sphalerite, galena, chalcopyrite, pyrite, marcasite, digenite, covellite, and tennantite/tetrahedrite (Figure 22A & 22D). It has been suggested that Cu minerals are supergene. In the geochemistry of the system, Cu is present in locally high concentrations up to 2000 ppm and is associated with the base-metal horizons also high in Bi, Pb, and Te (Margolis, 1997). This indicates that these minerals are probably a result of the skarn rather than supergene processes. It is from the copper-rich sulfides that native copper found in the Archimedes jasperoids are believed to have originated. While speculative, it is entirely possible that the reduced Carlin-type fluids mobilized the copper sulfide minerals and re-deposited them at higher levels in more oxidized conditions. Pyrite is ubiquitous throughout, and occurs as both an early and late phase. Earlier pyrite typically has a broken, rounded texture that would indicate some later hydrothermal event (Figure 22E). More distal retrograde skarn alteration consists of marbleized limestone with sparse base metal sulfides as well as pyrite.

Carlin-style Overprint Mineralization

It is clear from the garnet overgrowths and sulfide paragenesis that much of the iron sulfides were pre- or syn-skarn, but petrographic analysis has determined at least one other pyrite event that is likely much later. In the skarn zones there are locally cross-

cutting zones of kaolinite, dark-grey/black carbonaceous material, and sooty pyrite. It is herein referred to as the lower overprinted skarn, and is seen in hand sample in the lower image of Figure 21. This event includes precipitation of pyrite/marcasite as rims and disseminated grains around base metal sulfides as well as in the more carbonaceous sediments (Figure 22F). Some of these pyrite/marcasite rims are arsenian based on electron-dispersive spectra analysis (EDS). Locally, barite is common along with silicification and decarbonatization in the marbleized zone. Silicification is generally weak where skarn mineralization is well preserved, throughout the range of alteration haloes. Chemically, the skarn is characteristically enriched in Zn, Pb, Ag, Cd, Mn, Cu, As, Sb, Bi, W, Te, Se, and Sn. These elements are all commonly enriched in skarns and are not common, with the exception of As and Sb, in Carlin systems. It is worth noting that the Bi values increase with increasing depth into the most sulfidized portions of the skarn. Although Margolis (1997) mentions that rare grains of hedleyite were detected by microprobe, none were detected using SEM or X-ray diffraction techniques within the skarn suite during this study. Hedleyite is a bismuth-telluride mineral that has been found in many world-class gold-skarns throughout the world and is typically referred to when describing the characteristics of these deposits. While Bi is elevated in the deep East Archimedes gold mineralization, the bismuthinite ± hedleyite ± native bismuth found in other gold skarns is not present. The deposit as a whole can be considered enriched in these elements relative to other traditional Carlin-type deposits. Despite some geochemical characteristics that indicate Archimedes to be a skarn, more powerful evidence indicates that it is, in fact, a Carlin-type system.

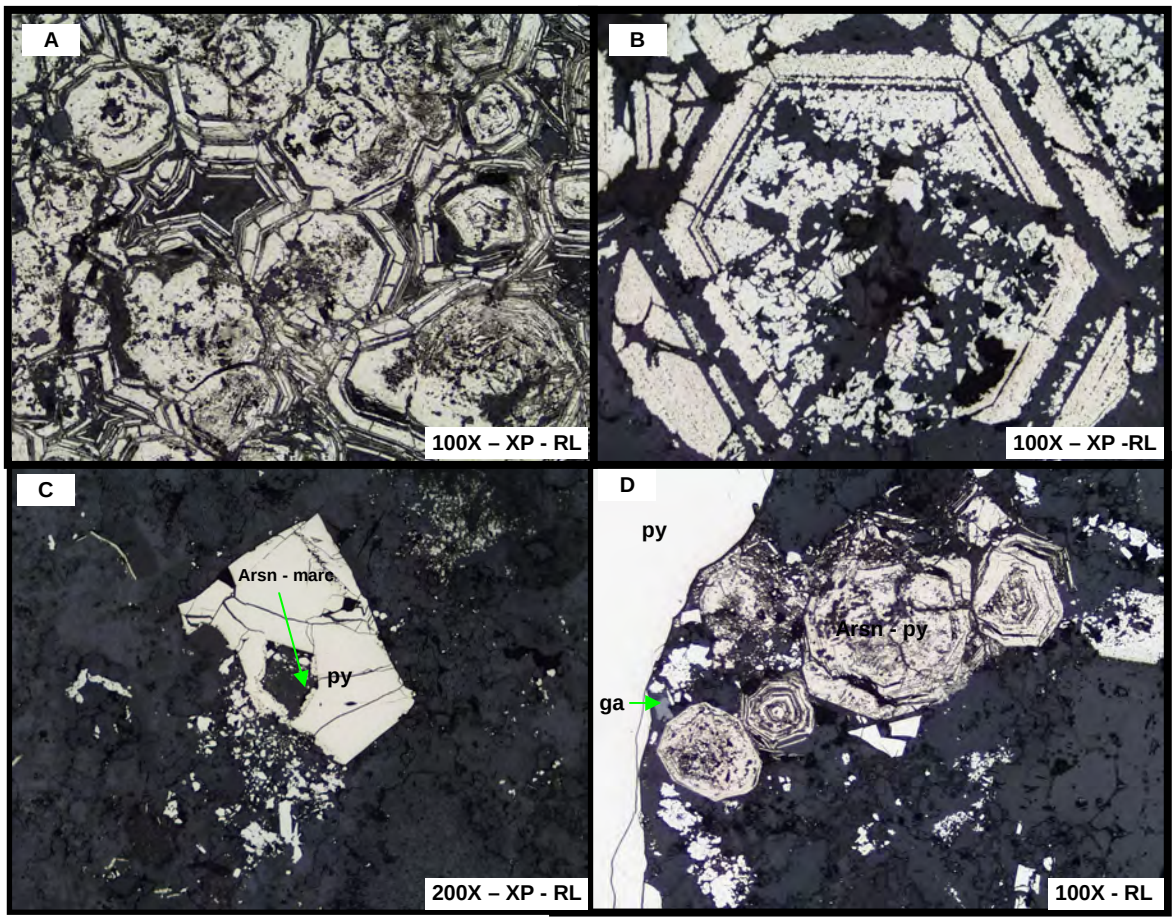

Figure 23. – Photomicrographs in reflected light from overprinted skarn zone in East Archimedes. A. – Garnets completely replaced by qtz and arsenian pyrite/marcasite; B. – Example of well-preserved garnet crystal structure despite total replacement by qtz and sulfides; C. - Pyrite grain rimmed in places by arsenian marcasite; D. – Pyrite and arsenian pyrite/marcasite both as garnet replacement and arsenian rims on pre-existing pyrite grains. FOV = (100x) 0.85 mm, (200x) 0.43 mm, (400x) 0.21mm

The pyrite/kaolinite that cuts the skarn at depth appears to be structurally controlled. The Blanchard fault is assumed to be the fluid pathway, as the overprinted zone appears to be focused around where the fault intersects the massive skarn. The Carlin-type fluids were characterized by multiple arsenian pulses evidenced by variable pyrite compositions in the replaced garnets (Figure 24). Slight color variations in the SEM backscatter images reflect varying compositions of the sulfides present. In the case observed in Figure 24,

these shifts are obvious. In Figure 25, they are not obvious, yet confirmed through EDS that the bands are indeed not the same composition. Replacement textures in this zone are fairly spectacular, and for the most part retain the original crystal structure of the garnets (Figure 23A, 23B, & 23D). SEM analysis of this zone has determined that the banding is arsenian marcasite/pyrite with quartz and carbonate in alternate bands. Pyrite also occurs as large (>5mm) euhedral cubes or as massive replacement of carbonates. Arsenian

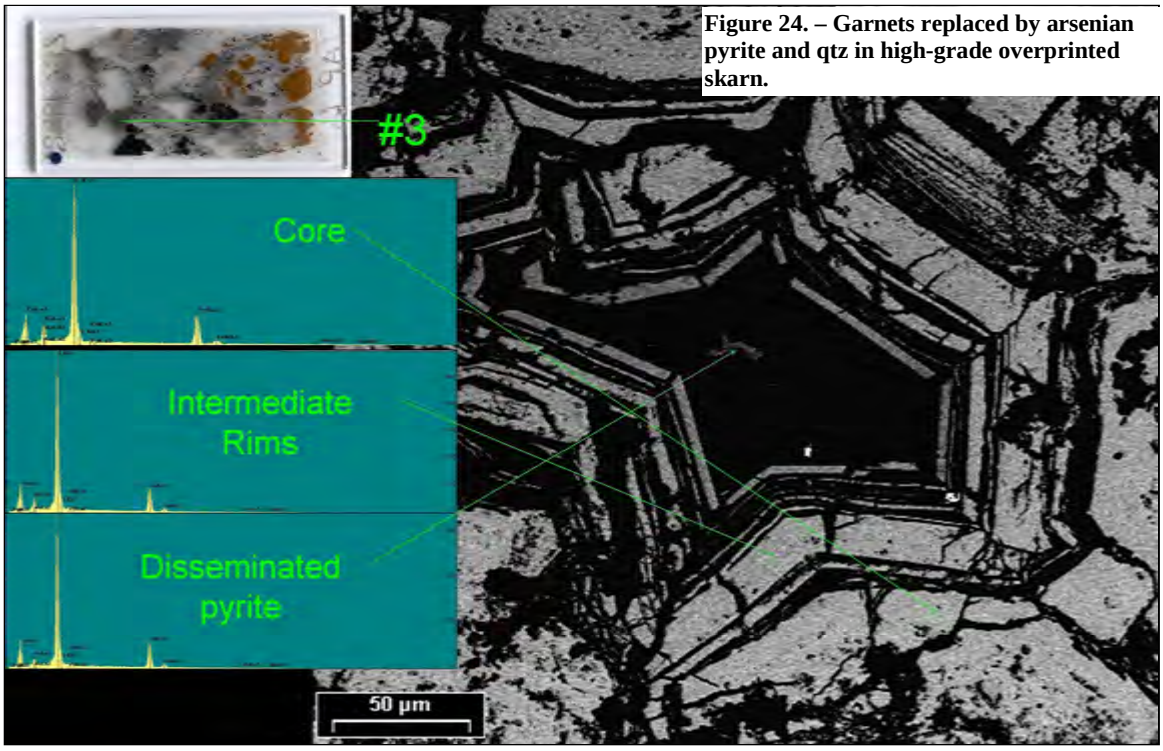

Figure 24. – Garnets replaced by arsenian pyrite and qtz in high-grade overprinted skarn.

marcasite occurs with pyrite and is commonly interbanded with arsenian pyrite and pyrite on the rims of other sulfides (Figure 23C). Characteristic radiating textures of marcasite on pyrite are present and are well-developed in the higher-grade intervals. This zone is also characterized by Pb-Zn replacement mineralization as massive galena and sphalerite. Base-metal sulfides are much more massive in this zone, with the exception of chalcopyrite, covellite, and digenite. Individual sphalerite and galena crystals in excess of

4 cm have been recovered. Sphalerite abundances are much higher than galena, and exhibit multiple stages of precipitation. Chalcopyrite is present as “disease” in sphalerite as well as cores in pyrite/marcasite grains. Arsenian marcasite was observed in the higher grade zones to occur as rims on sulfides such as galena and pyrite (Figure 26). The rim features on these sulfides are very similar to those found in the more obviously Carlin-type parts of Archimedes, as well as those found in many other Carlin-type systems (Folger et al., 2000). Silicification is relatively localized, but occurs as matrix in brecciated zones as well as chalcedonic quartz flooding. This indicates that silicification was not pervasive with any sort of prograde/retrograde skarn alteration, but was a component in the later, more restricted alteration that took place. Also common in this zone is massive barite with late calcite, occurring commonly as 7-12 in. thick bands intermittently with the highest grade base-metal lenses. This could be the reason for earlier interpretations that these high-grade intervals appeared to be manto-like due to the intermittent drop in grades from the massive barite horizons. These early observations have shown that higher gold grades appear to be associated with the replacement of the garnets by some later hydrothermal event. It is this event that is believed to have been the source for the gold mineralization that is so closely associated with the earlier skarn.

Gold concentrations in this zone are relatively high, with local intercepts having assays in excess of 1.7 oz/ton Au. It is worth noting that silver grades at depth increase to values in excess of several hundred ppm, and locally correlate well with Au-Pb-Zn grades

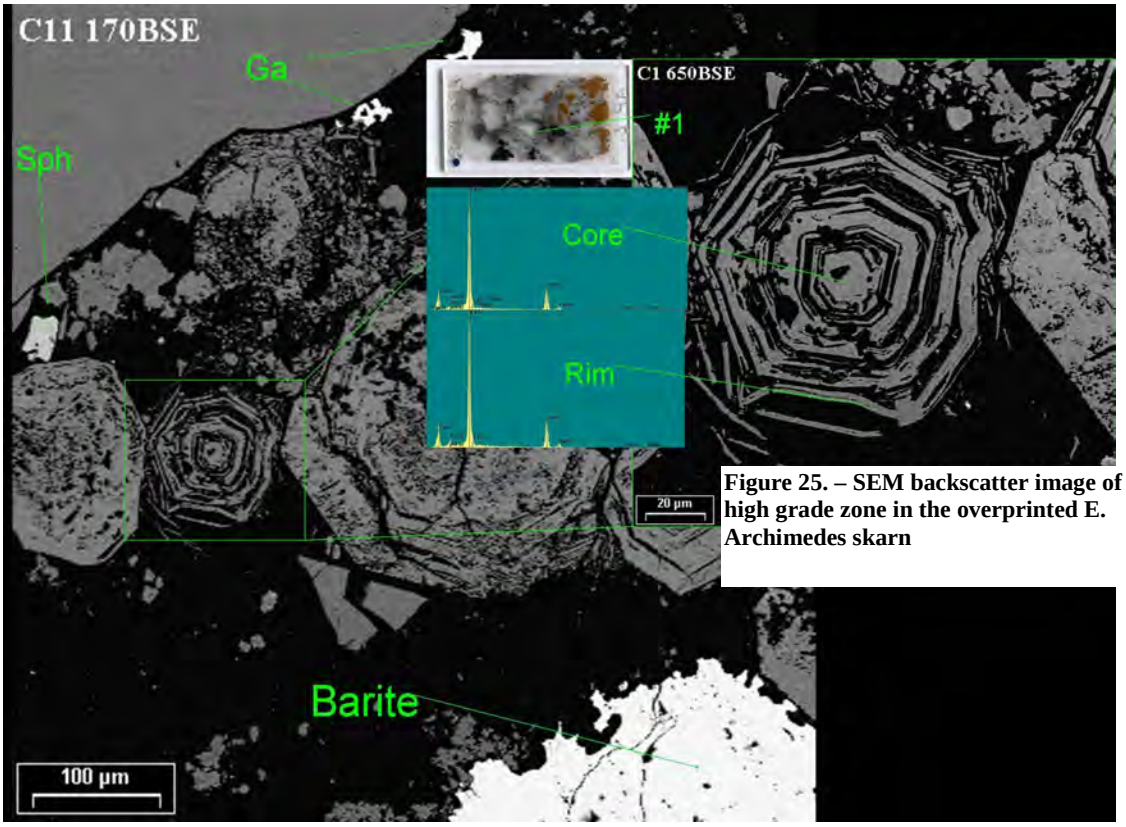

Figure 25. – SEM backscatter image of high grade zone in the overprinted E. Archimedes skarn

(Margolis, 1997). The most common elements that are correlative with gold in this zone are As, Hg, Tl, Ba, and Sn (Margolis, 1997).

These elements are certainly more diagnostic of Carlin-type deposits rather than traditional gold-bearing skarns. Although the geochemistry of the deep East Archimedes zone as a whole reflects the signature of the skarn, the gold is found to be more coeval with other more Carlin-style elements. One can draw the conclusion that the gold is, in turn, a product of the more localized Carlin-style overprinting event rather than some retrograde event during skarn emplacement.

Figure 26. – Late arsenian marcasite overgrowths on pyrite grains as well as interstitial to galena in the overprinted skarn. Infill of this arsenian overgrowth into the crystal lattice spaces of the galena grains is obvious.

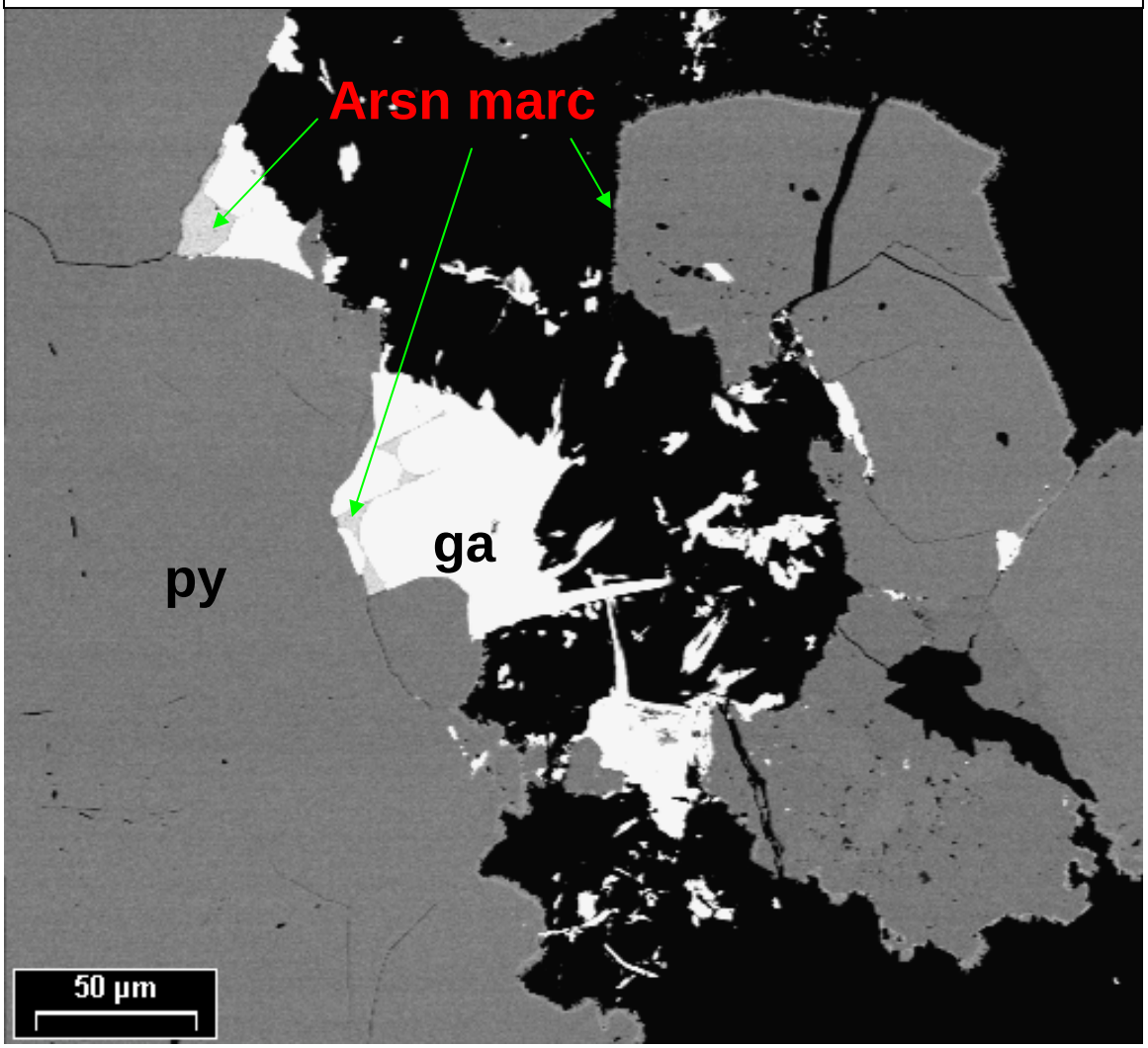

Sulfidized Carlin-type Gold Mineralization

Finally, the third type of gold mineralization is described as traditional Carlin-type mineralization. It is best exemplified in the Ruby Deeps orebody which is a lensoidal, discontinuous breccia complex found directly beneath and within the Bullwhacker Sill. Alteration in the sill to the east is very similar to the Graveyard Flats, with most of the plagioclase altered to sericite, kaolinite or calcite. Pyrite is also a common alteration product, but differs in intensity throughout the sill. Alteration assemblages in the sill vary as one approaches the mineralized zone at depth. Distal outcrops of the Bullwhacker Sill are weakly propylitized with an assemblage of chlorite ± calcite ± rutile ± iron-oxides (Langlois, 1971).

Figure 27. – Core from the Ruby Deeps orebody illustrating the more Carlin-type features of the system such as the dissolution/collapse breccias cemented by barite, calcite, and arsenic sulfides

The chlorite and iron-oxides that dominate in this assemblage appear to have been derived primarily from alteration of biotite and hornblende (Figure 12A & 12D). The sill

is moderately to intensely argillically altered at depth with a quartz-kaolinite dominant assemblage also characterized by less abundant pyrite and sericite. Deeper zones are known to have barite ± arsenic sulfides ± and arsenian pyrite/marcasite associated with high-grade gold mineralization in the Ruby Deeps orebody. In deep drill holes it would seem that the Bullwhacker Sill and the Graveyard flats are indeed the same rock, and that the textures observed in thin section corroborate this more than the geochemistry. It is believed that the Bullwhacker Sill functioned as a trap for mineralizing fluids, resulting in the orebody that is flush with the underside of the intrusive.. The orebodies are located approximately 1000 ft. below the Archimedes orebodies, and are similar in their lateral extent. Spectacular examples of this mineralization are seen as dissolution/collapse breccias within the Catlin and Bullwhacker members of the Windfall Formation (Figure 27). Breccia fragments are typically monolithic, comprised of variably decalcified silty limestone, and contain abundant fine-grained pyrite with arsenian marcasite/pyrite overgrowths (Figure 28E). Pyrite is found as both euhedral crystals and fine-grained disseminated granular mineralization. Later fractures and veinlets are characterized by orpiment/realgar ± massive barite ± calcite. These textures are very similar to the post-ore barite-cemented breccias found at the Meikle deposit (Emsbo & Hofstra, 2003). Gold grades are generally found to correspond with the arsenic values in Ruby Deeps. Pyrite is uncommon in the matrix, but does appear as breccia fragments in orpiment/realgar and barite veins (Figure 28D). Based on megascopic cross-cutting relationships visible in core, it can be said

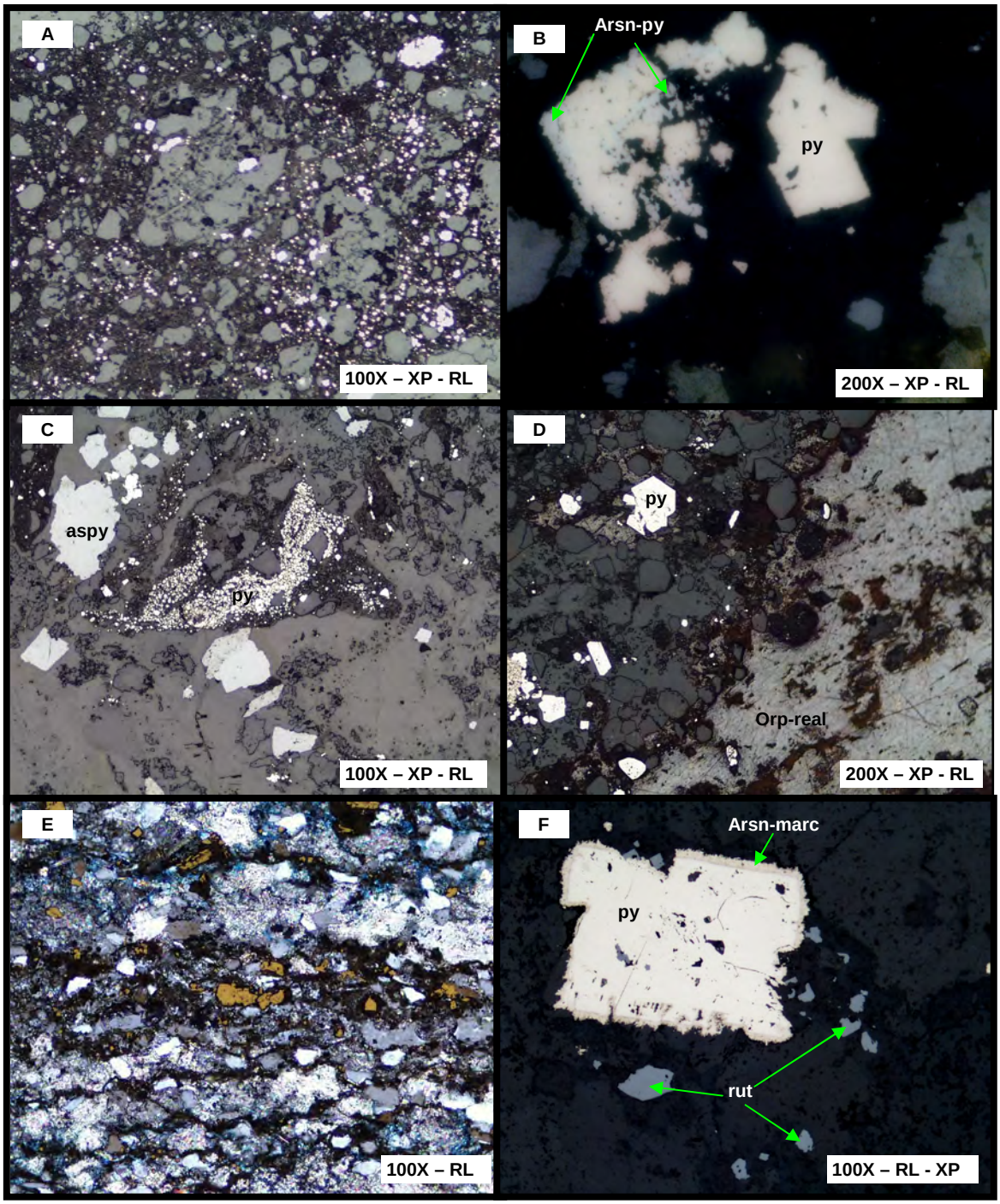

Figure 28. – Photomicrographs from the Ruby Deeps orebody; A. – Disseminated pyrite and arsenian pyrite in a dissolution/collapse breccia; B. – Arsenian pyrite and arsenian marcasite rims on preexisting pyrite grains; C. – Disseminated pyrite with sphalerite and galena in a matrix of barite, arsenic sulfide, and qtz; D. – Pyrite and arsenopyrite in qtz-barite breccia with late arsenic sulfide vein; E. – Less altered rock shows dissolution and compaction of the section, resulting in high concentrations of stylolites with preexisting pyrite grains rimmed by arsenian pyrite/marcasite. Note the abundance of qtz grains relative to carbonate; F. – Well-developed arsenian marcasite rim on euhedral pyrite grain with rutile grains. FOV = (100x) .85 mm, (200x) .43 mm, (400x) .21mm

that the sequence of events for this deposit follows as such: decarbonatization associated with sooty pyrite, dissolution/collapse breccias and the initiation of arsenian pulse with gold mineralization, and finally the late orpiment/realgar/barite veinlets and breccia matrix.

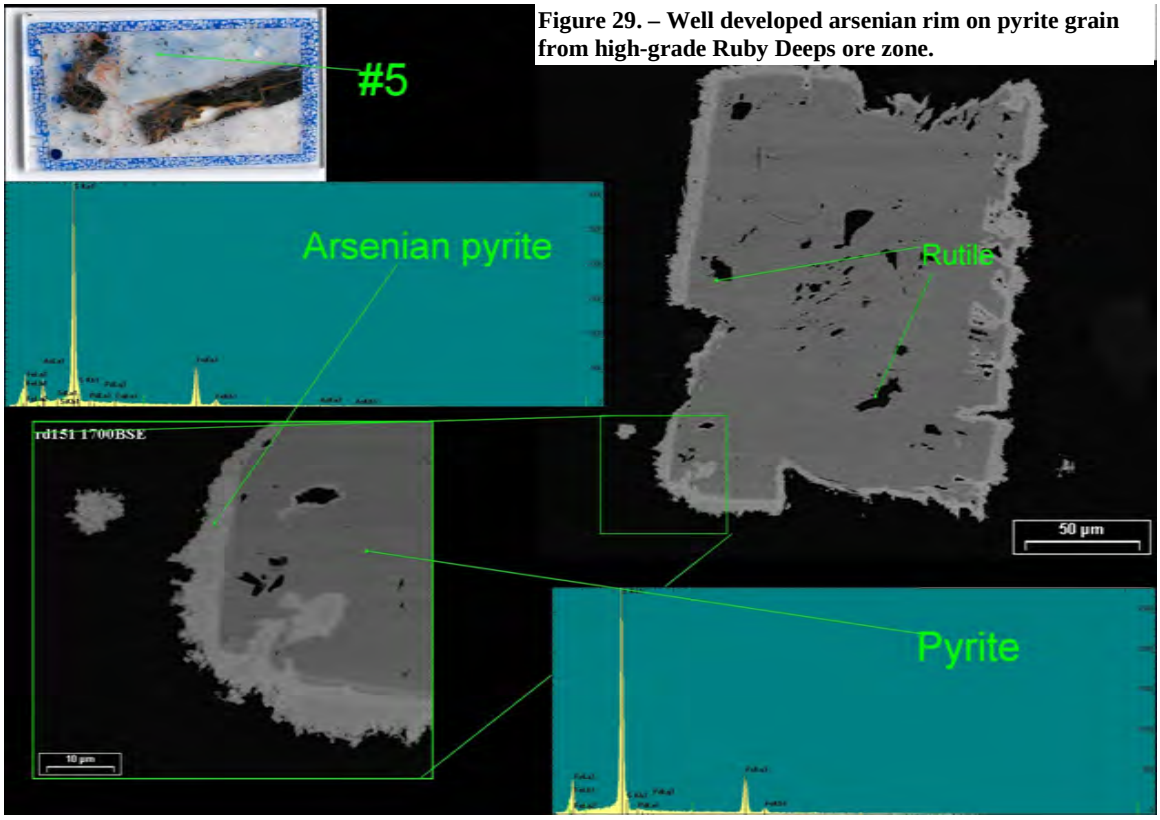

Figure 29. – Well developed arsenian rim on pyrite grain from high-grade Ruby Deeps ore zone.

In Ruby Deeps, like most Carlin-type systems, the gold is concentrated in the arsenian rims of these disseminated pyrite grains (Figure 28B & 28F). These rims are well-developed on pre-existing euhedral pyrite grains. In some samples, they exhibit spectacular variations in the arsenic content in marcasite within the rims (Figure 29 & 30). SEM and EDS analysis of these rims was instrumental in defining their compositions

relative to the cores, but was not successful in determining whether or not they were

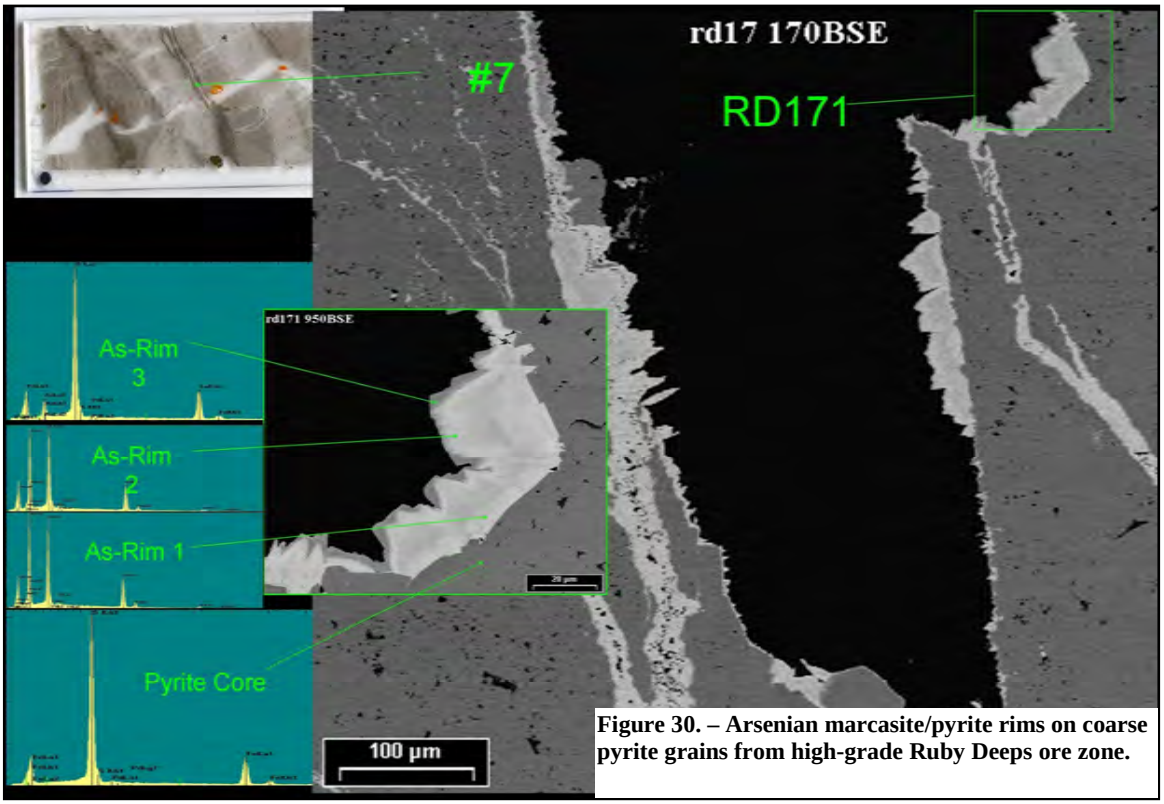

Figure 30. – Arsenian marcasite/pyrite rims on coarse pyrite grains from high-grade Ruby Deeps ore zone.

auriferous. However, unpublished secondary ion mass spectrometry (SIMS) work by Ghidotti and Barton from the University of Arizona suggests these rims to have elevated gold values (Personal Communication, Mark Barton, 2007).

Petrographic study of the different orebodies has been the most useful tool in describing their relationships to each other. A rough timeline can be established from the paragenetic relationships seen in this study (Figure 31). Early alteration is represented by the prograde contact metamorphic event due to emplacement of the 109 Ma Graveyard Flats quartz monzonite. Prograde alteration is represented by the garnet ± wollastonite assemblage that is developed in closest proximity to the intrusive. Other contact metamorphism includes well-developed marble further from the garnet skarn and intrusive contact. Shortly after this event, retrograde alteration began. This resulted in the

chlorite ± stilpnomelane ± calcite ± quartz ± adularia assemblage that is more distal from the massive garnet skarn, yet locally overprints it. During this time, Cu-sulfides were deposited along with Pb and Zn minerals as temperatures waned.

It is clear that significant leaching and destruction of the primary skarn mineralogy took place, and probably remobilized elements to new parts of the developing Carlin-type system. In the Graveyard Flats intrusive, the retrograde alteration and propylitic alteration are overprinted by moderate to intense argillization. In the carbonate units, early alteration associated with Carlin-type fluids resulted in decalcification and volume-loss within the Pogonip Group. High level mineralization was accompanied by late silicification in the form of jasperoids. Base-metal and iron sulfides were introduced early and include pyrite/marcasite, sparse sphalerite (lower Fe), and late tennantite/tetrahedrite. Introduction of gold into the system was likely coeval with later As-sulfides and the auriferous arsenian pyrite. There is significant petrographic evidence for multiple pulses of arsenic-rich fluids through the system, ending with consumption of Fe for complexing and precipitation of As-sulfides. Late barite/calcite matrix developed both in Ruby Deeps as well as Archimedes.

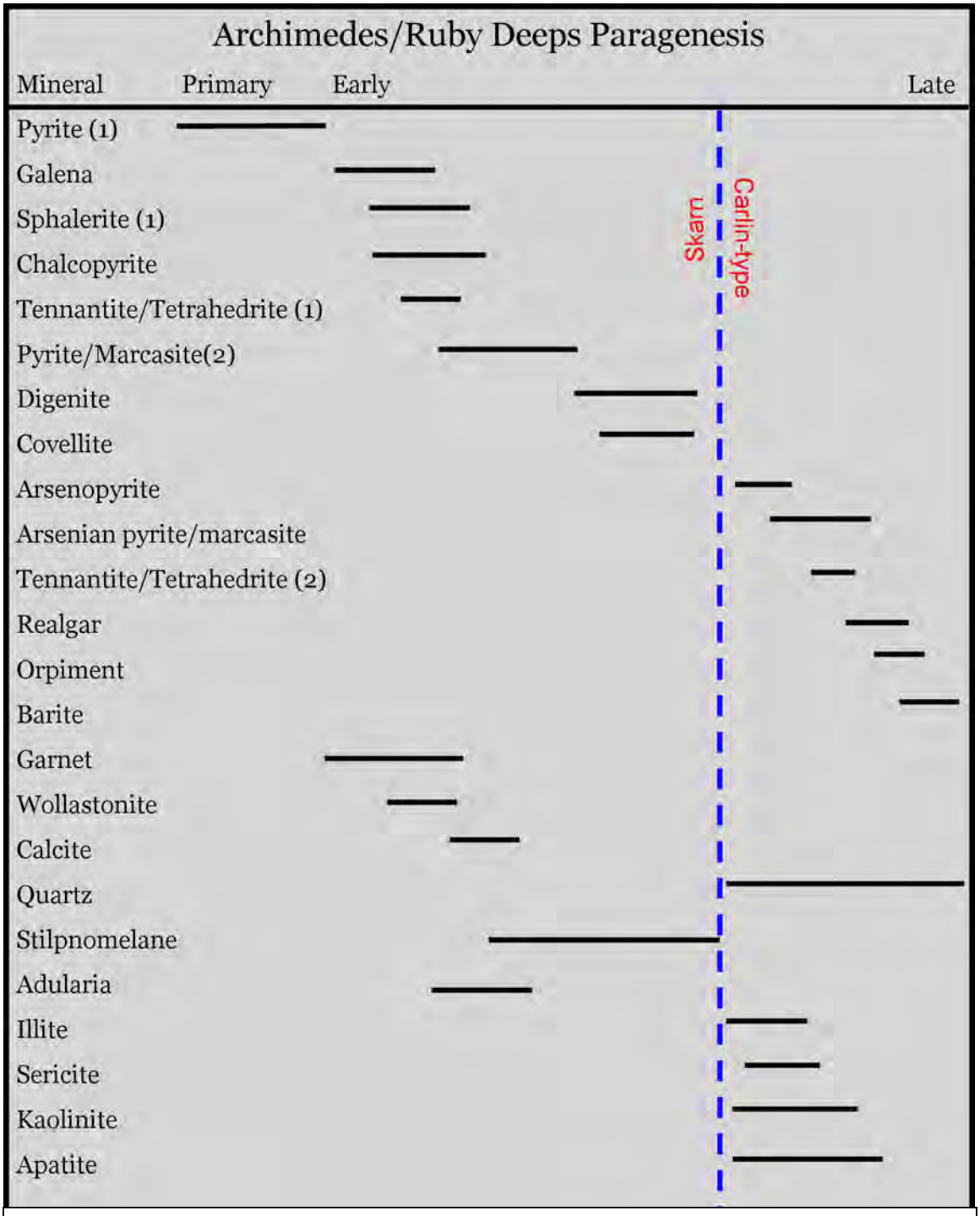

Figure 31. – Paragenetic diagram illustrating mineralogical differences between the two systems.

Age Dating

The skarn age has been relatively well constrained with adularia from the fresh skarn yielding a K-Ar age of 109 ± 2 Ma (Margolis, 1997). A whole-rock sample from the Graveyard Flats intrusive yielded a K-Ar date of 110 ± 5 Ma (Margolis, 1997), which corresponds roughly to other ages obtained on the Bullwhacker Sill (91.8 ± 1.8 and 103 ± 2 Ma, K-Ar, sericite) reported by Armstrong (1970) and Langlois (1971). This would indicate that zones of alteration associated with these intrusive rocks occurred during the Cretaceous, not the Eocene or Miocene. However, dating was not performed on the deeper kaolinite-altered zones of the Bullwhacker Sill that can be demonstrated to be associated with Carlin-type mineralization. Dating of Carlin systems has ever been an issue due to the lack of dateable alteration or ore minerals that can be demonstrated to be related to ore deposition (Arehart, 2003). Another issue contributing to this difficulty is the fact that the low temperatures of ore formation are in many cases insufficient to completely reset the K-Ar system. While the age of the intrusives themselves can be well-constrained, it is considerably more difficult to date the timing of later hydrothermal events. Although the dating of the Archimedes system has not been successful, it is safe to say that the emplacement of the Graveyard Flats quartz monzonite, the Bullwhacker Sill, and the sericitic alteration occurred from 110-90 Ma.

Apatite Fission-Track Dating

Apatite Fission-Track Dating (AFTA) was employed to place constraints on the ages of the mineralization events at Archimedes. This technique is commonly used by oil exploration companies to define uplift and thermal history of a basin, but is also useful for showing periods of heating and cooling associated with hydrothermal systems. The basic approach adopted for this study involves application of AFTA to constrain the cooling histories of paleo-thermal events. Figure 32 shows the spatial distribution of samples analyzed for AFTA.

The way that AFTA works is a relatively easy to understand concept, with very complicated undertones. A summary of the AFTA technique is provided in Appendix D,

Figure 32. - AFTA Samples (plotted on mine grid)

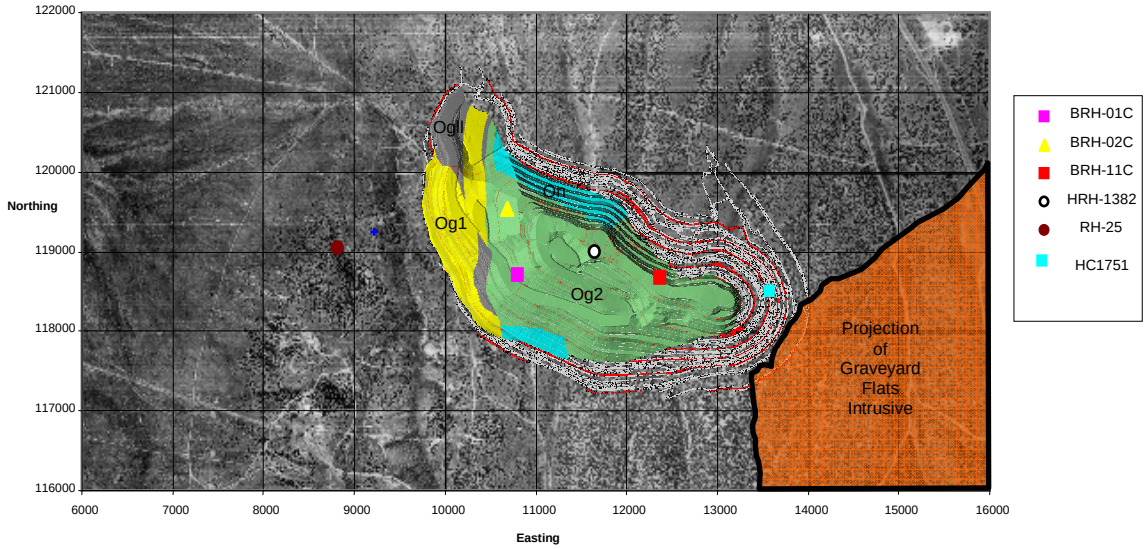

a set of appendices from the full report by the Australian lab Geotrack, Intl. For these purposes, the descriptions and principles in Gallagher (1995) suffice. Apatite fission

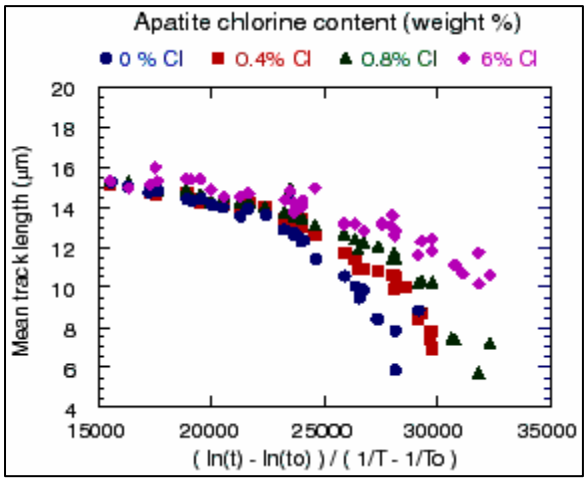

Figure 33. – Laboratory results from isothermal annealing experiment with apatites of four different Cl compositions. Mean track length in each apatite is plotted as a combined function of annealing temperature and time (Laslett et al., 1987) .

tracks are basically damage trails caused by radiation within detrital (and hydrothermal) apatites. The tracks themselves are produced by radioactive decay of atoms of U^{238} within the crystal lattice of the apatite. Because U^{238} has a known half-life, the amount of tracks present in an un-disturbed apatite grain is a function of the amount of uranium and the time since the formation of the apatite. Thus, amount of tracks can be directly correlated to the age of apatite grains due to the steady decay of the contained uranium. However, apatite exhibits an interesting property that makes this technique even more useful. Apatites that are subjected to prolonged temperatures in excess of about 120 ^{o}C display an annealing of fission-tracks completely, essentially resetting the apparent age of the apatite grains. There are a number of factors that influence this annealing effect on the apatites, the most notable of which is composition. The chemical formula of apatite is $Ca_5(PO_4)_3(OH, F, Cl)$. It has been demonstrated that Cl content of apatites has a pronounced effect on annealing temperatures. Most detrital and magmatic apatites are fluorapatites with little appreciable Cl content. Annealing temperatures are dependent upon the composition of the apatites. For example, fission tracks in chloroapatites anneal at higher temperature relative to fluorapatites. Thus, the thermal history reconstruction of an area must be evaluated based

on three factors: uranium content, time since cooling below the annealing temp, and Cl content.

The distribution of samples also took advantage of the variable depth from surface due to the shallowly-dipping nature of the Bullwhacker Sill back to the Graveyard Flats intrusive. A control sample was sent in from an overlying rhyodacite tuff unit that had not undergone any sort of hydrothermal alteration or uplift.

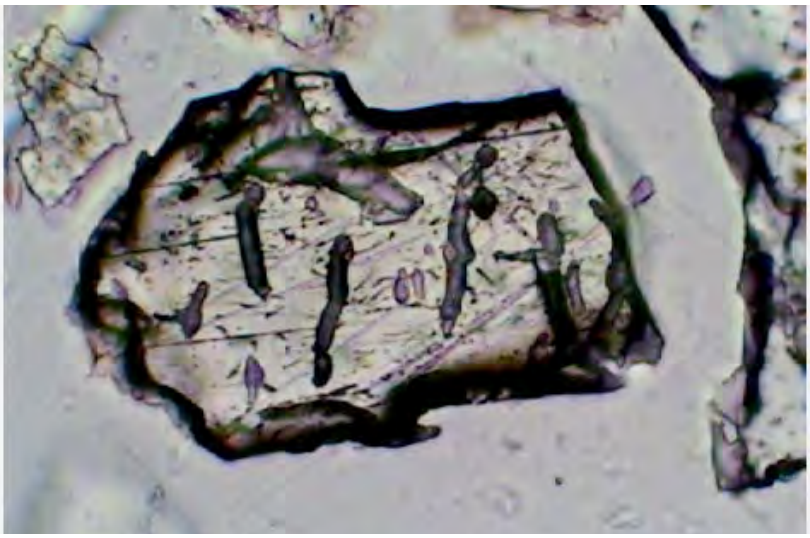

Figure 34. – Apatite grain exhibiting fission tracks (straight thin lines) as well as abundant dislocations and etched pits (large curved dark lines). This particular sample is not suitable for fission track analysis. Plane light photomicrograph; FOV= 195 µm

It was confirmed by AFTA that this tuff is, in fact, not tertiary. Apatites from this sample yielded an age of approximately 40 Ma from the onset of cooling. Based on the textures in the tuff, it is likely that this tuff has been reworked and transported from an unknown distance. This is not a difficult conclusion to believe given the lack of welding characteristics and rounded clasts contained within the tuff. Moreover, it is similar to other Oligocene-Eocene volcanics in the Eureka district, notably those exposed in the pit

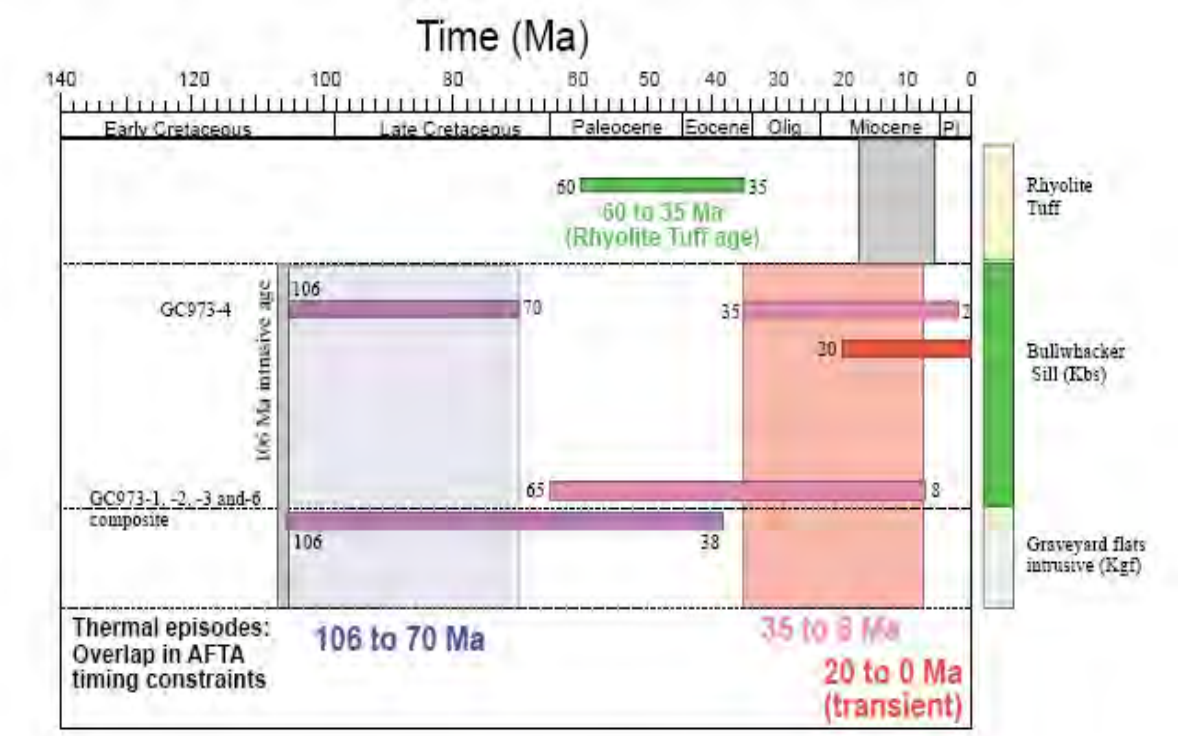

Figure 35. – Graphical representation of constraints on the onset of cooling periods derived from AFTA in samples from the Bullwhacker Sill and Graveyard Flats intrusive. The results define two post-Cretaceous thermal episodes with cooling beginning some time between intrusion at 106 Ma and 70 Ma, followed by a cooling period some time between 35 and 8 Ma. These episodes could be explained by regional burial followed by uplift and erosion, but are better explained by hydrothermal events. This conclusion is best represented by the "transient" thermal episodes observed in some samples that took place in the last 20 Ma.

at Rustler. The Pinto Peak rhyodacites are known to have erupted around 36 Ma which fits roughly with the 42 ± 5 Ma age date determined from AFTA. Excellent yields of apatites were obtained from all samples sent to the Geotrack lab in Australia. The overall quality of the apatite recovered from 4 of the six samples in this study was relatively poor, which has limited the amount of AFTA data that could be obtained from these samples. Any conclusions that can be drawn from this data and the modeling performed by Geotrack Intl. can be considered simply as a *possible* scenario for cooling histories. Data were particularly lacking in the only sample from the Graveyard flats intrusive (GC973-6) and three of the four samples from the Bullwhacker Sill (GC973-1, -2 and -3). In fact, margins of error for these samples were between 25 and 44 Ma. However, the

lack of useable data is an important piece of information in itself. As described in the report from GeoTrack, apatites from the Bullwhacker Sill and Graveyard Flats intrusive at depth almost universally showed signs of significant partial dissolution and recrystallization of hydrothermal apatites. These later rims of hydrothermal apatite are unsuitable for identifying tracks due to the large amounts of dislocations and fluid inclusions (Duddy, 2006). To improve the thermal history interpretation available from AFTA in these individual samples, the data have also been combined into a single composite sample as representative of the Cretaceous Bullwhacker Sill and Graveyard Flats intrusive. The data from the remaining samples, one from the Bullwhacker Sill (GC973-4) and one from the rhyolitic tuff (GC973-5) are of high quality. Apatite fission track age and mean track length data in the six samples are summarized in Table 1 and plotted as a function of relative stratigraphic position in Figure 35. The variation of fission track age and length versus relative stratigraphic position predicted from the Default Thermal History for these samples are also shown in Figure 33, for various apatite chlorine contents. Figure 37 summarizes the values of mean length and fission track age predicted from the Default Thermal History (Figure 36) modeled for each sample. These values take into account the range of chlorine contents measured in each sample (Duddy, 2006).

Table 1: Summary of apatite fission track data in shallow borehole and outcrop samples, Nevada (Geotrack Report #973)

Sample number	Source No.	Present temperature[*1] (°C)	Stratigraphic age (Ma)	Mean track length (μm)	Predicted mean track length[*2] (μm)	Fission track age (Ma)	Predicted fission track age[*2] (Ma)
GC973-1	BRH-01C	39	106	12.32 ± 0.63	13.8	37.6 ± 28.9	100
GC973-2	BRH-11C	52	106	12.48 ± 0.38	13.4	127.3 ± 28.5	98
GC973-3	HRH-1382	47	106	11.43 ± 0.57	13.4	82.6 ± 23.9	98
GC973-4	RH-25	15	106	12.49 ± 0.24	14.9	57.5 ± 13.8	106
GC973-5	HC1751	26	17-6	14.70 ± 0.26	14.7	41.7 ± 5.1	12
GC973-6	BRH-12C	44	106	12.04 ± 0.72	13.7	142.8 ± 44.2	100

All other AFTA samples were taken from the Cretaceous Bullwhacker Sill. AFTA analysis confirmed that the 110 ± 5 Ma age of the Graveyard Flats intrusive from the USGS data is not unreasonable. A graphical summary of the thermal history of the Bullwhacker Sill/Graveyard Flats intrusive is included in Figure 36. Assuming that the events revealed by AFTA in individual samples represent synchronous thermal episodes, the following time intervals for the onset of cooling are suggested:

1. 106 to 70 Ma (Cretaceous) – Cooling from maximum post-Albian paleotemperatures >100°C or more, occurred during this time interval.

2. 35 to 8 Ma (Oligocene-Late Miocene). Cooling from a peak in paleotemperatures, generally in the range 65 to 95°C, began during this time interval.

3. 20 to 0 Ma (Early Miocene to present-day). Cooling from locally elevated paleotemperatures >125°C began during this time interval.

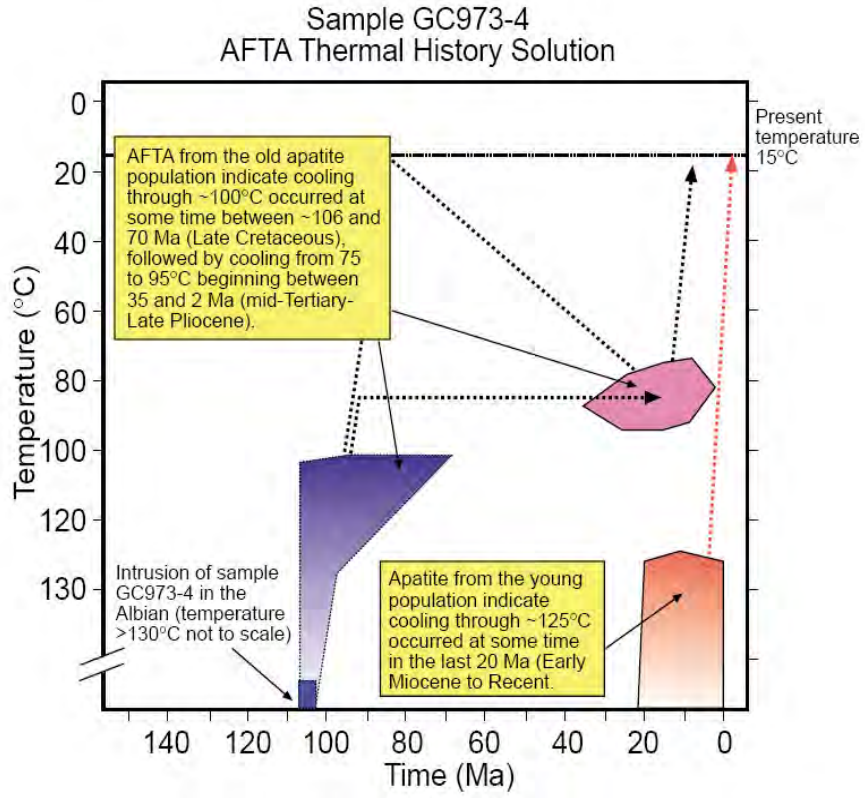

Figure 36.- Thermal history reconstruction of the composite sample representing the Cretaceous Bullwhacker Sill and Graveyard Flats Intrusive. This includes the high-quality data as well as lower quality data from the composite.

The data generated by the AFTA has the potential for raising more questions than it answers. The cooling period between 106 and 70 Ma is likely representative of the high heat flow in the district during the Cretaceous and before later uplift. The 35 to 8 Ma period, while broad, would fit with the rhyolitic and andesitic volcanic rocks in the district. It is also possible that any uplift during this time could be responsible for the age of cooling. Based on the alteration of these rocks, however, the more likely conclusion has to deal with the magmatic-hydrothermal systems and the potential for later hydrothermal events. This age falls within the 28 to 41 Ma age range from other deposits

on the Carlin trend (Arehart et al., 2003). Perhaps the most interesting result is the Miocene cooling age. Interestingly enough, the initial report prepared by Geotrack Inc. could not relate this localized heating event to any sort of uplift and instead speculated that the transient episode (20 to 0 Ma) revealed by AFTA in sample GC973-4 may have been associated with a pulse of heated fluids involved with dissolution of primary igneous apatite and/or precipitation of secondary apatite (Duddy, 2006). While it does not explicitly date the mineralization of Archimedes or Ruby Deeps, these data do offer a

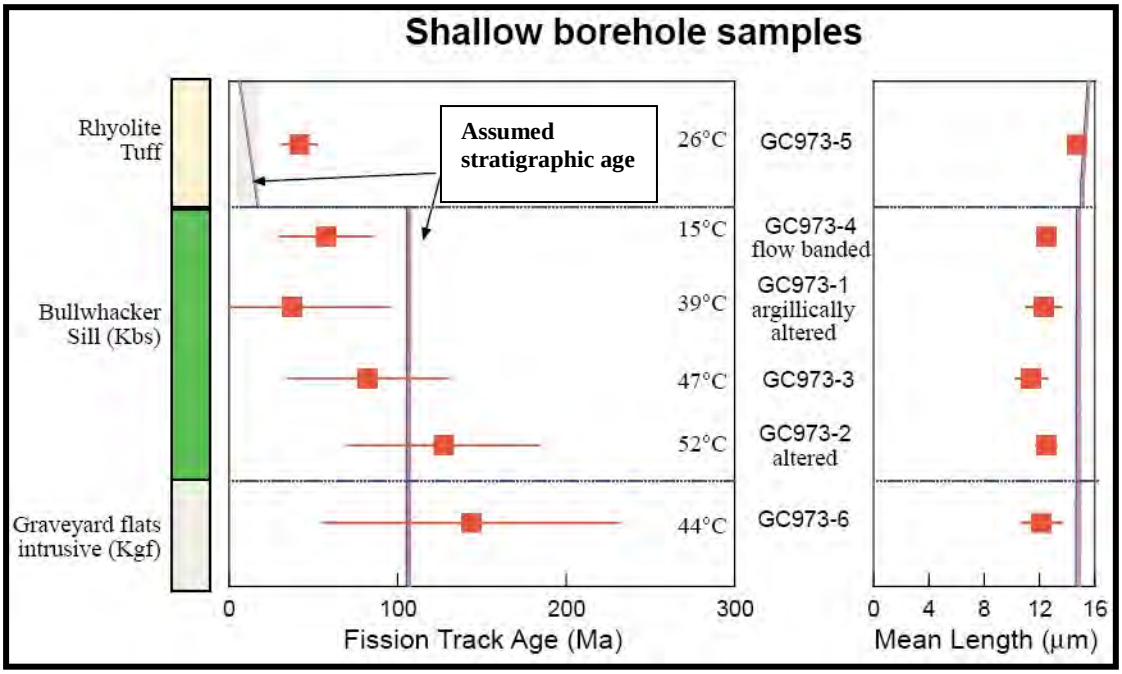

Figure 37. - Average AFTA parameters plotted against relative stratigraphic position for Cretaceous and Tertiary samples from Ruby Hill, Nevada. Present-day temperatures are estimated assuming a geothermal gradient of 57°C/km (~3.1°F/100 feet) and an average surface temperature of 15°C (59°F), as explained in the Geotrack Report in Appendix D The fission track ages for the Bullwhacker Sill samples are either significantly younger than, or similar to, the values expected from the Default Thermal Histories while the mean track lengths are all much shorter. These patterns indicate cooling from paleotemperature significantly higher than the present temperatures at some time well after initial intrusion. The fission track age of the rhyolite tuff sample is much older than the Middle to Late Miocene age attributed to it, while the length is similar to that predicted from the Default History. These features suggest the tuff is significantly older than the Middle to Late Miocene.

possibility for higher heat flow during time periods that are typical of many other Carlin-type systems. The complex tectonic and volcanic history of the Eureka district does not make this task any easier, yet apatite fission track analysis has shown conclusively that later thermal episodes, even as recently as the Miocene, could be responsible for the disseminated Au mineralization at Archimedes and Ruby Deeps.

Stable Isotope Analysis

Ninety samples from the vicinity of the Archimedes pit as well as unaltered carbonates to the south were analyzed for stable isotope ratios for oxygen and carbon. The purpose of this investigation was to determine how much, if any, isotopic exchange had occurred between ore fluids and rocks in mineralized zones. Values for these samples are presented in Appendix B. Sample locations are shown on Plates 1 & Plate 3. Samples are also projected onto the cross-section in Plate 2. Background samples were taken from unaltered limestone to the south from the same units that are exposed in the pit. The background $\delta^{18}O$ levels appear to be around -12 to -5 per mil VPDB. Carbon isotope samples average around .5 per mil VPDB for these background carbonates. The $\delta^{18}O$ and $\delta^{13}C$ isotopic values do not exhibit any significant pattern that would be useful for differentiating multiple populations within the data (Figure 38). When plotting the samples that were separated specifically from calcite veinlets vs. wall rock, the range of values is very similar for both (Figure 39). However, it can be suggested that vein samples tend to skew towards more depletion. More samples making this differentiation might help to discern between different populations. Based on the shotgun patterns for C and O isotopes in this study, it suggests that the scale at which the isotopic exchange took

place during alteration was greater than the veinlet/wall rock effects seen in hand samples. The O and C isotope samples in the area of the pit are shown in Figures 40-41. Values have been thematically arranged to attempt to show any sort of changes in isotopic ratios. The range breaks are determined according to an algorithm such that the difference between the data values and the average of the data values is minimized on a per range basis. Carbon isotopic exchange does not exhibit any obvious pattern relative to the oxygen values. Both carbon and oxygen isotopes appear depleted in zones of intense contact alteration proximal to the Graveyard Flats skarn. This indicates the likelihood of the depleted zones being related to magmatic waters during skarning, a characteristic observed in other magmatic/hydrothermal systems (Rye & Ohmoto, 1974).

Figure 38. Carbon vs. oxygen isotopic ratios from hand samples and core taken from the vicinity of the Archimedes pit.

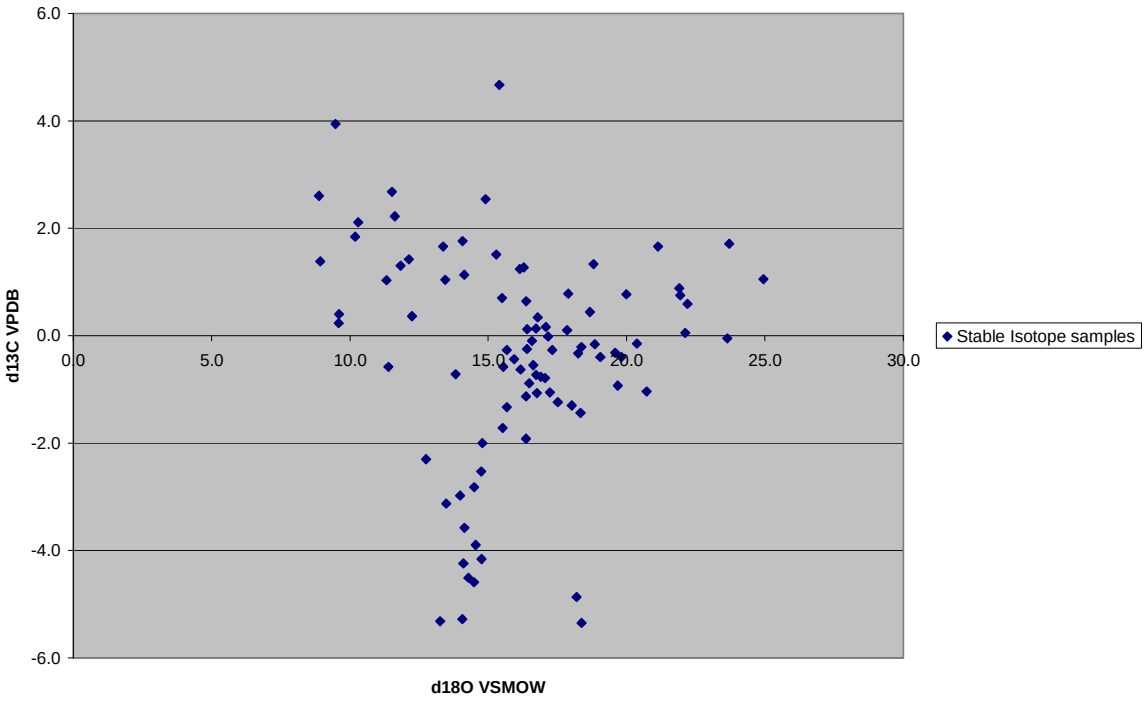

The restriction in the depleted $\delta^{13}C$ isotope values to the immediate skarn area can be attributed to the increased intensity of fluid/rock reactions taking place immediately adjacent to the intrusive during metasomatism.

Figure 39. – Plot of isotopic exchange ratios for samples taken from veins vs. wall-rock that illustrates the slight $\delta^{18}O$ and $\delta^{13}C$ depletions observed in vein carbonates relative to the altered limestone adjacent to the veins. Baseline values taken from the same stratigraphic units in unaltered rock have a remarkably similar spread.

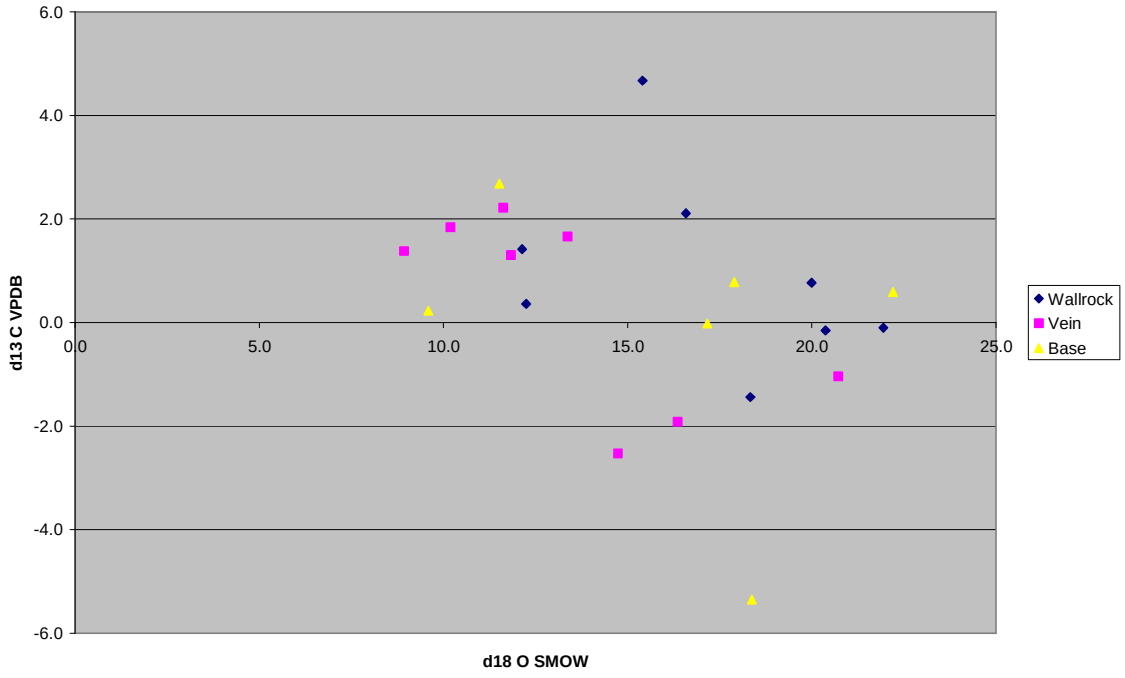

It is suggested that the observed fluctuations in $\delta^{13}C$ isotope values is related to the original magmatic system that produced the deep East Archimedes skarn whereas the $\delta^{18}O$ isotope depletions define a broader and more extensive halo of isotopic exchange. This occurs most notably around mineralized structures such as the 150 and Holly faults. This same effect is seen in other ore deposits associated with skarns and carbonate replacement mineralization (Vasquez et al., 1998). Another interpretation is that the fluids responsible for O isotope exchange that took place along mineralized faults and

fractures in West Archimedes are different from those that produced the more restricted C isotope halo. This could be a pH effect, as carbonate speciation varies with pH and thus changes the isotopic composition of calcite deposited during mineralization (Rye and Ohmoto, 1979). As pH increases, the likelihood for H_2CO_3 as the dominant species increases as well. The fractionation between H_2CO_3 and calcite is more temperature dependent than that of HCO_3 and calcite, particularly at pH's in excess of 6. This is possible in a skarn system with a buffering effect and cooling over time. Thus, in zones where fluid/rock reactions are high, the relative isotopic exchange in C isotopes increases. With fluids that are decreasing in temperature and increasing in pH, the $\delta^{13}C$ values skew towards more depletion. This is a possible explanation of the depletion seen in the more intensely altered zones. As seen in Fig. 41, $\delta^{18}O$ VSMOW isotopic ratios are depleted to the east, immediately adjacent to the Graveyard Flats intrusive. Many of these carbonate separates came from the marbleized zone as well as the moderately silicified high-grade zones associated with the Blanchard Fault at depth. Values are also depleted in mineralized fault zones such as the 150-Holly fault system as well as carbonate veining associated with these faults. In most cases, samples taken from these carbonate veinlets are depleted whereas wall-rock immediately adjacent to them retains the background $\delta^{18}O$ ratios or is only slightly depleted. There are a number of factors that affect isotopic exchange rates in carbonates. The extent of isotopic exchange is dependent upon initial grain size, the permeability of the rocks, the fluid/rock ratio, and the temperature of the hydrothermal system (Vasquez et al., 1998).

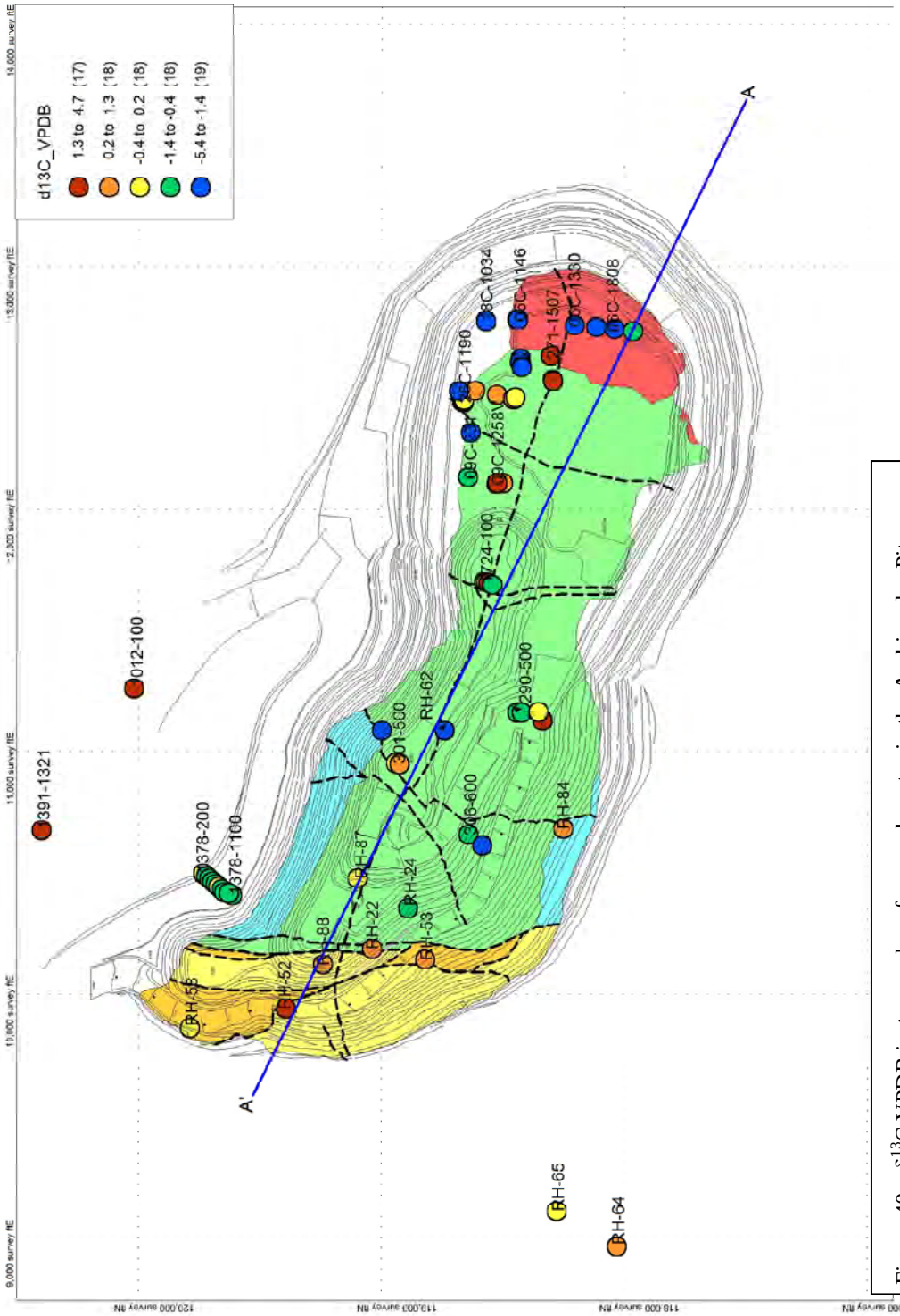

Figure 40 – $\delta^{13}C$ VPDB isotope values from carbonates in the Archimedes Pit area

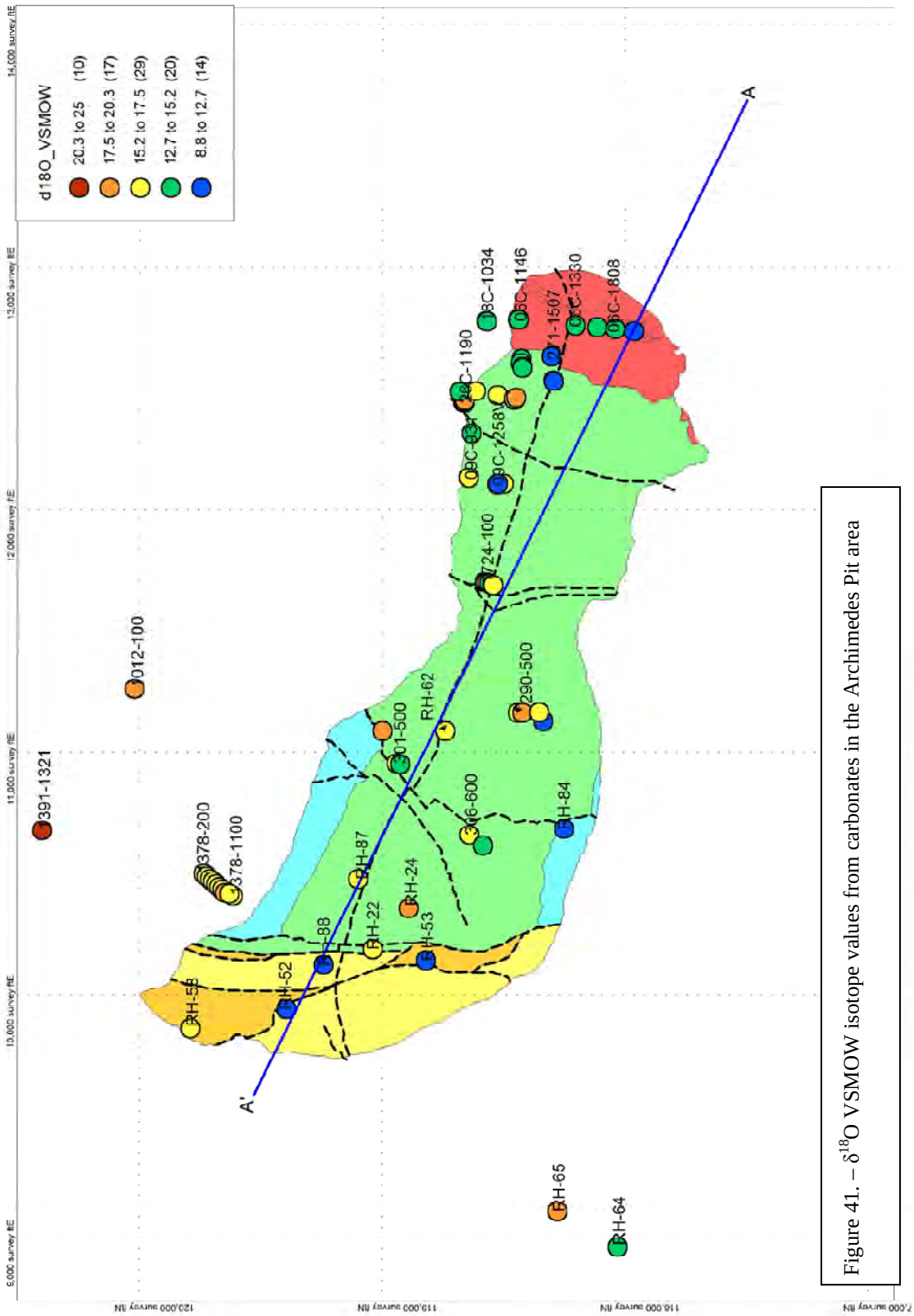

Figure 41. – $\delta^{18}O$ VSMOW isotope values from carbonates in the Archimedes Pit area

Also a factor is the original isotopic composition of the fluid. All of the above could account for the wide variations observed in the Archimedes deposit. However, it is more likely that the fluid/rock reactions taking place in mineralized faults and zones of high permeability were greater than the buffering effects of the carbonate section. Like the carbon isotopes, this results in more extensive isotopic exchange. Archimedes does exhibit a general depletion in oxygen isotopes with a relatively less-obvious depletion in carbon, much like other Carlin-type deposits (Heitt et al., 2003, Holland et al., 1988, Williams et al., 2000). For example, the El Mochito Pb-Zn orebody in Honduras has background isotopic compositions in Cretaceous carbonates that are similar to those unaltered carbonates in the Eureka district. Approaching the orebodies, there is a distinct depletion in both carbon and oxygen that is also very similar to the depletions observed at Archimedes (Vazquez et al., 1998).

The results obtained in this study can not conclusively differentiate between Carlin-type and skarn systems using water types as a classification tool. However, they give more insight into defining fluid pathways and providing data on the differences that can be observed along them. The depleted $\delta^{14}C$ isotopes that are distributed mainly around the contact metamorphic aureole of the intrusive are something that would be expected of any metasomatic alteration. However, $\delta^{18}O$ values show a similar depletion both in the skarn as well as in the mineralized ***post-intrusion*** faulting. This fact alludes to the possibility that the isotopic exchange observed in the mineralized structural zones took place after the faulting, which is thought to be considerably later than the intrusion of the Graveyard Flats porphyry. This suggests that although the Graveyard Flats Intrusive likely caused some isotopic exchange in the carbonate section due to contact

East Arch. Skarn		
Sample ID	Mineral	$\delta^{34}S_{VCDT}$ (‰)
18C-1481	Sphalerite	16.6
18C-1481	Pyrite	18.7
18C-1481	Galena	16.9
18C-1481	Barite	30
28C-1187	Sphalerite	14.7
28C-1187	Barite	22.7
28C-1226	Sphalerite	17.8
28C-1226	Barite	29.9
28C-1226	Galena	15.4
28C-1226	Pyrite	18.3
Ruby Deeps		
Sample ID	**Mineral**	$\delta^{34}S_{VCDT}$ (‰)
1393A-1967	Realgar	16.3
1393A-1967	Barite	21.1
1393A-2062	Realgar	15.2
1393A-2062	Barite	27.9

Table 2. – $\delta^{34}S$ Isotope values for some sulfide and sulfate minerals in the Archimedes system

metamorphic effects, a later system also provided some depleted waters that caused the exchange along the mineralized faults in the high-grade parts of the West Archimedes orebody. Whether these waters were solely magmatic, metoric, or some mixture of the two is subject for a more detailed isotopic study in the future.

Stable isotopes of sulfur were also analyzed from sulfide and sulfate minerals in the deep East Archimedes overprinted skarn as well as the Ruby Deeps ore zone (Table 2). Sulfur isotopes from the major sulfides (i.e. pyrite, galena, sphalerite, orpiment/realgar) As many of these sulfides are found in equilibrium in groups of three, the possibility for extracting sulfide pairs geothermometry data is good. Typically, the pyrite-galena-sphalerite assemblage is found in equilibrium in the skarn portion of the Deep East Archimedes mineralization. Conversely, the sulfides in the Ruby Deeps mineralization typically are pyrite-realgar-sphalerite. As barite is present in both these zones, sulfide-sulfate pairs were also analyzed for geothermometry and fluid source isotopic signatures. The sulfur isotopes in this system reveal that the sulfides have a somewhat meteoric signature. Barites typically average around 26 per mil, with the sulfides averaging around 16 per mil. At this point, the sulfur isotopes are not conclusive enough to differentiate between the two orebodies, although numbers from the sulfide and sulfate-sulfide geothermometry average approximately 419 ^{o}C. This temperature is

high for most Carlin-type systems, and could reflect the isotopic exchange between the magmatic system and the later Carlin-type system.

Discussion

Evidence supporting the discussion that follows is summarized as:

- Relationships of mineralized structures to the Cretaceous intrusive rocks
- Observed cross-cutting relationships in the various styles of Au mineralization
- Presence of another clearly Carlin-type orebody along the same structural trend
- Likelihood of at *least* two heating and cooling episodes in the last 100 Ma. Indicated by AFTA

Based on the data presented, the timing constraints for the development of the Archimedes system are as follows. The first mineralizing event at Archimedes took place around 106 Ma with the emplacement at some depth of the Graveyard Flats/Bullwhacker Sill quartz monzonites. The timing of this event is well-understood from radiometric dating (Vikre, 1998). This intense heating and release of magmatically-derived fluids into relatively clean carbonate rocks produced the garnet-dominant calcic skarn that is seen in the deep portions of East Archimedes. During retrograde cooling of the magmatic/hydrothermal system, sulfide minerals of Pb, Zn, and Cu were deposited along with lower temperature alteration assemblages in the skarn. As much as 60 Ma later, a new pulse of magmatism began in the Eureka area. This 40-30 Ma period roughly coincides with the Pinto Peak volcanics as well as the Richmond andesites to the east (Blake et al., 1975). It is believed that during this time, meteoric waters convecting from

deeper in the crust came up along preexisting structures around the Graveyard Flats intrusion and into the same Ordovician carbonates as the original Cretaceous skarn. These gold-bearing fluids used extension-related NS faults as well as the older EW trending Blanchard fault to ascend to the still-reactive carbonates. Some of the displacements on these mineralized post-intrusion faults are well-understood from drilling and are clearly offsetting the Bullwhacker Sill, most notably the Holly-150 system. These fluids also appear to have locally pooled against the underside of the Bullwhacker Sill, producing the Ruby Deeps orebodies. The skarn was overprinted at depth, particularly near the Blanchard Fault, with a more Carlin-type assemblage including sooty arsenian pyrite/marcasite, orpiment/realgar, and barite. Locally, garnet replacement textures are well-developed and provide excellent arguments for an overprinting event. At higher levels and particularly along structures, development of jasperoids were pervasive and resulted in the high-grade oxidized portions of Archimedes (Dilles et al., 1996). Post-mineral faulting then dropped down the Archimedes deposit to the east and is probably responsible for its preservation near the surface today. To better understand why this explanation best fits the observations, it is important to look at the many similarities and then to define the key differences.

Variations in the mineralization and alteration seen within the Archimedes system could theoretically all be classified as different types of systems, were they to be observed with no context. This is the main problem in dealing with questions of classification in ore deposits. Because it is sometimes advantageous in exploration for ore deposits to develop models for their development and locations, the attempt to pigeonhole systems sometimes forces the interpretation of their characteristics. Perhaps

in some cases it is more useful to observe the characteristics and make interpretations regarding the ore-forming processes, which are more important than the classification itself. Trying to fit a deposit into a stringent set of classifying rules limits the interpretation and the assumptions that can lead to intuitive discoveries. Thus, rather than making the geology try to fit a model, it is more useful to compare the alteration styles and overprinting characteristics of Archimedes to both skarn and Carlin-type systems and identify their similarities and dissimilarities. Distinctly different alteration assemblages and mineralization types occur in the Archimedes system and exhibit characteristics that can be found in several different types of gold deposits in Nevada. The controversy that surrounds the Archimedes deposit regarding its genesis is due mainly to the similarities between Au-rich distal disseminated carbonate replacement deposits, disseminated Au-rich skarns, and Carlin-type deposits associated with possible intrusives at depth. In Archimedes, all of these characteristics can occur within 500 m of each other, and thus add to the confusion. While precise dating and unequivocal evidence for their genesis cannot be determined through this study, there are several lines of evidence to support the conclusion that Archimedes and Ruby Deeps are not part of the Cretaceous magmatic-hydrothermal associated with the Graveyard Flats intrusive. The aforementioned timing constraints, the paragenetic relationships in mineralized zones, and a comparative study are all supportive of this claim.

Archimedes as a Skarn

Earlier work has called into question the similarity of Archimedes to the distal and disseminated gold mineralization found in some skarns (Margolis, 1996). The

primary evidence used in this case was the compelling geochemical relationships in the ore zones as well as the proximity to the Graveyard Flat intrusion. Thus, it is a major objective of this study to provide evidence that either proves or disproves the relationship of the Archimedes system to the Cretaceous base-metal sulfide rich skarn to the east. Much can be gleaned about the relationships between the two systems by examining the characteristics of well-known gold skarns and comparing them to what is seen at Archimedes. Gold skarns can be broken up into two distinct groups based on their relative oxidation state: reduced and oxidized gold skarns (Meinert, 1992). Characteristics of each type are listed in Table 3. The reduced skarns are characterized by higher grades, reduced ilmenite-bearing diorite-granodiorite plutons and dike/sill complexes, and high-Fe pyroxene dominant calc-silicate assemblages. The classic example of this type is the Nickel Plate mine in the Hedley District, British Columbia (Meinert, 1992).

Table 3. Comparison of different types of Au skarns (Meinert, 1992)

Characteristic	Calcic Reduced	Calcic Oxidized
Metals mined	Au, Ag	Au
Avg Size, Grade	.2 Mt; 9g/t Au, 5 g/t Ag	.4 Mt; 4 g/t Au
Examples	Fortitude, NV; Crown Jewel, WA; Elkhorn & Beal, MT	McCoy, NV; Nambija, Ecuador
Associated Intrusive	reduced, ilmenite-bearing granodiorite plutons	oxidized diorites and granodiorites
Protolith	clastic-rich limestones	massive limestone/dolostone
Alteration	Wide hornfelsed halos (100's of meters); marbleization; Low garnet/pyroxene ratios	dolomitization; jasperoid formation; skarning; high garnet/pyroxene ratios
Ore minerals	abundant sulfides (pyrrhotite, arsenopyrite) with dominant pyrrhotite; gold is associated with pyrrhotite and small amounts of chalcopyrite, arsenopyrite, and bismuth minerals	low total sulfides; ubiquitous minor chalcopyrite, sphalerite, galena; pyrite is dominant Fe-sulfide; gold associated with K-feldspar and quartz
Geochemistry	distinctive Au-Bi-Te-As signature	variable; some described as having Au-Mo-As-Bi-Sb signatures

A relevant example of gold mineralization associated with Cretaceous intrusions is that found in the Robinson district just east of Archimedes outside of Ely, Nevada. Robinson well-known for its world-class copper production as well as its complexity of multiple ore deposit types. Robinson contains porphyry copper mineralization, iron-oxide-copper-gold skarns, and jasperoid-hosted gold mineralization (James, 1976). The gold deposits have been described as being very similar to Carlin-type deposits, yet are believed to be related to the multiple Cretaceous intrusions responsible for the porphyry-copper mineralization (Albino, 1995). The Kranovich deposit in particular bears many similarities to Carlin-type systems. Eleven of these small deposits are concentrated on the eastern margins of the intrusive complex at Robinson. Disseminated gold mineralization

is hosted in Devonian-aged decalcified and silicified calcareous limestones as well as Permian sandstones. Locally, host rocks are moderately to strongly argillized. Gold deposits in most cases lie immediately adjacent to copper mineralization controlled by a combination of structural and stratigraphic features generally in shallow-dipping tabular form (Seedorff, 2000). The deposits are deeply oxidized to the point of almost no preservation of original sulfides. However, these deposits are believed to be genetically related to the Cretaceous magmatism. Their spatial distribution outboard of the main copper ore zones is consistent with their interpretation as distal disseminated deposits related to the magmatic-hydrothermal system. Also, they are found to be associated with enriched base-metals, bismuth, and tellurium, which is more consistent with distal disseminated gold deposits (Albino, 1995).

Another local example is the Fortitude gold skarn found in Northern Nevada. There are some general geologic characteristics that are used to classify these systems that can be compared to Archimedes. Firstly, Archimedes is associated with a quartz monzonite intrusive, rather than a more reduced ilmenite-bearing granodiorite. The skarns at Fortitude and Hedley also have a relatively characteristic calc-silicate skarn assemblage. This assemblage is pyroxene-rich and garnet poor, with a biotite ± K-feldspar distal alteration assemblage. Both at Fortitude and Hedley, gold grades increase in assemblages where pyroxene is the dominant calc-silicate phase. In Fortitude's main ore zone, pyroxene is iron-rich and exhibits a silver enrichment on the most distal margins of the skarn (Kotlyar *et al.,* 1998). Pyrrhotite along with pyrite, marcasite, loellingite, and arsenopyrite are the dominant sulfides in the ore zones of these deposits (Meinert, 1998). Other sulfides that are commonly present include chalcopyrite, pyrite,

sphalerite, hedleyite ($Bi_{2+X}Te_{1-X}$), native bismuth, gold, galena, and maldonite (Au_2Bi) (Ettlinger, 1990). Elevated bismuth is a uniform characteristic of all of these systems, and generally is the best indicator of high grade gold zones. Commonly, native bismuth and coarse bismuthinite are described in the highest grade intervals within several of these deposits (Meinert, 1992). Few of these characteristics occur at Archimedes.

The oxidized gold skarns are a group classified based on their dramatically different mineralogy and alteration styles (Brooks, 1991). However, the Cove-McCoy system in Northern Nevada serves as an excellent example thanks both to its proximity and similarities to Carlin-type deposits. Moreover, McCoy has been well-studied and the temporal and spatial relationship between gold mineralization and the petrology of the associated intrusive rocks is well constrained (Brooks, 1994). McCoy is centered around the Brown Stock, a relatively reduced hornblende-biotite granodiorite dated at about 39 Ma. This deposit exhibits alteration zoning that is very different from that of the reduced skarns. The most distal alteration is early hornfelsing with biotite and hornblende. The hornfelsing is overprinted approaching the intrusive contact by a garnet-dominant assemblage that is comprised of andraditic garnet with minor pyroxene (Meinert, 1998). Zones most proximal to the intrusive show complete obliteration of primary sedimentary structures by massive garnet – pyroxene skarn, with the highest pyroxene concentrations occurring in this zone (around 10%) (Brooks, 1994). Later retrograde alteration overprints the massive garnet skarns with a quartz ± pyrite ± kaolinite ± K-feldspar assemblage which is not altogether unlike that of some Carlin-type deposits (Johnston, 2003).

The Cove deposit is a gold deposit that appears to be intimately related to the McCoy system and occurs more distally from the intrusive. Silicification is commonly expressed as jasperoids in the distal Carlin-style orebodies at Cove. The jasperoids are auriferous, enriched in manganese, and appear to be comprised of silicified dissolution-collapse breccias of the original carbonate units (Johnston, 2003). The similarities between this and the observed textures at Archimedes are apparent. The decarbonatized limestones at McCoy are also very similar to those seen at Archimedes, particularly the sanding textures due to liberation and accumulation of insoluble quartz during removal of carbonate. Another compelling similarity of the oxidized skarns to the mineralization at Archimedes is the fact that gold mineralization is not always associated with sulfide assemblages dominated by pyrrhotite. Pyrite is generally dominant to pyrrhotite in these deposits (Meinert, 1992). Also, gold is present as lower grade, disseminated mineralization associated with pyrite and not calc-silicate dominant skarn rocks (Brooks, 1994). Sulfides present at McCoy include, pyrite, pyrrhotite, sphalerite, galena, arsenopyrite, chalcopyrite, bornite, gold, hedleyite, native bismuth, and hessite (Brooks 1994). The elevated Bi values are accompanied by high Mn, Cu, Pb, Zn, and Ag (Johnston, 2003). Archimedes also displays elevated values in these elements (except for Ag), most notably an enrichment in Mn.

Both Archimedes and Cove-McCoy have distal auriferous jasperoids, gold-rich skarns at depth, similar alteration styles, and similar mineralogies. Perhaps the most compelling argument is the simple fact that there is a definite spatial relationship to the Graveyard Flats intrusive. However, there are several dissimilarities. For example, Archimedes lacks an abundance of bismuth minerals or significant biotite hornfels. Also,

there has been no pyrrhotite discovered at Archimedes, whereas in every other gold skarn it is considered a major sulfide phase. In addition, alteration and mineralogy at the Ruby Deeps orebody is very different from anything described at Cove-McCoy and many other reduced gold skarns.

Archimedes as a Carlin-type deposit

Although Archimedes displays characteristics similar to those of some disseminated oxidized gold skarns, it is useful to attempt to reinterpret these features as related to a later Carlin-type event. Whereas the geochemistry and skarn minerals present at Archimedes serve to support its origins as an oxidized gold skarn, they can potentially be explained by the process of overprinting. As was mentioned earlier, the most positive correlations with gold values are As, Hg, Tl, Ba, and Sn, despite the enrichment in other elements such as Bi, Pb, Zn, Ag, and Mn. Widespread enrichment in elements that are diagnostic of skarns in general could potentially reflect mobility of these elements as the later Carlin-type fluids pulsed through the skarn. Warm, acidic fluids pulsing through a pre-existing skarn can be demonstrated to have replaced the original garnet textures and potentially remobilize or redeposit elements distally from the actual skarn. While speculative, the overprinting textures are well-developed and the possibility of remobilization of skarn related elements cannot be ruled out. The more correlative elements suggest its origins as a Carlin-system.

Most deposits that are considered Carlin-type lack any sort of obvious genetic relationship to intrusive rocks (Weiss et al., 2000). There has been substantial discussion

on the so-called Carlin-type deposits that are closely associated with Eocene-Miocene intrusive rocks. Additionally, extensive discourse has developed regarding the classification of these sedimentary-rock hosted gold deposits as Carlin-type rather than simply distal disseminated deposits related to a magmatic-hydrothermal system. The discussions that take place in the literature regarding the nomenclature of these deposits are many and widely variable. There has also been much controversy regarding studies focused on determining origins of the sediment-hosted gold deposits of Nevada. Recent data regarding δD and δO isotopic ratios in ore-stage minerals tends to be more conclusive, but has not been performed widely. Use of these isotopic studies to denote the presence of magmatic or meteoric waters seems to work for some deposits and remain inconclusive for others. The most convincing example of this isotopic characteristic is found at the Deep Star deposit (Folger et al., 2000). In Deep Star, values of fluids that produced ore-stage kaolinite appear to be zoned from the center of the orebody outward (Heitt et al., 2003). Kaolinites at the center of the deposit appear to plot near the magmatic water field while waters on the periphery have a more mixed appearance. The implications for this are potentially great, due to the fact that Deep Star occurs in what could be interpreted as one of the main feeder zones for the entire Carlin-trend (Heitt et al., 2003). The localized depletions in stable isotopes of O and C that are found in Archimedes are indicative of isotopic exchange with either magmatic or deep-cycled meteoric fluids. Their association with mineralized faults such as the Holly-150 fault system offers some intuition as to the fact that it was later Carlin-style fluids that influenced the isotopic exchange associated with the gold mineralization at Archimedes. Other than the timing constraints of occurring between the late Cretaceous intrusion of

the Graveyard Flats/Bullwhacker Sill intrusion and the Oligocene-Eocene extension-related faults that are mineralized, there is still little known about the exact age of Archimedes. As the AFTA data show, multiple heating and cooling events have likely affected the northern Eureka district. This includes loosely-bracketed periods of heating and cooling in both the Cretaceous and the Oligocene-Eocene. Therefore, while it does not rule out the possibility of Archimedes as a Cretaceous distal disseminated deposit, it does provide evidence for other events that could have been responsible. The fact that many of the apatite grains displaying this strong bias towards an Oligocene-Eocene event were partially dissolved and reprecipitated by hydrothermal fluids is a compelling line of evidence as well. Another powerful argument for the temporal relationships suggested by this study comes from characteristics and paragenetic relationships observed in the different ore-zones.

As noted, the alteration styles and mineralogy of Archimedes are very similar to those developed in other deposits traditionally described as Carlin-type. These deposits are described as sedimentary rock-hosted, stratigraphically and structurally controlled, disseminated gold deposits (Arehart, 1996). Archimedes has been shown to exhibit these characteristics, and they have been known for a number of years by those who've worked at the mine. However, the fact that Archimedes meets these three generalized requirements is not conclusive in of itself. Other compelling qualities that might classify Archimedes as a Carlin-type deposit are the morphologies of the gold mineralization, the definitive Carlin-style textures within ore zones, and the geochemical characteristics of altered rock in the deposit. Also, the relatively new discovery of the Ruby Deeps mineralization provides what is almost incontrovertible evidence linking Archimedes to

other Carlin-type systems. While the auriferous jasperoids and decalcified limestones of Archimedes are relatively similar to distal portions of carbonate replacement deposits or oxidized gold-bearing skarns, the style of alteration and mineralization in Ruby Deeps is almost exclusively Carlin-style. Ruby Deeps exhibits decarbonatization, collapse-dissolution, and extensive barite-calcite development. These bear striking resemblances to the post-ore dissolution-collapse breccias found at the Meikle and Deep Post deposits (Emsbo & Hofstra, 2003). Also, ore horizons in Ruby Deeps often have a strong positive correlation between As and Au. Development of extensive orpiment/realgar as a relatively late phase in the gold mineralizing event is characteristic that is similar to other intrusive-related Carlin-type deposits such as the Betze-Post and Deep Star systems (Heitt et al., 2003). Other examples of Carlin-type systems associated with Eocene intrusive rocks include the Meikle, Griffin, Genesis, and Beast deposits which are all partially hosted in coeval Eocene dikes (Johnston, 2003, Heitt et al., 2003, Ressel et al., 2000b). While these systems all occur in or around these Eocene intrusive rocks, there are very few mentions of overprinted skarn mineralization associated with high-grade gold mineralization. The coincidence of the pulse of Eocene magmatism in Eureka, if nothing else, offers a contemporaneous heating event that is roughly coeval with AFTA results found in the Bullwhacker Sill. It is generally accepted that the deposits of the Carlin trend are related to a widespread pulse of magmatism in the Eocene (Arehart et al., 2000, Hofstra, 1994). Much of the constraints on ages come from cross-cutting relationships of Eocene intrusive rocks as well as dating of ore-stage galkhaite on Getchell, Twin Creeks, and Rodeo (Tretbar, 2001). There are no mentions in literature of Carlin-type deposits associated with Cretaceous magmatism. This does not preclude that a Cretaceous Carlin-

type system is impossible. The close association of Archimedes with a Cretaceous intrusive does not fit with any other known Carlin-type system in Nevada, and thus its contemporaneity is immediately suspect.

It is proposed through this study that the Archimedes system as a whole encompasses both the West and East Archimedes orebodies, as well as the Ruby Deeps mineralization. These orebodies all appear to have been controlled by the Blanchard fault system, as well as other N-NE trending extension-relate faults. The disseminated gold mineralization occurs along structures that cut the Graveyard Flats intrusive and the Bullwhacker Sill at depth. It is difficult to reconcile this with the interpretation of some sort of syn-genetic mineralizing event for Archimedes. The similarities between Archimedes and other Carlin-type systems are too many to be ignored, and the close association of it with a Cretaceous intrusive is not enough evidence to provide for interpretation as a distal part of a magmatic-hydrothermal system.

Conclusions

The “Carlin-style” mineralization of the Archimedes and Ruby Deeps orebodies is not related to Cretaceous magmatism in the northern Eureka District. As much as 60 million years later, data suggests that renewed magmatism in the area was associated with the development of a new hydrothermal system around the original Graveyard Flats intrusive. This new system was likely derived from convecting meteoric waters and developed a Carlin-type system in the structurally complex area around the intrusive. Thus, the Pb-Zn skarn at depth is Cretaceous, but exhibits an Oligocene-Miocene overprint that developed locally as a result of Carlin-style mineralizing fluids. The Ruby

Deeps mineralization is a well-preserved representative of deeper, sulfide-rich Carlin-type mineralization. Ruby Deeps also does not display any of the unusual skarn-related mineralogy or geochemistry. The variations in the appearances of different parts of the Archimedes system were likely produced by fluids interacting with different mineralogy and fluids at different levels within the system. The same can be said for the highly variable geochemistry of the deposit. Mobility and redistribution of original elements associated with skarning was likely the culprit for the unusual geochemistry and mineralogy seen in Archimedes. Bimodal Oligocene-Miocene volcanics are likely surficial expressions of the heat engine that drove the hydrothermal system responsible for Archimedes. Results from AFTA on the Bullwhacker Sill at depth show multiple cooling events, with a particularly intense period taking place in the Eocene-Miocene time. This period can only be attributed to hydrothermal fluids from the developing Carlin-type system. Archimedes exhibits many of the characteristics of porphyry-related, distal-disseminated gold deposits, but also several key differences. However, due to the lack of hard evidence regarding a direct heat source to drive the mineralization, Archimedes can be classified in the same scheme with traditional Carlin-type deposits.

Works Cited

Albino, G. V., 1995, Porphyry Copper deposits of the Great Basin—Nevada, Utah and adjacent California in Porphyry Copper deposits of the American Cordillera, Arizona Geological Society Digest 20, Pierce, F. W., and Bolm, J. G., ed.

Arehart, G.B., 1996, Characteristics and origin of sediment-hosted disseminated gold deposits: a review: Ore Geology Reviews, v. 11, p. 383-403.

Arehart, G.B., Chakurian, A.M., Tretbar, D.R., Christensen, J.N., Donelick, R.A. and McInnes, B.A., 2003, Evaluation of radioisotope dating of Carlin-type deposits in the Great Basin, western North America, and implications for deposit genesis; Economic Geology, v. 98, p. 235-248.

Armstrong, R.L., 1970. K-Ar dating using neutron activation for Ar analysis: comparison with isotope dilution Ar analysis: Geochimica et Cosmochimica Acta, v. 34, p. 233-236

Bau M., 1991., Rare-earth element mobility during hydrothermal and metamorphic fluid-rock interaction and the significance of the oxidation state of europium. Chemical Geology 93 (3-4): 219 - 230.

Blake, M.C., McKee, E.H., Marvin, R.F., Silberman, M.L., and Nolan, T.B., 1975, The Oligocene volcanic center at Eureka, Nevada: U.S. Geological Survey Journal of Research, v. 3, no. 5, p. 605412.

Blakey, R., (2006) Geologic History of the Western U.S. Retrieved January 8th from Northern Arizona University's Department of Geology Website: http://jan.ucc.nau.edu/~rcb7/RCB.html

Brooks, J.W., Meinert, L.D., Kuyper, B.A., and Lane, M.L., 1991, Petrology and geochemistry of the McCoy gold skarn, Lander County, NV: in Raines, G.L., Lisle, R.E., Schafer, R.W., and Wilkinson, W.H. (eds.), Geology and Ore Deposits of the Great Basin, Geol. Soc. Nevada, Reno, v. 1, p. 419-442.

Brooks, J.W., 1994. Petrology and geochemistry of the McCoy gold skarn, Lander County, Nevada. Unpublished Ph.D. thesis, Washington State University, Pullman, Washington, 607 p.

Burchfiel, B.C., Cowan, D.S., and Davis, G.A., 1992, Tectonic overview of the Cordilleran orogen in the Western United States, *in* Burchfiel, B.C., Lipman, P.W., and Zoback, M.W., editors, The Cordilleran orogen: Conterminous U.S.: Geological Society of America, The Geology of North America, v. G-3, p. 407-480

Christiansen, R.L., and Yeats, R.S., 1992, Post-Laramide geology of the U. S. Cordilleran region: Geological Society of America, American Geology of North America, v. G-3, p. 261–406.

Curtis, J.S., 1884, Silver-lead deposits of Eureka, Nevada: U.S. Geologic Survey Monograph 7, 200 p.

Dilles, P.A., Wright, W.A., Monteleone, S.E., Russell, K.D., Marlowe, K.E., Wood, R.A., and Margolis, J., 1996, The geology of the West Archimedes deposit: a new discovery in the Eureka mining district, Eureka County, Nevada *in* Coyner, A.R., and Fahey, P.L., eds., Geology and Ore Deposits of the American Cordillera: Geological Society of Nevada Symposium Proceedings, Reno/Sparks, Nevada, April 1995, p. 159-171.

Duddy, I.R., 2006, Thermal history reconstruction in the Ruby Hill area using apatite fission track analysis (AFTA); Geotrack Report 973, 113 pages.

Emsbo, P., Hofstra, A.H., Origin and Significance of Postore Dissolution Collapse Breccias Cemented with Calcite and Barite at the Meikle Gold Deposit, Northern Carlin Trend, Nevada; Economic Geology, v. 98; no. 6; p. 1243-1252

Ettlinger, A.D., 1990, A geological analysis of gold skarns and precious metal enriched iron and copper skarns in British Columbia, Canada; Unpublished Ph.D. Thesis, Washington State University , 246 pages.

Fletcher, C.C. and Pollard, D.D., 1981, Anticrack model for pressure solution surfaces; Geology, Vol. 9, pp. 419-24.

Folger, H.W., Hofstra, A.H., and Cline, J.S., 2000, Alteration and mass transfer in igneous dikes at the Getchell Carlin-type gold deposit, Nevada, *in* Cluer, J.K., Price, J.G., Struhsacker, E.M., Hardyman, R.F., and Morris, C.L., eds., Geology and Ore Deposits 2000: The Great Basin and Beyond, May 15-18, 2000: Reno, Nevada, Geological Society of Nevada, Symposium Proceedings, p. A4.

Gallagher, K., 1995. Evolving temperature histories from apatite fission-track data: Earth and Planetary Science Letters, vol. 136, Issue 3-4, pp.421-435

Grauch, V.J.S., Rodriguez, B.D., Wooden, J.L., 2003, Geophysical and Isotopic Constraints on Crustal Structure Related to Mineral Trends in North-Central Nevada and Implications for Tectonic History, Economic Geology; v. 98; no. 2; p. 269-286

Hague, A., 1892, Geology of the Eureka District, Nevada., U.S. Geological Survey Monograph 20, 419 p.

Heitt, D.G., Dunbar, W.W., Thompson, T.B., Jackson, R.G., 2003, Geology and Geochemistry of the Deep Star Gold Deposit, Carlin Trend, Nevada. Economic Geology, Vol. 98, 2003, pp. 1107–1135

Hofstra, A.H., 1994, Geology and genesis of the Carlin-type gold deposits in the Jerritt Canyon district, Nevada: Boulder, Colorado, University of Colorado, Ph.D. dissertation, 719 p.

Hofstra, A.H., Snee, L.W., Rye, R.O., Folger, H.W., Phinisey, J.D., Loranger, R.J., Dahl, A.R., Naeser, C.W., Stein, H.J., and Lewchuk, M., 1999, Age constraints onf Jerritt Canyon and other Carlin-type gold deposits in the western United States: Relationship to Mid-Tertiary extension and magmatism: Economic Geology, v. 94, p. 769-802

Holland, P.T., Beaty, D.W., and Snow, G.G., 1988, Comparative elemental and oxygen isotope geochemistry of jasperoid in the northern Great Basin; evidence for distinctive fluid evolution in gold-producing hydrothermal systems: Economic Geology, v. 83, p. 1401-1423

Jaffee, J.W., and others, 1959, Lead-alpha determinations of accessory minerals of igneous rocks(1953-1957): U.S. Geologic Survey Bulletin 1097-B. p. 65-148

James, L.P., 1976, Zoned Alteration in Porphyry Copper Deposits, Ely, Nevada: Economic Geology, v. 71, p. 488-512

Johnson, T.W., 2000, Metal and mineral zoning at the Greater Midas Au-Cu-Ag skarn deposit (Battle Mountain district), Lander County, Nevada, in Cluer, J.K., Price, J.G., Struhsacker, E.M., Hardyman, R.F., and Morris C.L., eds., Geology and ore deposits 2000: The Great basin and beyond: Symposium, Reno/Sparks, Nevada, Proceedings, v. 1, p. 1083–1106. Kotlyar, B.B., Theodore, T.G., Singer, D.A., Moss, K., Campo, A.M.,

Johnston, Marcus K., 2003, Geology of the Cove Mine, Lander County, Nevada, and a Genetic Model for the McCoy-Cove Magmatic-Hydrothermal System, PhD. Dissertation, University of Nevada, Reno, 353 p.

Kim, E., 2007, Paragenesis and Mineral Chemistry of the Geodo Gold Skarn Deposit, Korea. Geological Society of America Abstracts with Programs, Vol. 39, No. 6, p. 625

Kotlyar, B.B., Theodore, T.G., Singer, D.A., Moss, K., Campo, A.M. & Johnson, S.D. (1988): Geochemistry of the gold skarn environment at Copper Canyon, Battle Mountain mining district, Nevada. In Mineralized Intrusion-Related Skarn Systems (D.R. Lentz, ed.). Min. Assoc. Can. Short Course 26, p. 415-443.

Langlois, J.D., 1971, Hydrothermal alteration of intrusive igneous rocks in the Eureka mining district, Nevada [M.S. thesis]: University of Arizona, 113 p.

Laslett, G.M., Green, P.F., Duddy, I.R. & Gleadow, A.J.W. 1987. Thermal annealing of fission tracks in apatite 2. A quantitative analysis. *Chemical Geology (Isotope Geoscience Section)*, 65, 1-13.

Lovering, T.G., 1962, The origin of jasperoid in limestone, Economic Geology, v. 57, no. 6, pp. 861-879

Margolis, J., 1997, Gold paragenesis in intrusion-marginal sediment-hosted gold mineralization at Eureka, Nevada, *in* Vikre, P., and others, eds., Carlin-type Gold Deposits Field Conference: Society of Economic Geologists, Guidebook Series Volume 28, p. 213-221

McKee, E.H., Silberman, M.L., Marvin, R.F., and Obradovich, J.D., 1971, A summary of radiometric ages of Tertiary volcanic rocks in Nevada and eastern California, Part I, central Nevada: Isochron/West, no. 2, p. 21-42

Meinert, L.D., 1992, Skarns and skarn deposits: Geoscience Canada, v. 19, p. 145-162.

Meinert, L.D., 1998, A review of skarns that contain gold, in Lentz, D.R., ed., Mineralized intrusion-related skarn systems: Mineralogical Association of Canada Short Course Series, v. 26, p. 359–414.

Miller, E.L., Miller, M.M., Stevens, C.H., Wright, J.E., and Madrid, R., 1992, Late Paleozoic paleogeographic and tectonic evolution of the western U.S. Cordillera, in Burchfiel, B.C., Lipman, P.W., and Zoback, M.L., eds., The Cordilleran orogen: Conterminous U.S.: Geological Society of America, The Geology of North America. v. G-3, p. 57–106.

Mollinelli, L., 1879, Eureka and its resources: Eureka, Nevada, Molinelli, Lambert, and Co., reprinted by Univ. of Nev. Press, 1982

Myers, G.L., 1994, Geology of the Copper Canyon-Fortitude skarn system,Battle Mountain, Nevada: Unpublished Ph.D. thesis, Pullman, Washington, Washington State University, 356 p.

Nakamura, N., Determination of REE, Ba, Fe, Mg, Na and K in carbonaceous and ordinary chondrites, Geochimica et Cosmochimica Acta, vol. 38, Issue 5, pp.757-775

Nutt, C.J., Hofstra, A.H., Hart, K.S., and Mortensen, J.K., Structural setting and genesis of gold deposits in the Bald Mountain-Alligator Ridge area, east-central Nevada, Geology and Ore Deposits 2000: The Great Basin and Beyond, May 15-18, 2000: Reno, Nevada Geological Society of Nevada Symposium Proceedings, p 513-537

Nolan, T.B., 1962, The Eureka Mining District Nevada: U.S. Geological Survey Professional Paper 406, 78 p.

Nolan, T.B. and Hunt, R.L., 1968, The Eureka Mining District, Nevada, in Ore Deposits of the United States, v. 1, J.D. Ridge (ed.): New York, Am. Inst. Mining Engineers, p. 966-991

Oldow, J.S., 1984, Spatial variability in the structure of the Roberts Mountains allochthon, western Nevada: Geological Society of America Bulletin, v. 95, p. 174-185.

Ray, G.E., Webster, I.C.L., Dawson, G.L., and Ettlinger, A.D., 1993, A Geological Overview of the Hedley Gold Skarn District, Southern British Columbia; B.C. Ministry of Energy, Mines and Petroleum Resources, Paper 1993-1, pages 269-279.

Ressel, M.W., Noble, D.C., Henry, C.D., and Trudel, W.S., 2000b, Dike-hosted ores of the Beast deposit and the importance of Eocene magmatism in gold mineralization of the Carlin trend, Nevada: Economic Geology, v. 95, p. 1417-1444.

Robinson, B. W., 1975, Carbon and oxygen isotope equilibria in hydrothermal calcite[abs.]: Geochemical Journal, v. 9, p. 43046

Russel, K., 1996, West Archimedes Gold Deposit, in Green, S.M., and Struhsacker, E., eds., Geology and Ore Deposits of the American Cordillera: Geological Society of Nevada Field Trip Guidebook Compendium, 1995, Reno/Sparks, NV, v. 1, p. 316-319

Russel, K., Chadwick, T., 2002, Unpublished geologic mapping of the Archimedes pit, Ruby Hill Mine, Eureka, Nevada

Ohmoto, H. and Rye, R.O. (1979) Isotopes of sulfur and carbon: in H.L. Barnes ed., Geochemistry of Hydrothermal Ore Deposits, Second Edition: John Wiley & Sons, 509-567.

Scambelluri, M., Rampone, Elisabetta, Piccardo, G.B., Fluid and element cycling in subducted serpentinite; a trace-element study of the Erro-Tobbio high-pressure ultramafites (Western Alps, NW Italy) in Orogenic lherzolites and mantle processes, Anonymous,) Journal of Petrology (January 2001), 42(1):55-67

Seedorff, E., 1991a, Magmatism, extension, and ore deposits of Eocene to Holocene age in the Great Basin--Mutual effects and preliminary proposed genetic relationships, *in* Raines, G. L., Lisle, R. E., Schafer, R. W., and Wilkinson, W. H., eds., Geology and ore deposits of the Great Basin: Geological Society of Nevada, Symposium, Reno/Sparks, April 1990, Proceedings, v. 1, p. 133-178.

Seedorff, E., 2000b, Summary of the gold-silver deposits of the Robinson district, with descriptions of the Northwest Ruth, J. D. Hill, and Star Pointer deposits, *in* Gans, P. B., and Seedorff, E., eds., Cenozoic tectono-magmatic evolution of White Pine County, Nevada: Core complexes, Eocene-Oligocene volcanic centers, episodic extension and shortening, and disseminated gold deposits: Geological Society of Nevada Symposium 2000 Field Trip Guidebook No. 11, p. 141-166.

Speed, R.C., Sleep, N.H., 1982, Antler orogeny and foreland basin; a model, Geological Society of America Bulletin, v. 93, p. 815-828

Theodore, T.G., and Blake, D.W., 1975, Geology and geochemistry of the Copper Canyon porphyry copper deposit and surrounding area, Lander County, Nevada: U.S. Geological Survey Professional Paper 798-B, 86 p.

Tosdal, R.M., Wooden, J.L., and Kistler, R.W., 2000, Inheritance of Nevadan mineral belts from Neoproterozoic continental breakup, *in* Cluer, J.K., Price, J.G., Struhsacker, E.M., Hardyman, R.F., and Morris, C.L., eds., Geology and Ore Deposits 2000: The Great Basin and Beyond: Geological Society of Nevada Symposium Proceedings, May 15-18, 2000, p. 451-466.

Tretbar, D., 2001, The distribution, chemistry, and dating of galkhaite, an uncommon but important accessory mineral in Carlin-type gold deposits: Geological Society of Nevada Membership Directory 2001-2002, p. 95-96

Vazquez, R., Venneman, T.W., Kesler, S.E., Russell, N., 1998, Carbon and Oxygen Isotope Halos in the Host Limestone, El Mochito Zn-Pb-(Ag) Skarn Massive Sulfide-Oxide Deposit, Honduras; Economic Geology, v. 93, 1998, pp. 15-31

Vikre, P.G., 1998, Intrusion-related, polymetallic carbonate replacement deposits in the Eureka District, Eureka County, Nevada., Nevada Bureau of Mines and Geology., Bulletin 110, 52 p.

Weill, D.F., Drake, M.J., 1973, Europium Anomaly in Plagioclase Feldspar: Experimental Results and Semiquantitative Model; Science 180 (4090): 1059 – 1060

Weiss, S. I., Percival, T.J., Noble, D.C., and Ressel, M.W., 2000, The “Carlin-type” – “Carlin-like” dichotomy revisited: The general association of sedimentary rock-hosted gold deposits with magmatic activity, *in* Cluer, J.K., Price, J.G.,

Struhsacker, E.M., Hardyman, R.F., and Morris, C.L., eds., Geology and Ore Deposits 2000: The Great Basin and Beyond, May 15-18, 2000: Reno, Nevada, Geological Society of Nevada, Symposium Proceedings, p. A4.

Williams, C.L., Thompson, T.B., Powell, J.L., Dunbar, W.W., 2000, Gold-Bearing Breccias of the Rain Mine, Carlin Trend, Nevada; Economic Geology, v. 95, 2000, pp. 391-404

Wilson, W.L., 1986, Geology of the Eureka-Windfall gold deposit, *in* Tingley, J.V., and Bonham, H.F., Jr., eds., Sediment-hosted precious-metal deposits of Northern Nevada: Nevada Bureau of Mines and Geology Report 40, p. 81-82

Zoback, M. L., McKee, E.H., Blakey, R.J., and Thompson, G.A., The northern Nevada rift; regional tectono-magmatic relations and middle Miocene stress direction, Geological Society of America Bulletin, vol.106, no.3, pp.371-382

Appendix A – Table 4
Eureka District Whole-Rock Geochemistry
Analysis performed by ALS Chemex

Method	ME-ICP06	ME-ICP06	ME-ICP06	ME-ICP06	ME-ICP06	ME-ICP06	ME-ICP06	ME-ICP06	ME-ICP06
Sample Description	SiO2	Al2O3	Fe2O3	CaO	MgO	Na2O	K2O	Cr2O3	TiO2
	%	%	%	%	%	%	%	%	%
Richmond Mtn Rhyolite-tuff	69.4	12.65	1.51	1.1	0.64	2.19	4.68	0.04	0.09
Target Hill Rhyolite	73.3	12.85	0.78	1.08	0.12	3.16	5.04	0.02	0.07
Graveyard Flats Intrusive	68.1	15.75	2.67	3.26	0.45	3.21	3.83	0.02	0.64
Lamprophyre dike	54.8	15.05	6.89	7.08	1.64	2.11	2.65	0.01	1.27
Basaltic Andesite	60.5	14.6	6.67	5.4	3.34	2.65	3.56	0.04	0.93
Basaltic Andesite 2	61.9	15.6	6.03	4.62	1.99	2.87	3.92	0.02	0.89
Fine-Grained Basaltic Andesite	57.5	15.2	8.46	7.14	4.19	2.46	2.2	0.03	1.07
Bullwhacker Sill S.	54.4	15.25	7.21	8.63	3.99	2.07	3.48	0.02	0.73
Ruby Hill Stock	64.1	16.45	5.04	3.47	1.38	2.49	3.16	0.04	0.5
Tuff in alluvium	63.4	15.05	2.49	3.1	2.41	1.82	0.81	0.03	0.21

Method	ME-ICP06	ME-ICP06	ME-ICP06	ME-ICP06	C-IR07	S-IR08	ME-MS81	ME-MS81	ME-MS81
Sample Description	MnO	P2O5	SrO	BaO	C	S	Ag	Ba	Ce
	%	%	%	%	%	%	ppm	ppm	ppm
Richmond Mtn Rhyolite-tuff	0.06	0.03	0.01	0.03	0.06	0.01	<1	245	67.4
Target Hill Rhyolite	0.02	0.07	0.01	0.04	0.09	<0.01	<1	323	49.4
Graveyard Flats Intrusive	0.02	0.25	0.09	0.16	0.06	<0.01	<1	1425	140
Lamprophyre dike	0.11	0.39	0.07	0.15	1.2	0.18	<1	1330	105
Basaltic Andesite	0.1	0.31	0.07	0.17	0.09	0.01	<1	1530	103
Basaltic Andesite 2	0.09	0.28	0.07	0.15	0.04	<0.01	<1	1310	112
Fine-Grained Basaltic Andesite	0.1	0.27	0.09	0.11	0.06	<0.01	<1	967	103.5
Bullwhacker Sill S.	0.11	0.31	0.07	0.45	0.58	0.07	<1	4050	98.5
Ruby Hill Stock	0.07	0.23	0.06	0.13	0.04	<0.01	<1	1190	67
Tuff in alluvium	0.04	0.26	0.07	0.04	0.03	0.01	1	390	74.6

Method	ME-MS81	ME-MS81	ME-MS81	ME-MS81	ME-MS81	ME-MS81	ME-MS81	ME-MS81	ME-MS81
Sample Description	Co	Cr	Cs	Cu	Dy	Er	Eu	Ga	Gd
	ppm	ppm	ppm	ppm	ppm	ppm	ppm	ppm	ppm
Richmond Mtn Rhyolite-tuff	0.8	240	4.26	<5	5.49	3.1	0.8	18.9	6.26
Target Hill Rhyolite	1	150	3.84	<5	4.24	2.22	0.77	20	5.03
Graveyard Flats Intrusive	7.9	140	4.86	14	3.18	1.48	1.96	22.4	7.1
Lamprophyre dike	20.8	100	16.35	44	5.03	3.09	1.95	20.3	7.29
Basaltic Andesite	19.5	310	2.06	18	4.98	2.93	1.77	20.2	7.29
Basaltic Andesite 2	14	120	2	13	5.01	2.84	1.78	21.2	7.42
Fine-Grained Basaltic Andesite	27.4	230	0.84	19	4.82	2.77	1.9	19.9	7.21
Bullwhacker Sill S.	23.6	180	3.93	42	3.89	2.29	1.51	19.6	6.18
Ruby Hill Stock	7.1	270	5.19	14	4.15	2.34	1.55	20.2	5.65
Tuff in alluvium	6	220	27.7	23	4.44	2.3	1.93	20.3	6.54

Method	ME-MS81	ME-MS81	ME-MS81	ME-MS81	ME-MS81	ME-MS81	ME-MS81	ME-MS81	ME-MS81
Sample Description	Hf	Ho	La	Lu	Mo	Nb	Nd	Ni	Pb
	ppm	ppm	ppm	ppm	ppm	ppm	ppm	ppm	ppm
Richmond Mtn Rhyolite-tuff	4.4	1.08	31.7	0.44	3	33	29	<5	31
Target Hill Rhyolite	4.4	0.82	27.8	0.29	2	25.9	22.4	<5	28
Graveyard Flats Intrusive	7.7	0.53	78.9	0.14	2	34.1	52.3	7	18
Lamprophyre dike	7	1.01	53.3	0.37	2	30.1	44.9	16	89
Basaltic Andesite	6.5	1.02	54.2	0.38	2	26.6	44.1	37	65
Basaltic Andesite 2	6.8	1	59.1	0.38	3	27.2	45.8	12	16
Fine-Grained Basaltic Andesite	6.7	0.97	54.3	0.36	<2	17.5	45.5	18	18
Bullwhacker Sill S.	5.8	0.79	53.9	0.32	<2	16.4	39.1	21	17
Ruby Hill Stock	5.1	0.82	34	0.34	<2	15.9	31	9	9
Tuff in alluvium	4	0.84	44.9	0.29	<2	27.9	34	16	72
Method	ME-MS81	ME-MS81	ME-MS81	ME-MS81	ME-MS81	ME-MS81	ME-MS81	ME-MS81	ME-MS81
Sample Description	Pr	Rb	Sm	Sn	Sr	Ta	Tb	Th	Tl
	ppm	ppm	ppm	ppm	ppm	ppm	ppm	ppm	ppm
Richmond Mtn Rhyolite-tuff	8.19	169.5	6.55	3	90.4	2.8	1	26.9	0.6
Target Hill Rhyolite	6.64	221	5.25	4	105	3.2	0.81	25.7	0.8
Graveyard Flats Intrusive	15.25	133	8.52	2	825	2.2	0.84	19.4	<0.5
Lamprophyre dike	12	105	8.4	2	615	1.6	1.03	12.75	1.2
Basaltic Andesite	12	111	8.16	2	587	1.6	1.03	15.75	<0.5
Basaltic Andesite 2	12.7	117	8.47	2	599	1.6	1.05	17.4	<0.5
Fine-Grained Basaltic Andesite	12	61.4	8.34	2	826	0.9	0.97	11.35	<0.5
Bullwhacker Sill S.	10.9	117.5	6.92	2	589	1	0.82	18.4	<0.5
Ruby Hill Stock	8	110	6.37	2	555	1.2	0.81	8.94	<0.5
Tuff in alluvium	9.29	81.5	7.21	2	637	2	0.96	15.4	20
Method	ME-MS81	ME-MS81	ME-MS81	ME-MS81	ME-MS81	ME-MS81	ME-MS81	ME-MS81	ME-MS42
Sample Description	Tm	U	V	W	Y	Yb	Zn	Zr	As
	ppm	ppm	ppm	ppm	ppm	ppm	ppm	ppm	ppm
Richmond Mtn Rhyolite-tuff	0.47	7.23	<5	3	28.8	2.94	52	106	1.2
Target Hill Rhyolite	0.31	4.67	<5	2	22.8	2.02	31	101	0.9
Graveyard Flats Intrusive	0.15	2.68	37	17	14.4	0.98	61	287	0.6
Lamprophyre dike	0.37	2.41	156	7	25.7	2.41	195	263	13.8
Basaltic Andesite	0.4	3.07	115	14	26.2	2.46	125	245	8.6
Basaltic Andesite 2	0.38	3.34	104	11	25.8	2.44	91	253	1.4
Fine-Grained Basaltic Andesite	0.37	1.67	175	18	24.6	2.33	101	260	1.8
Bullwhacker Sill S.	0.31	2.98	143	14	20.5	2	100	215	1.3
Ruby Hill Stock	0.32	1.61	55	14	21.9	2.08	49	186	6.7
Tuff in alluvium	0.3	1.57	17	11	24.1	1.87	327	128	1.2

Method	ME-MS42	ME-MS42	ME-MS42	ME-MS42	ME-MS42	OA-GRA05	TOT-ICP06
Sample Description	Bi	Hg	Sb	Se	Te	LOI	Total
	ppm	ppm	ppm	ppm	ppm	%	%
Richmond Mtn Rhyolite-tuff	0.02	0.075	0.89	0.2	0.01	5.19	97.6
Target Hill Rhyolite	0.02	0.068	0.83	0.3	<0.01	1.16	97.7
Graveyard Flats Intrusive	0.02	0.013	0.6	<0.2	<0.01	1.56	100
Lamprophyre dike	0.04	0.084	2.58	<0.2	0.01	8.31	100.5
Basaltic Andesite	0.04	0.035	0.48	<0.2	0.01	1.6	99.9
Basaltic Andesite 2	0.02	0.01	0.17	<0.2	<0.01	1.32	99.8
Fine-Grained Basaltic Andesite	0.02	0.015	0.18	<0.2	<0.01	1.15	100
Bullwhacker Sill S.	0.02	0.011	0.17	<0.2	0.01	3.37	100
Ruby Hill Stock	0.06	0.014	0.73	<0.2	0.01	2.72	99.8
Tuff in alluvium	0.11	2.99	3.4	<0.2	0.02	10.05	99.8

Appendix B – Table 5. O & C Stable Isotope values for Archimedes Samples

Sample ID	Easting	Northing	Elevation	$\delta^{18}O$ **VSMOW**	$\delta^{18}O$ VPDB	$\delta^{13}C$ VPDB
06C-1146	12783.001	118446.46	5339.4029	14.1	-16.3	-4.2
06C-1166	12782.629	118442.68	5299.8136	14.1	-16.3	-3.6
06C-1330	12759.704	118209.29	5215.1859	14.5	-15.9	-2.8
06C-1604	12750.979	118120.47	4956.0874	13.3	-17.1	-5.3
06C-1808	12743.676	118046.12	4766.1842	12.8	-17.6	-2.3
06C-2060	12736.052	117968.51	4526.4074	11.4	-18.9	-0.6
09C-1258V	12089.129	118526.48	5232.4325	11.8	-18.5	1.3
09C-1258W	12104.153	118531.48	5233.8008	20.0	-10.6	0.8
09C-1379	12107.044	118504.37	5116.0837	16.1	-14.3	1.2
09C-931	12132.156	118648.79	5548.1334	15.5	-14.9	-0.6
1012-100	11262.42	120023.14	6323.49	19.8	-10.8	-0.4
1012-200	11262.42	120023.14	6223.49	16.4	-14.1	0.1
1012-300	11262.42	120023.14	6123.49	18.4	-12.2	-0.2
1012-400	11262.42	120023.14	6023.49	19.6	-11.0	-0.3
1012-600	11262.42	120023.14	5823.49	15.7	-14.8	-0.3
1012-700	11262.42	120023.14	5723.49	18.8	-11.8	1.3
11C-2035	12316.819	118636.58	4471.7593	14.0	-16.4	-3.0
1378-1100	10408.309	119619.77	5368.3649	15.9	-14.5	-0.4
1378-200	10499.699	119739.8	6255.63	17.1	-13.4	0.2
1378-300	10489.135	119726.79	6157.045	16.7	-13.8	-0.7
1378-400	10479.003	119713.43	6058.4599	16.8	-13.7	-1.1
1378-500	10467.629	119701.06	5959.8749	16.5	-14.0	-0.9
1378-600	10456.966	119688.12	5861.2899	17.2	-13.3	-1.1
1378-700	10445.629	119675.74	5762.7049	16.4	-14.1	-0.3
1378-800	10435.084	119662.71	5664.1199	16.9	-13.6	-0.8
1378-900	10421.611	119652.15	5565.5349	17.5	-13.0	-1.2
1391-1321	10679.378	120405.25	5097.0366	23.7	-7.0	1.7
1724-100	11702.383	118582.38	5840.0053	13.8	-16.6	-0.7
1724-300	11700.774	118573.35	5640.216	18.7	-11.9	0.4
1724-500	11696.557	118564.94	5440.4267	14.9	-15.5	2.5
1724-800	11692.07	118551.92	5140.7427	15.3	-15.2	1.5
1725-900	11689.85	118547.82	5040.848	16.2	-14.3	-0.6
18C-1034	12776.672	118575.26	5436.1632	14.5	-15.9	-3.9
18C-1135	12775.334	118574.34	5363.5788	14.8	-15.6	-2.0

24C-1300	8337.7917	116362.43	5339.987	18.3	-12.3	-0.3
24C-361V	8546.1411	116171.59	6240.0957	8.9	-21.3	1.4
24C-361W	8543.5421	116175.13	6242.3577	15.4	-15.1	4.7
24C-547	8475.2004	116231.03	6078.6415	23.6	-7.1	-0.1
24C-707	8427.3681	116274.89	5931.885	22.1	-8.5	0.1
24C-830V	8387.3262	116311.95	5821.5821	8.9	-21.4	2.6
24C-830W	8388.6043	116313.47	5818.3579	20.4	-10.2	-0.2
26C-1190	12443.108	118672.12	5292.7047	21.1	-9.5	1.7
26C-1270V	12441.736	118668.08	5215.5259	10.2	-20.1	1.8
26C-1270W	12442.402	118666.03	5215.526	12.2	-18.1	0.4
26C-1400	12441.253	118667.44	5085.6135	14.1	-16.3	1.8
26C-1597	12445.798	118665.15	4888.4442	16.6	-13.9	-0.6
26C-1708	12450.589	118665.55	4777.398	17.9	-12.7	0.1
271-1507	12634.218	118307.24	5054.0947	9.5	-20.8	3.9
28C-1187	12622.639	118431.46	5324.5814	14.5	-15.9	-4.6
28C-1226	12605.56	118434.75	5283.9205	14.3	-16.1	-4.5
28C-1267	12590.04	118428.89	5243.5221	13.5	-16.9	-3.1
28C-1269	12585.098	118428.62	5241.4148	14.1	-16.3	-5.3
28C-1720	12534.625	118301.02	4812.2699	21.9	-8.7	0.9
28C-1748V	12528.793	118298.46	4785.0648	13.4	-17.0	1.7
28C-1748W	12528.793	118298.46	4785.065	12.1	-18.2	1.4
290-500	11164.1	118445.03	6015.8191	16.4	-14.1	-1.1
290-600	11162.659	118426.44	5916.0175	18.0	-12.5	-1.3
301-500	10953.498	118945.54	5990.5372	17.3	-13.2	-0.3
301-600	10949.354	118930.59	5890.377	13.4	-17.0	1.0
306-600	10661.315	118644.79	5877.1072	15.7	-14.8	-1.3
30C-1071	12489.569	118620.26	5471.9333	16.3	-14.2	1.3
30C-1369	12472.976	118530.16	5188.2032	15.5	-15.0	0.7
30C-1593	12452.096	118461.54	4974.9451	15.5	-14.9	-1.7
30C-1625	12455.84	118463.45	4940.1125	16.4	-14.1	0.6
30C-1737	12461.506	118453.37	4825.6005	18.9	-11.7	-0.2
30C-987	12487.039	118686.42	5537.9979	14.8	-15.7	-4.2
RH-22	10188.148	119043	6400	16.8	-13.7	0.3
RH-23W	10615.05	118589.22	6550	18.3	-12.2	-1.4
RH-24	10357.075	118895.58	6300	19.7	-10.9	-0.9
RH-52	9940.744	119397.8	6600	11.6	-18.7	2.2
RH-53	10143.048	118824.18	6400	10.3	-20.0	2.1
RH-57	10143.048	118824.18	6500	9.6	-20.7	0.2

RH-58	9862.696	119793.66	6400	17.2	-13.3	0.0
RH-59	11128.233	118340.89	6500	11.5	-18.8	2.7
RH-60V	11165.43	118357.96	6450	20.7	-9.9	-1.0
RH-60W	11165.43	118357.96	6450	16.6	-13.9	-0.1
RH-62	11088.191	118744.22	6500	16.4	-14.1	-1.9
RH-63	8852.997	116625.97	6500	21.9	-8.7	0.8
RH-64	8960.741	118034.73	6500	14.1	-16.3	1.1
RH-65	9106.148	118282.74	6550	19.1	-11.5	-0.4
RH-84	10683.6	118256.2	6500	9.6	-20.7	0.4
RH-87	10477.9	119102.8	6500	16.7	-13.8	0.1
RH-88	10125.4	119245.6	6450	11.3	-19.0	1.0
RH-89	11089.3	119003.4	6500	18.2	-12.3	-4.9
1378-1000	10417.774	119633.63	5466.9	17.1	-13.4	-0.8
RH-23V	10615.05	118589.22	6550	14.7	-15.7	-2.5
RH-33	14521.04	101827.63	6550	18.4	-12.2	-5.4
RH-78	11637.972	102141.57	6500	25.0	-5.8	1.1
RH-34	13769.13	103492.91	6600	22.2	-8.5	0.6
RH-37	13628.968	102893.25	6550	17.9	-12.6	0.8

Appendix C.
Table 6. - Ruby Hill Thesis AFTA Samples

*Coordinates in RH mine grid (U.S. State Plane NV Central) survey ft.

Hole ID	Footage	Lithology	Description	Easting	Northing	Sampled Elevation	Collar Elevation
HRH-1312	1805	Kbs	Argillized Bullwhacker sill	10486	118453	4719	6524
BRH-01C	1388	Kbs	Argillically altered Bullwhacker sill, abundant AsS, ore grade	10801	118703	4709	6097
BRH-02C	1850	Kbs	argillically altered Bullwhacker sill	10689	119537	4632	6482
BRH-11C	2108	Kbs	Altered Bullwhacker sill, possible preservation of phenocrysts?	12367	118674	4653	6761
HRH-1382	1840	Kbs	Bullwhacker sill- Mild argillization with abun. pyrite	11648	119000	4702	6542
RH-25	surface	Kbs	Flow banded Bullwhacker sill by TL	8813.59	119038.8	6357	
HC-1393A	1840	Kbs	Mineralized Bullwhacker Sill	10673.6	119581	4619	6459
RH-68	surface	Kbs	Mineralized Bullwhacker Sill	9213	119247	6412	
BRH-26C	1689	Kbs	Argillized Bullwhacker sill	12437.4	118657.4	4793.6	6482.6
HC-1399A	1825	Kbs	Mineralized Bullwhacker Sill	10836	120064.7	4629.2	6454.2
HC1751	640	Trt	Rhyolite tuff overlying E. Arch – possibly transported?	13574.6	118505.5	5836.4	6476.4
BRH-12C	1663	Kgf	Graveyard Flats intrusive	12936	118662.1	4790.8	6453.8

Sent to Geotrack for AFTA

Retained

Appendix D. –Attached Full Report from Geotrack Intl. #973
(See Supplemental Documents)